TRAPPING SODIUM WITH LIGHT

by

Eric Lowell Raab

A.B. Columbia College, New York, NY
(1982)

Submitted to the Department
of Physics
in Partial Fulfillment of
the Requirements for the Degree of

DOCTOR OF PHILOSOPHY

at the

MASSACHUSETTS INSTITUTE OF TECHNOLOGY

January, 1988

Signature of Author Signature redacted
Department of Physics
January 8, 1988

Certified by Signature redacted
David E. Pritchard
Thesis Supervisor

Accepted by Signature redacted
George F. Koster
Chairman, Department Commitee
on Graduate Studies

Trapping Sodium with Light

by

Eric Lowell Raab

Submitted to the Department of Physics
on January 8, 1987, in partial fulfillment of the
requirements for the degree of Doctor of Philosophy

Abstract

This thesis reports the conception and realization of a radiation pressure trap for neutral sodium atoms. The trapping and damping forces are provided by three counter-propagating laser beams situated along mutually orthogonal axes. A weak magnetic field having a constant gradient is superimposed with the lasers at their intersection, allowing the atoms to distinguish between the beams and absorb more light from the laser(s) propagating toward the center of confinement. The theory of radiative forces on atoms is presented, from which we make predictions of the trap dynamics for sodium to compare with the experiment. The trap is the first radiation pressure trap for neutral atoms which utilizes continuous-wave lasers.

Thesis Supervisor: Dr. David E. Pritchard

Title: Professor of Physics

To my parents

CONTENTS

CHAPTER I — INTRODUCTION

Electromagnetic traps for neutral atoms have been recently become a reality. Since Migdall *et al.* reported the first magnetic trap for neutrals in 1984 (MPP85), several other groups have succeeded in demonstrating different varieties of such traps (CBA86,BLM87,HKD87,RPC87,WIE87,GOU87). Neutral atom traps are interesting primarily because they provide a novel way to manipulate and observe large ($>10^{13}$ — HKD87) or small (<500 — CBA86) numbers of atoms. As trap technology develops, we can anticipate the use of trapped, cooled samples of atoms for testing the basic predictions of quantum mechanics as well as other fundamental concepts of physics.

The ability to trap particles electrodynamically is not a recent development. Ions and electrons are the easiest particles to trap, since they experience a fairly large force in an electric field; the spectroscopy of trapped ions is already a fairly advanced science (WDW78,BPI85,WIB87). Neutral particles are considerably more difficult to manipulate, but they have been confined using the relatively small interactions of their higher-order electromagnetic moments with either static or optical fields. Heer was the first to suggest a confinement scheme for neutral particles, proposing that a beam of neutrons be stored in a superconducting toroid (HEE63). Kugler *et al.* constructed a magnetic trap for neutrons in 1978 based on this proposal (KPT78), despite the difficulties imposed by the relatively small size of the neutron's magnetic moment. The development of traps for neutral atoms was contingent on the demonstration of a practical source of cold (<1 K) atoms; this was accomplished first in 1982 by Phillips

et al. (PPM82), who used a solenoid magnet with a longitudinally varying field to keep decelerating atoms resonant with a cw "slowing" laser. Shortly thereafter, Migdall (MPP85), Bagnato (BLM87), Hess (HKD87) and their colleagues confined sodium or hydrogen about a magnetic field minimum, and Chu *et al.* trapped sodium in the waist of an off-resonant laser beam (CBA86).

The most novel feature of an atom trap is the ultra-low temperature of the gas it contains. Indeed, since these traps have limited depths (typically <1 K), atoms *must* be pre-cooled to less than ~1 K before they can be trapped. Once confined, the trapping fields deflect the atoms away from surfaces which may adsorb or perturb them. They may then be further cooled — one proposal for cooling trapped atoms predicts ultimate temperatures (for sodium) as low as $\sim 10^{-6}$ K (PRI83).

An ultra-low temperature trapped gas can provide the opportunity to conduct some unique experiments. Collisions can be analyzed in the unusual regime where the deBroglie wavelength of the atoms is comparable to the P-wave impact parameter (cf. Chapter V); sodium will satisfy this condition below about .25 mK. Only the first partial wave in this case will contribute significantly to the cross-section, simplifying collisional dynamics. At still longer deBroglie wavelengths, one may begin to observe quantum collective effects such as Bose condensation or degenerate Fermi statistics, depending on the spin of the atom. If these degenerate systems are divided into two distinct regions, one may test the prediction of Javanainen (JAV86) of oscillations between two degenerate Bose systems. By reducing the random atomic motion, one

reduces the second-order Doppler broadening, a boon for spectroscopy.

Atom traps come in two basic varieties, each of which has advantages in performing certain types of experiments on the ultra-cold gas. *Magnetic* traps confine paramagnetic atoms about a magnetic field minimum (MPP85,BLM87,HKD87). Such traps can be relatively large (as much as 1 liter in volume (BLM87)) and potentially can hold an enormous number of atoms. Since the magnetic traps contain a spin-polarized atomic gas, they may be used for observing certain types of low-energy collisions and collective effects such as degenerate Bose and Fermi systems. In addition, the trap of Bagnato *et al.* has a large region of uniform field, possibly useful in performing experiments in high-resolution spectroscopy. Besides the second-order Doppler suppression, the long interrogation time feasible in traps may abet such spectroscopy, since it reduces the broadening inherent in a short measurement.

Light traps confine atoms using laser beams. The major benefit one gains from a light trap is that the gas contained can be relatively dense. This situation is well-suited for studies of low-energy collisions (GAP88), long-range molecules, and laser-induced molecular formation (WEI80). Many types of spectroscopy are advantageously performed since there is no line broadening due to the first-order Doppler shift — $v \ll \lambda\Gamma/2\pi$, where v is the atomic velocity, and λ the wavelength and Γ the linewidth of the atomic transition.

There are two types of light forces on an atom: the *dipole* force and

radiation pressure (cf. II.1.1). The dipole force is the force exerted by a laser beam due to its intensity gradient. Focused laser beams have been used by Ashkin to trap small dielectric particles (ASH70) (more recently, bacteria) and by Chu *et al.* to trap sodium atoms (CBA86). For dipole traps, the depth increases with the intensity (cf. II.1.3), so a reasonably strong trap commonly has a small volume, typically μm^3; the consequent dearth of atoms places limitations on the overall signal. Dipole traps have the additional problem that the strong intensity gradients tend to heat the atoms once they are trapped (cf. II.1.5), necessitating periodic use of additional lasers for cooling. In addition, the perturbations induced by the trapping beams preclude investigations in high-resolution spectroscopy.

This thesis describes a trap which is large, deep, and straightforward to implement. We constructed a trap which relies on radiation pressure to provide both the restoring and damping forces necessary to form a stable trap. The radiation is in the form of collimated, counter-propagating laser beams situated along three mutually orthogonal axes; the trap is at the common intersection of the six beams. The beams all contain the same frequencies, so they can be generated by a single laser modulated by an electrooptic crystal. The trap they form can be ~1 K deep and several cm^3 in volume.

The fundamental physics governing radiation pressure has been known for quite some time (PHI86). The existence of radiation pressure was initially hypothesized many centuries ago and first tested in the early part of this century. In 1619, Keppler

hypothesized that light pressure from the sun was responsible for deflecting the tails of comets. James Clerk Maxwell quantified the existence of radiation pressure in the late 19th century in his treatise on electromagnetic theory (MAX91). Einstein proved in 1917 that a photon imparts a quantum of momentum to an atom on absorption and emission by considering the thermodynamic equilibrium between a gas of atoms (or molecules) and the surrounding blackbody radiation (EIN17). In 1933, Frisch used radiation pressure to deflect a beam of sodium atoms (FRI33). More recent experiments involving radiation pressure are discussed in Section II.2.

The novelty of our trap is that it is the first to use radiation pressure to provide the confinement force. It was not evident until recently that this was feasible (see sec. II.2). The reason is that radiation pressure is simply the transfer of momentum from photons to an object: if two counter-propagating beams of equally intense light are trained on a dielectric sphere, the sphere will scatter an equal number of photons from each and experience no net force. The situation would be the same with lasers shining on an atom, *except* that an atom has an internal structure; its resonance frequency and quantization axis, for example, can be manipulated to make it interact more strongly with a laser having a particular tuning and/or polarization. A judicious arrangement of lasers and other influences such as magnetic fields or optical pumping effects *can* form a radiation pressure trap for atoms (PWR86). As a bonus, the trapping lasers can be configured to simultaneously provide damping forces as well as restoring forces (CHB85), eliminating the need for a second laser and/or exotic chopping scheme. We

were able to achieve a record low temperature for trapped atoms (< 1 mK).

The successful design of *any* cw radiation pressure trap must rely in some way on the internal structure of the trapped atom. This is a consequence of the "optical Earnshaw theorem" (ASG83), which extends the well-known theorem from electrostatics to show that a dielectric particle cannot be trapped by cw radiation pressure exclusively (cf. II.2.3). In 1986, Pritchard *et al.* published several specific ideas for circumventing this theorem to construct a radiation pressure trap for atoms (PWR86). This paper is presented as Appendix A, and a brief review of the proposed traps is given in Section II.2.

Our implementation of the seminal ideas of Appendix A is a trap formed by three pairs of counter-propagating laser beams placed along mutually orthogonal axes (x,y, and z). The two beams along any given axis are given opposite circular polarizations with a pair of quarter-wave plates. By superimposing a weak "spherical quadrupole" magnetic field (MPP85) over the region formed by the intersection of the beams, we can induce an atom to absorb more photons from the beam(s) propagating towards the origin and consequently form a stable trap. The details of this trapping arrangement are given in Section II.2.

The dynamics of this trap for a sodium atom are analyzed using the theory in Section II.1 and the computer model described in Section II.3. It is found that despite the complexities which arise due to the multiplicity of states in the primary transitions

of sodium, the trap provides restoring and damping forces not only along the coordinate axes, but in the full three-dimensional space.

The trap was demonstrated in collaboration with S. Chu, M. Prentiss, and A. Cable by adapting their apparatus at AT&T Bell Laboratories. The additions made to their system and an analysis of the data obtained are given in Chapter III and Appendix B. Highlights of the results include:

- Trapped atom lifetimes of several minutes;
- Trapped atom temperatures of less than 1 mK;
- The highest published density of trapped neutral sodium atoms;
- The first measurement of optical absorption in a gas of trapped atoms; and
- Evidence of collisions between the atoms in the trap.

The success of the Bell experiment led us to design and build a light trap at M.I.T. The M.I.T. trap design has a number of advantages over the one at Bell, the most important being that it will load the atoms continuously into the trap region (instead of in pulses) and that the magnets are superconducting. This should allow us to obtain still higher densities than previously, and to study atomic interactions in regimes thus far unexplored. A description of the M.I.T. apparatus along with the principles for its operation is given in Chapter IV. The thesis concludes with a discussion of some experiments that may be conducted in the new apparatus.

CHAPTER II — THEORY

II.1 Light Forces On Atoms

II.1.1 Introduction

There are two types of forces which an atom can experience in the presence of radiation (DHS87, ASH70, COO79). One is referred to as the *dipole*, *stimulated*, *induced*, or *gradient* force; the other is called *radiation pressure*, or the *scattering* or *spontaneous* force. The dipole force is a result of the non-zero electric susceptibility of an atom: the electromagnetic field induces an electric dipole moment in the atom, which in turn interacts with the field to produce a force along the field gradient. Radiation pressure is a consequence of the fact that photons carry momentum; a beam of light will push an atom in its direction of propagation as a stream of water would push an object in its direction of flow. In this section we will present a brief derivation of the expression for the force exerted on an atom by electromagnetic radiation, analyze the velocity dependence and fluctuations of the force, and discuss some of the ramifications of our results.

II.1.2 Classical Expression for the Light Force

The quantum mechanical expression for the light force on an atom can be motivated by a classical analogy. A hydrogenic atom can be treated classically as an electron of charge -e and mass m harmonically bound to a charge +e fixed to the point

$\vec{x}_0$, with resonance frequency ω_0 and damping coefficient γ. We illuminate this atom with a general monochromatic electromagnetic wave where the electric field has the form

$$\vec{E}(\vec{x},t) = \hat{\varepsilon}E(\vec{x})\cos(\theta(\vec{x})+\omega t) = \mathrm{Re}\left\{\hat{\varepsilon}E(\vec{x})\,e^{i(\theta(\vec{x})+\omega t)}\right\} \tag{1}$$

where $\hat{\varepsilon}$ is the polarization, $E(\vec{x})$ the (real) amplitude, $\theta(\vec{x})$ the phase, and Re denotes "the real part of." The force on the electron in the dipole approximation ($|\nabla\theta(\vec{x}_0)(\vec{x}-\vec{x}_0)|\ll 1$) is (SML78)

$$\begin{aligned}\vec{F}_{class} &= \mathrm{Re}\left\{(\vec{p}\cdot\hat{\varepsilon})\nabla\vec{E}\right\} \\ &= \mathrm{Re}\left\{(p_\varepsilon)\left[\nabla E(\vec{x}_0) + iE(\vec{x}_0)\nabla\theta(\vec{x}_0)\right]e^{i(\theta(\vec{x}_0)+\omega t)}\right\} \\ &= \left[(\mathrm{Re}\,p_\varepsilon)\nabla E(\vec{x}_0) + (\mathrm{Im}\,p_\varepsilon)E(\vec{x}_0)\nabla\theta(\vec{x}_0)\right]e^{i(\theta(\vec{x}_0)+\omega t)}\end{aligned} \tag{2}$$

where $\vec{p}$ is the (complex) dipole moment of the electron and $p_\varepsilon \equiv \vec{p}\cdot\hat{\varepsilon}$.

In taking the real part of (2) to find the physical force, we see that the gradient of the field amplitude multiplies the real part of $\vec{p}$, while the gradient of the phase multiplies the imaginary part of $\vec{p}$. The real part of $\vec{p}$ gives rise to a scattered wave with a real wave-vector and hence corresponds to *elastic* scattering of the incident field, while the imaginary part of $\vec{p}$ yields an imaginary wave-vector and therefore corresponds to *absorption* (which is followed by spontaneous emission) (JAC75). Hence the field amplitude gradient contributes to elastic scattering, while the phase

gradient contributes to absorption.

We shall solve for $\vec{p}$ explicitly and obtain an expression for the force. In the dipole approximation, the effect of displacing the electron is ignored, so the equation of motion for the electron is

$$m\ddot{\vec{\xi}} + \gamma\dot{\vec{\xi}} + m\omega_0^2\vec{\xi} = -e\,\hat{\varepsilon}E(\vec{x}_0)e^{i(\theta(\vec{x}_0)+\omega t)} \tag{3}$$

where $\vec{\xi} \equiv \vec{x} - \vec{x}_0$ is a complex vector whose real part is the electron's displacement. Defining $\Gamma \equiv m\gamma$, we solve (3) in the usual way and get

$$\vec{p} = -e\vec{\xi} = \frac{e^2/m}{\omega_0^2 - \omega^2 + i\,\omega\Gamma}\,\vec{E}(\vec{x}_0,t)$$

which near resonance ($\omega \approx \omega_0$) becomes

$$\approx \frac{e^2/2m\,\omega_0}{(\omega_0 - \omega) + i\,\Gamma/2}\vec{E}(\vec{x}_0,t)$$

$$= \frac{e^2/2m\,\omega_0}{(\omega_0-\omega)^2 - (\Gamma/2)^2}\left[(\omega_0-\omega) + i\,(\Gamma/2)\right]\vec{E}(\vec{x}_0,t)\,. \tag{4}$$

We see that the real part of $\vec{p}$ oscillates in (or π out of) phase with the applied field, while the imaginary part of $\vec{p}$ oscillates $-\pi/2$ out of phase (Figure II.1). Since the total E-field is the sum of the incident and scattered fields and the latter is in phase with $\vec{p}$, radiation associated with Re $\vec{p}$ (i.e. stimulated emission) will add (or subtract) coherently to the applied field, while scattering associated with Im $\vec{p}$ (spontaneous emission) will be incoherent.

We get the classical expression for the force by substituting Eq. (4) into Eq. (2):

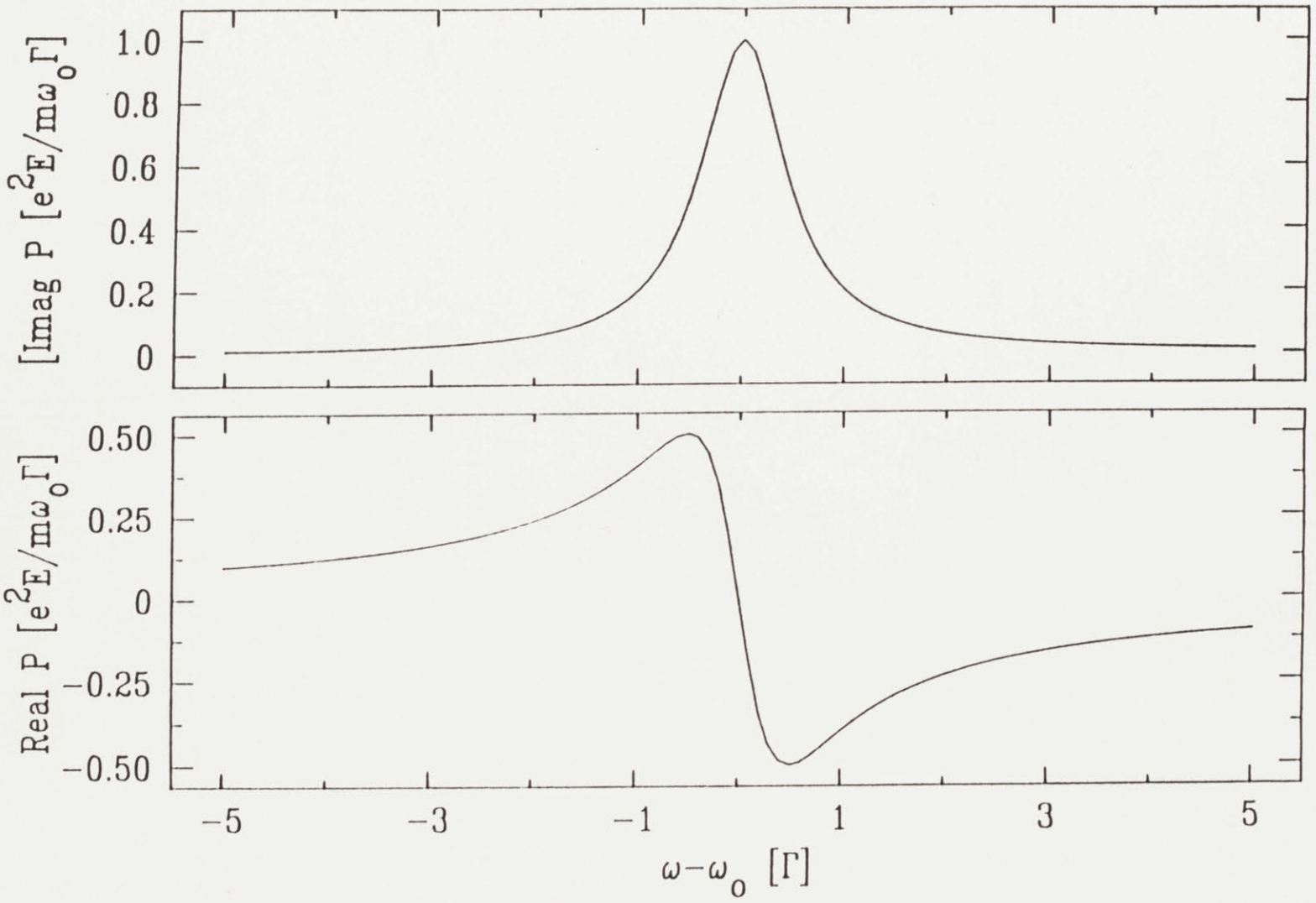

Figure II.1: The real and imaginary amplitudes of the dipole moment p of an atom subject to an electric field $E_0 e^{i\omega t}$ as a function of ω. The atom is modeled classically as a mass m having charge e bound to a point with a spring of resonance frequency ω_0 and damping rate Γ. The imaginary part of p (top) represents absorption of the incident wave; it has a Lorentzian lineshape with a FWHM of Γ. The real part of p (bottom) represents the elastic scattering of the incident radiation; it has a dispersion lineshape which changes sign through resonance, corresponding to the index of refraction becoming less than one when $\omega > \omega_0$.

$$\vec{F}_{class} = -\frac{e^2}{m\omega_0}\frac{\delta\nabla E^2 + \Gamma E^2\nabla\theta}{4\delta^2+\Gamma^2}, \tag{5}$$

where $\delta \equiv \omega - \omega_0$.

We may compare this classical relation with the quantum mechanical expression for the force on a stationary two-level atom in the low intensity limit (e.g. COO79)

$$\vec{F} \approx -\frac{\hbar\Gamma\Omega^2\nabla\theta + \hbar\delta\nabla\Omega^2}{4\delta^2+\Gamma^2} \qquad (\Omega/\Gamma \ll 1) \tag{6}$$

where $\Omega \equiv \vec{\mu}\cdot\vec{E}/\hbar$ is the Rabi frequency, with $\vec{\mu} \equiv -e <final\ |\vec{x}|\ initial>$ the atomic dipole moment. If one defines the *oscillator strength* (COS33)

$$f_{fi} \equiv \frac{m\omega_0\mu^2}{e^2\hbar} \tag{7}$$

then we may write

$$\vec{F} = f_{fi}\,\vec{F}_{class}\,. \tag{8}$$

We see therefore that at low field intensities, the force on a quantum mechanical two-level system is equal to the force on a classical damped oscillator of frequency $\omega_0 = (E_2 - E_1)/\hbar$, times a dimensionless number f_{fi}. At higher intensities, we must account additionally for the effects of saturation; there is no classical analogue for this.

II.1.3 Quantum Mechanical Expression for the Light Force

The general quantum mechanical expression for the force can be derived in the semi-classical approximation by viewing the atom as a two-level system with the hamiltonian

$$H = \frac{P^2}{2M} + H_0 - \vec{\mu}\cdot\vec{E}(\vec{x}_0,t) \tag{9}$$

where $\vec{P}$ is the center-of-mass momentum, M the atomic mass, H_0 the hamiltonian for the unperturbed atom, and $-\vec{\mu}\cdot\vec{E}$ the coupling in the dipole approximation. Note that as in the classical picture, the field is evaluated at the center-of-mass of the atom, a step valid in the dipole approximation. H_0 has energy eigenstates |1>, |2> with energies E_1, E_2 respectively.

We will assume that the electric field has the same form as in II.1.2, namely

$$\vec{E}(\vec{x},t) = \mathrm{Re}\left\{\hat{\varepsilon}E(\vec{x})\,e^{i(\theta(\vec{x})+\omega t)}\right\}. \tag{2}$$

The perturbed system will be described by the wavefunction

$$|\psi(t)> = a_1(t)\,|1> + a_2(t)\,|2>;$$

by substituting this into the Schrodinger equation

$$i\hbar\frac{\partial}{\partial t}\,|\psi(t)> = H\,|\psi(t)> \tag{10}$$

we obtain the equations of motion for the density matrix ρ, whose elements are defined as $\rho_{mn} \equiv a_m a_n^*$. These are commonly expressed in terms of the matrix σ, where

$$\begin{aligned} \sigma_{11} &= \rho_{11}, \\ \sigma_{22} &= \rho_{22}, \\ \sigma_{12} &= \sigma_{21}^* = \rho_{12}e^{-i(\theta(\vec{x})+\omega t)}. \end{aligned} \tag{11}$$

Defining:

$\omega_0 \equiv \frac{E_2-E_1}{\hbar}$, the atomic resonance frequency;

$\mu_\varepsilon \equiv \vec{\mu}\cdot\hat{\varepsilon}$; and

$\Omega \equiv \frac{\mu_\varepsilon E}{\hbar}$, the Rabi frequency,

the equations of motion can be written as

$$\dot{\sigma}_{11} = -\frac{i}{2}\Omega(\sigma_{12} - \sigma_{21}), \qquad (12)$$
$$\dot{\sigma}_{22} = \frac{i}{2}\Omega(\sigma_{12} - \sigma_{21}),$$

and

$$\dot{\sigma}_{12} = -i(\delta + \dot{\theta}(\vec{x}))\sigma_{12} + \frac{i}{2}\Omega(\sigma_{22}-\sigma_{11})$$

where terms oscillating at twice the optical frequency have been discarded (rotating wave approximation).

We now must add a relaxation mechanism to account for the spontaneous decay of the atom from level 2 (the excited state) to level 1 (the ground state). In the case of radiative relaxation, this can be done rigorously by adding a term to a "dressed" (atom + field) hamiltonian which couples the dipole moment of the atom to the field modes of the vacuum (LOU64). We shall expedite matters by simply adding a damping term to the equations of motion,

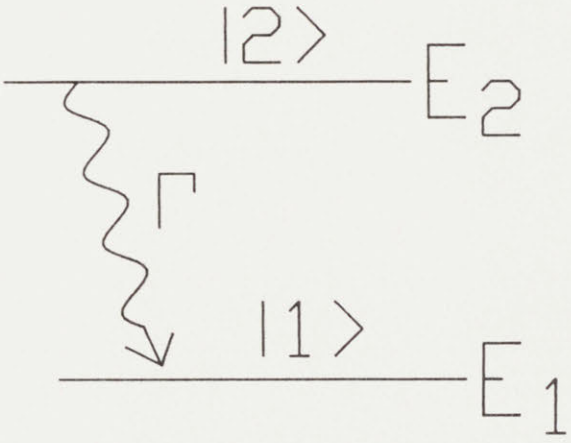

Figure II.2

with the understanding that we are considering radiative damping although it could include other contributions to the relaxation as well (such as collisions). If Γ is the

decay rate from |2> to |1> (see Figure II.2) then (12) becomes

$$\dot{\sigma}_{11} = -\frac{i}{2}\Omega(\sigma_{12} - \sigma_{21}) + \Gamma\sigma_{22} \; ; \tag{13}$$
$$\dot{\sigma}_{22} = \frac{i}{2}\Omega(\sigma_{12} - \sigma_{21}) - \Gamma\sigma_{22} \; ;$$

and

$$\dot{\sigma}_{12} = -i\,(\delta + \dot{\theta}(\vec{x}))\sigma_{12} + \frac{i}{2}\Omega(\sigma_{22}-\sigma_{11}) - \frac{\Gamma}{2}\sigma_{12}.$$

Here, $\Gamma = A = \dfrac{4\omega_0{}^3\mu^2}{3\hbar c^3}$, the Einstein A coefficient. These equations are commonly referred to as the "Optical Bloch Equations" (O.B.E.) (ALE75).

If the atomic velocity is so low that the atom travels much less than a wavelength in a typical excited state lifetime ($v/\Gamma \ll \lambda$; for the sodium D2 transition, $v \ll 6m/s$), σ assumes steady state values. The solution for σ is then readily obtained by setting all time derivatives to zero and solving the resulting system of coupled algebraic equations.

The expectation value $\langle\mu_\varepsilon\rangle = Tr(\rho\mu) = \mu_\varepsilon(\rho_{12} + \rho_{21})$ (CDL77); the steady state force can then be found using the Ehrenfest theorem:

$$\begin{aligned} \dot{\vec{P}} &= \frac{i}{\hbar}[H,\vec{P}] = -\nabla H \\ \Rightarrow \vec{F} &= \langle\dot{\vec{P}}\rangle = \langle\nabla\vec{\mu}\cdot\vec{E}\rangle \\ &= \langle\mu_\varepsilon\rangle\,\nabla E(\vec{x},t)\;. \end{aligned} \tag{14}$$

After some algebra, again invoking the rotating wave approximation, we obtain

$$\vec{F} = -\frac{\hbar\Gamma\Omega^2\nabla\theta + \hbar(\delta+\dot{\theta})\nabla\Omega^2}{4(\delta+\dot{\theta})^2 + \Gamma^2 + 2\Omega^2}\;. \tag{15}$$

We shall evaluate this expression for two simple varieties of electric field: a traveling wave in one dimension and a standing wave in one dimension.

II.1.3a: Light force in a one-dimensional traveling wave

For a traveling wave propagating along, say, the z-axis, we have

$$E(\vec{x},t) = E_0 \cos(-kz + \omega t) = \mathrm{Re}\left\{E_0 e^{i(-kz+\omega t)}\right\}$$

where a positive wavevector k indicates propagation in the +z-direction. In this case, $\theta = -kz$, and the gradient $\nabla\Omega^2$ is zero. ($-\dot{\theta} = k v_z$, the Doppler shift in the direction of the atom's motion). Substituting these into (15), we obtain

$$\vec{F} = \frac{\hbar\Gamma\Omega_0^2 k}{4(\delta - k v_z)^2 + \Gamma^2 + 2\Omega_0^2}\,\hat{z} \qquad (1\text{–}D \textit{ traveling wave}) \qquad (16)$$

where

$$\Omega_0 \equiv \mu E_0/\hbar\,. \qquad (16a)$$

This corresponds to the scattering force, and is always in the direction of propagation of the wave. If we define the *saturation parameter*

$$s \equiv \frac{2\Omega_0^2}{\Gamma^2 + 4(\delta - k v_z)^2}$$

we may then write

$$\vec{F}_{scat} = (\hbar\vec{k})(\Gamma)\left[\frac{s}{2(s+1)}\right] \qquad (16b)$$

$$= (\textit{photon momentum}) \times (\textit{decay rate}) \times (\textit{fraction of time in excited state}),$$

i.e. the force results from the momentum transferred to the atom from absorbed photons and their subsequent spontaneous emission. Since the incident photons are propagating with a particular direction but are re-radiated (nearly) isotropically, there is a net push in the direction of the incident beam. This effect was first experimentally demonstrated for sodium by Frisch in 1933 (FRI33), but was not exploited to cool and trap atoms until recently (PHM82,PPM82,BLS84 — cf. Chapter I).

II.1.3b: Light force in a one-dimensional standing wave

Now consider the case of a one-dimensional standing wave. We have a field

$$E(x,t) = 2E_0 \cos kz \cos \omega t \ .$$

In this case $\theta = 0$, and we get

$$\vec{F} = \frac{-2\hbar k \delta \Omega_0^2}{4\delta^2 + \Gamma^2 + 2\Omega^2} \sin 2kz \ \hat{z} \ , \qquad (1\text{–}D \ \textit{standing wave}) \tag{17}$$

where Ω, Ω_0 are the Rabi frequencies of the individual traveling waves (Ω_0 has the spatial dependence removed — see Eq. (16a)). Equation (17) is commonly written in terms of the total spatially dependent Rabi frequency as

$$\vec{F} = \frac{-\hbar \delta \nabla \Omega^2}{4\delta^2 + \Gamma^2 + 2\Omega^2} \ . \qquad (1\text{–}D \ \textit{standing wave}) \tag{18}$$

The expression (18) corresponds to the induced dipole force. We may write this as $\vec{F}_{dip} = -\nabla U$ (ASH78), where

$$U = \frac{\hbar \delta}{2} \ln \left[\frac{4\delta^2 + \Gamma^2 + 2\Omega^2}{4\delta^2 + \Gamma^2} \right] . \tag{19}$$

This potential corresponds to the free energy of the atom in the radiation field

(LAL60).

We make three observations about this expression: first, the force is derived from a *conservative* potential. This is a consequence of the fact that the dipole force arises from the *coherent* redistribution of the field quanta by the atom (DAC85), i.e. absorption followed by stimulated emission. An atom therefore cannot be *cooled* using the dipole force alone. If the atom experiences an occasional spontaneous decay, however, the coherence of the system is destroyed; the atom may then be biased into seeing more "uphill" than "downhill" regions of potential, resulting in very efficient cooling (ACH86).

Second, the sign of the potential, and hence the force, depends on the laser detuning δ. In particular, for $\delta<0$, the potential draws the atom to a region of strong field, allowing one to trap atoms in the waist of a focused laser beam (ASH79,CBA86) or to collimate an atomic beam by laser focusing (BFA78). For $\delta>0$, an atom is drawn to weaker fields, leading to proposals for trapping atoms in the center of a $TEM_{1,0}$ "donut mode" of a laser (STW84,YSH86), or at the nodes of a three-dimensional standing wave (LMP76).

Third, the depth of the potential and hence the dipole force increases monotonically with the laser intensity Ω^2. The scattering force, on the other hand, saturates at $\hbar k\Gamma/2$. The dipole interaction, therefore, can potentially exert much more force on an atom than radiation pressure. Specifically, if the condition $\Omega \gg \delta$ is

satisfied, the dipole force will exceed the spontaneous force by approximately the ratio δ/Γ. For example, if we focus a 100 mW laser beam to a 3 μm waist, we will have $\Omega \approx 10^4\Gamma$, so a detuning of $\delta \sim 1000\Gamma$ from resonance will result in a dipole force ~3 orders of magnitude greater than the maximum attainable scattering force.

II.1.4 Velocity Dependence of Radiation Pressure in a 1-D Standing Wave

We now examine how the scattering force in one dimension depends on the atomic velocity. Consider a two-level atom as described in II.1.3 moving with velocity v along the z-axis. The atom is illuminated with a monochromatic standing plane wave $\vec{E}(z,t) = \hat{\varepsilon}E(z,t)$ where $\hat{\varepsilon}$ is a transverse polarization vector and $E(z,t) = 2E_0 \cos kz \cos \omega t$.

The physical effect of the atom's motion through the standing wave is to Doppler shift the counterpropagating beams so that in the rest frame of the atom, one of the beams appears to have a slightly higher frequency than the other. From the perspective of radiation pressure, this will cause the atom to scatter more photons from the beam whose Doppler shifted frequency is closer to resonance. The *rate* of scattering will be reduced, however, by the effects of stimulated emission. Since the standing wave has a field gradient, dipole forces will be present; but it is not clear how to obtain the velocity dependence of the dipole force from the results thus far presented.

A complete and correct approach to the problem of an atom moving through a standing wave is to solve the optical Bloch equations (13) in the non-stationary case.

The exact relation for the force cannot be obtained in closed form, but a continued fraction expansion was found by Minogin and Serimaa for the force averaged over a wavelength (MIS79). An alternative approach is to simplify the set of exact equations by considering only low velocities such that the atom travels much less than a wavelength during an excitation-spontaneous decay cycle: $v/\Gamma \ll \lambda$, or $kv \ll \Gamma$ — the Doppler shift is much less than the natural linewidth. For the sodium D2 line, $\Gamma = 2\pi\times 10$ MHz, and the requirement is $v \ll \Gamma/k = 6\,m/s$. ‡ The O.B.E. can then be expanded in terms of the small parameter kv/Γ, and a solution to the force is found of the form (DHS87)

$$F \simeq F(v=0) - \alpha v . \tag{20}$$

When $\alpha<0$, the force and the velocity are co-linear, causing the atom to heat. When $\alpha>0$, the force opposes the atomic velocity; α is then called the *damping coefficient*. The characteristic *damping time* of the system is then given by $\tau \equiv M/\alpha$; it determines how quickly an atom will be slowed to 1/e of its initial velocity. It was found (DHS87), in the low velocity regime, that

$$\frac{1}{\tau} = \frac{\hbar k^2}{M\Gamma}\,\frac{2\delta}{(1+4s_0)^{3/2}}\left\{\frac{\Gamma^2 s_0(1+2s_0)}{\delta^2+\Gamma^2/4} - [(1+6s_0+6s_0^2-(1+4s_0)^{3/2}]\right\}, \tag{21}$$

s_0 being the saturation parameter at zero velocity for *one* of the traveling waves. The

‡ This corresponds to a temperature of ~0.1 K, implying that the atoms are already quite cold; they are still several orders of magnitude hotter than the minimum temperature which they can achieve, however (cf. II.1.5).

behavior of α ($\equiv M/\tau$) versus s_0 for various detunings is plotted in Figure II.3. We see that for a given positive detuning, the sign of the damping coefficient changes from negative to positive as the intensity increases. For negative detuning (not shown), just the opposite is true: the force damps at low intensities, and heats at high intensities. Thus to cool atoms at high intensity, the laser must be tuned above resonance, while at low intensities the laser must be tuned to the red (DAC85).

The low intensity behavior of the damping force can be found by taking the $s_0 \to 0$ limit of the above expression. We can obtain the same result, however, if we note that the atom's kinetic energy in this regime will be much greater than the depth of the potential wells of the dipole interaction: $M\,\mathrm{v}^2 \gg \Omega^2 > U$. The dipole force will then be negligible, and the damping will simply be given by the total scattering force imparted by the two counter-running traveling waves viewed independently.

If we expand the expression (16a) for the scattering force in a traveling wave to first order in $k\,\mathrm{v}/\Gamma$ about v=0, we get

$$F_{scat} \approx \frac{\Gamma\hbar k\,\Omega^2}{\Gamma^2+2\Omega^2+4\delta^2}\left[1+\frac{8\delta\Gamma}{\Gamma^2+2\Omega^2+4\delta^2}\,\frac{k\,\mathrm{v}}{\Gamma}\right]$$

$$= \frac{\Gamma\hbar k}{2}\,\frac{s_0}{s_0+1}\left[1+\frac{8\delta}{s_0+1}\,\frac{k\,\mathrm{v}}{\Gamma^2+4\delta^2}\right] \qquad (22)$$

where s_0 is the single traveling wave saturation parameter. The two traveling waves will have opposite signs for k, so in a standing wave,

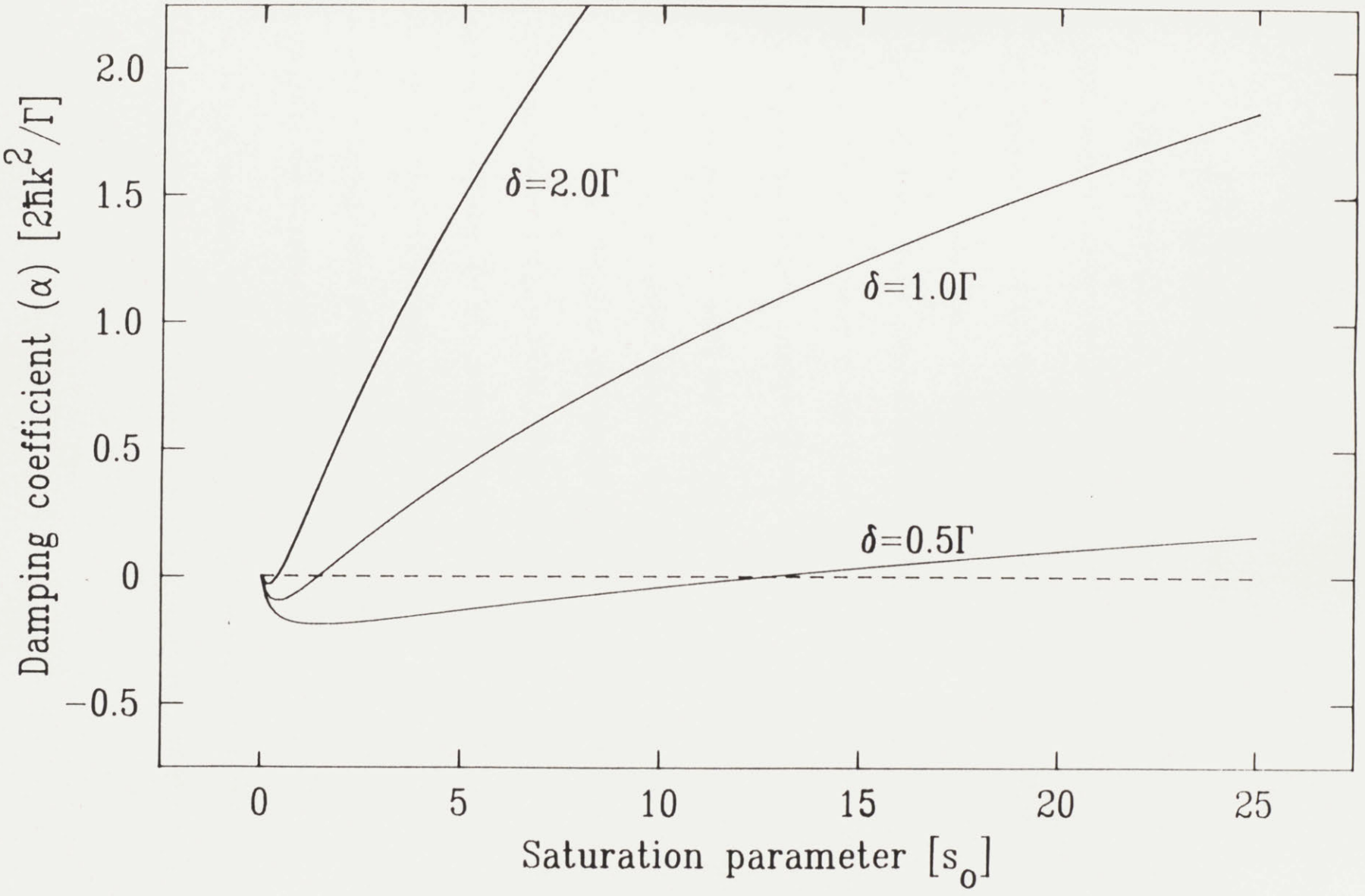

Figure II.3 Damping coefficient α versus saturation parameter $s_0 \equiv (\Omega/2)/(\Gamma^2/4 + \delta^2)$ for various values of positive detuning. As the intensity increases, α changes sign from negative to positive, indicating that the force damps at high intensities.

$$F_{scat} \approx \frac{\Gamma\hbar k}{2} \frac{s_0}{s_0+1} \frac{16\delta}{s_0+1} \frac{k\,v}{\Gamma^2+4\delta^2} \tag{23}$$

$$\Rightarrow \alpha \rightarrow -\frac{8\Gamma\hbar k^2\delta}{\Gamma^2+4\delta^2} \frac{s_0}{1+2s_0} . \qquad (\textit{low intensity})$$

This force is proportional to $-v\,\delta$, so for negative detunings it opposes the velocity and thus damps the motion of the atom, in agreement with our previous result.

This approximation for α is compared to that obtained using Eq. (21) in Figure II.4a. We see that at saturation intensity $\Omega=\Gamma$, the approximation deviates quite a bit from its correct value. Since saturation occurs at a relatively low laser intensity (~12 mW/cm^{2}for sodium), one must be careful to use the correct expression for the damping force when analyzing experimental data.

The dependence of α on s_0 and δ at low intensities is plotted in Figure II.4b. We see that for a given velocity, the damping is a maximum when $s_0 = 1$ and $\delta = -\Gamma/2$. We find that the characteristic damping time under these optimum conditions is $\tau_{scat} = 2M/\hbar k^2 \approx 6\mu s$ for sodium. On a macroscopic time scale this is very fast; for this reason this arrangement has been dubbed "optical molasses" (CHB85) in analogy to the highly viscous derivative of sugar cane. Counter-propagating beams placed along the three Cartesian axes have been used to cool a gas of sodium atoms and hold them for times up one second (CHB85).

At high intensities, tuning *above* resonance causes the standing wave to quickly damp the atomic velocity — this has been dubbed "blue molasses" (DAC85,SDA87).

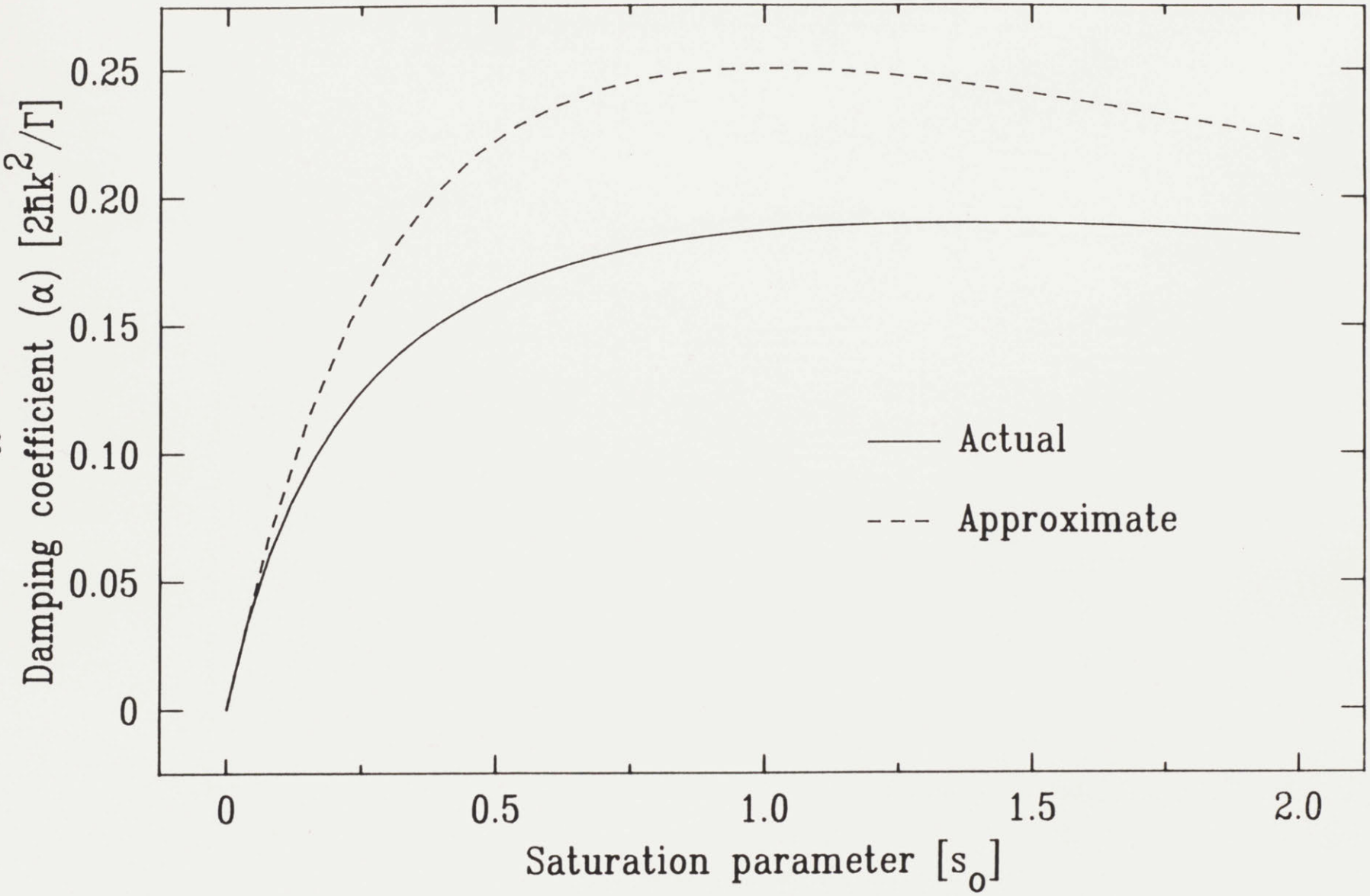

Figure II.4a: The first order damping coefficient α obtained by solving the velocity-dependent Bloch equations (solid line) is compared to the approximate coefficient obtained by adding the radiation pressure of two counter-propagating waves (dashed line). The two agree only for very small intensities; as s_0 increases, saturation causes a reduction in the damping not accounted for in the radiation pressure approximation.

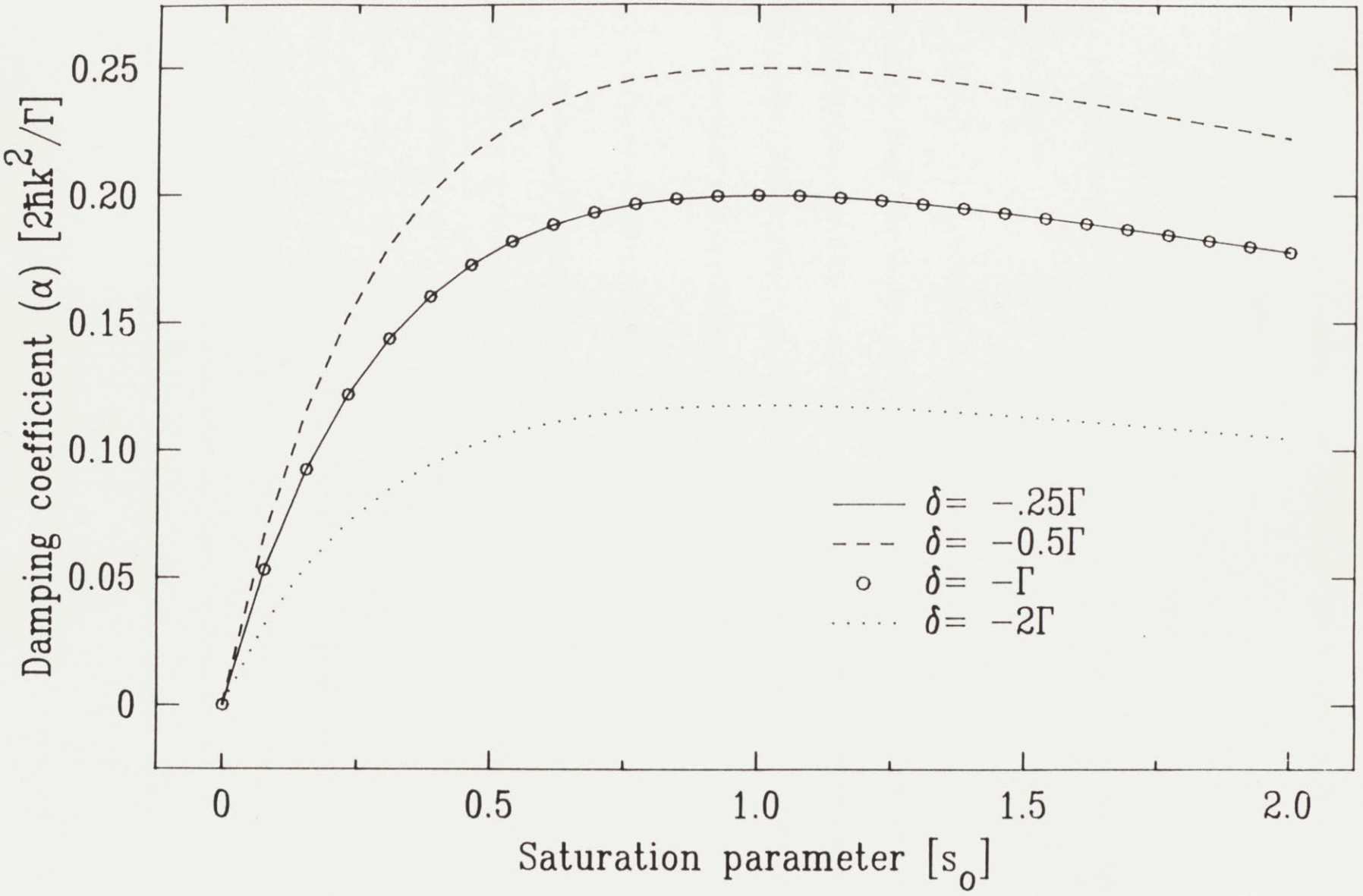

Figure II.4b: The approximate damping coefficient α due to radiation pressure versus saturation parameter s_0 for various laser detunings δ. The damping is optimized for $s_0 = 1$ and $\delta = -\Gamma/2$.

The behavior of the damping coefficient in this regime can be found by taking the leading terms in s_0 in the polynomial (21):

$$\alpha \rightarrow -\frac{\hbar k^2}{\Gamma} \frac{2\delta s^2{}_0}{(1+4s_0)^{3/2}} \left\{ \frac{\Gamma^2}{\delta^2+\Gamma^2/4} - 6 \right\}. \qquad (high\ intensity) \qquad (24)$$

When the detuning satisfies $\Gamma \ll |\delta| \ll \Omega$, $s_0 \rightarrow \Omega_0^2/2\delta^2$, and the above expression yields the damping time

$$\tau \approx \frac{2\sqrt{2}}{3} \frac{M}{\hbar k^2} \frac{\Gamma}{\Omega} = 3 \frac{\Gamma}{\Omega} \mu sec \ . \qquad (\Gamma \ll |\delta| \ll \Omega)$$

Thus the damping time at high intensities can be shorter than at low intensities by approximately the ratio Γ/Ω. In a focused beam, this can be a factor of several orders of magnitude. This is why a high intensity blue tuned laser has been suggested as an efficient means of slowing a thermal atomic beam (DAC85,SDA87).

II.1.5 Heating and Ultimate Temperature

The processes described in the previous section can be used to damp the atomic motion, but not without limit. In reality, there are uncertainties inherent to these cooling processes which introduce randomness to the system and consequently, heating. There are two primary sources of this uncertainty: one, when an atom absorbs a photon and undergoes a spontaneous decay, the spatial distribution of the emitted photon is determined only probabilistically, leading to heating at a rate proportional to the rate of spontaneous emission. Two, the dipole moment of the atom will experience zero-point fluctuations which couple to the gradient of the electric

field, giving rise to uncertainty in the the absorption of photons and the dipole force (GOA80). The minimum or "ultimate" temperature which is theoretically attainable will result from the balance between the directed cooling and random heating processes.

We will utilize two frequently referenced approaches to calculate a relation for the ultimate temperature. The procedure common to both is to find an expression for the kinetic energy "component" $K_i = \frac{1}{2}M v_i^2$ along the i-axis, then to solve for its minimum steady-state value. The minimum temperature is subsequently defined by the relation $\frac{1}{2}k_B T_{\min} = (K_i)_{\min}$, where k_B is the Boltzman constant (even though a radiatively cooled gas of atoms may not be in thermal equilibrium). The two approaches give the same result in the regime of *low* optical intensity; one approach is more general and will allow us to solve for the minimum temperature in the *high* intensity regime as well.

The first approach is attributed to Wineland and Itano (WII79). They reason that when an atom undergoes a photon absorption followed by a spontaneous emission, its kinetic energy will change by an amount equal to the difference in energy of the two photons:

$$\Delta K = \hbar(\omega_{abs} - \omega_{em}) \tag{25}$$

where ω_{abs} (ω_{em}) is the frequency of the absorbed (emitted) photon. The frequencies will in general be different because of the Doppler shift and atomic recoil. On resonance, if we neglect terms of order $(v/c)^2$ and beyond, these frequencies are

$$\omega_{abs} = \omega_0 - \vec{k}_{abs}\cdot\vec{v} + R/\hbar, \tag{26a}$$

$$\omega_{em} = \omega_0 - \vec{k}_{em}\cdot\vec{v}' - R/\hbar, \tag{26b}$$

where $\vec{v}$ ($\vec{v}'$) is the velocity of the atom in the ground (excited) state, and the recoil energy $R = \hbar^2k^2/2M$. Since the emitted radiation is approximately isotropic, the second term on the r.h.s. of (26b) averages to zero, and Eq. (25) becomes

$$\Delta K = \hbar\vec{k}\cdot\vec{v} + 2R\ , \tag{27}$$

where we have set $\vec{k} \equiv \vec{k}_{abs}$.

The *rate* of energy change is simply ΔK times the absorption rate:

$$\frac{dK}{dt} = \frac{I}{\hbar\omega}\sigma(\vec{v})\Delta K \tag{28}$$
$$= (photon\ flux)\times(absorption\ cross\text{-}sec'n)\times(energy\ change\ per\ event)\ .$$

The atomic cross-section for absorption of *each* traveling wave is given by (LOU73)

$$\sigma(\vec{v}) = \sigma_0\frac{\Omega^2}{4(\delta - \vec{k}\cdot\vec{v})^2 + 2\Omega^2 + \Gamma^2}\ , \tag{29}$$

where $\sigma_0 = \lambda^2/2\pi$; note that we have included saturation effects (which WII79 neglects).

We can now estimate the cooling limit for the atom. Assume the atom is illuminated with a *weak* laser counter-propagating along the z-axis, and has a velocity v_z. The rate of energy change along this axis is then the sum of the rates induced by the two beams:

$$\frac{dK_z}{dt} \propto \sigma(v_z)(\hbar k v_z + 2R) + \sigma(-v_z)(-\hbar k v_z + 2R)\ . \tag{30}$$

Note that we must use the full recoil energy $2R$ per event, and not the average

projection along the z-axis. This is required in our case because there are cooling beams parallel to the x and y-axes as well. The recoil from absorption and emission from the x and y-axis beams will contribute to heating along z; similarly, recoil in this dimension will cause heating in the other two. We can account for this simply by taking advantage of the symmetry of the situation and using the *full* recoil in Eq. (30). This correction is also required for finding the cooling limit in a three-dimensional atom trap even if only one molasses beam is present, since the trap will mix all degrees of translational freedom. Some authors (e.g. COO80) do in fact take the projection of the recoil along one axis, and consequently arrive at a lower value for the temperature. These authors are only *interested* in one-dimensional heating, however (as in an atomic beam), and the remaining dimensions are uncoupled.

At the low velocities we are considering, we may expand the cross-section to first order in v_z and obtain an expression proportional to Eq. (23). If we substitute this into Eq. (30) and set it to zero, we find the minimum kinetic energy along the z-axis:

$$(K_z)_{\min} = \frac{\hbar}{2}(s_0+1)\frac{\Gamma^2+4\delta^2}{8\delta} \tag{31}$$

where we recall that s_0 is the saturation parameter of *one* of the beams. As the laser intensity gets very weak ($s_0 \to 0$), we find the minimum temperature

$$T_{\min} \to \frac{\hbar}{k_B}\frac{\Gamma^2+4\delta^2}{8\delta} \; . \tag{32}$$

This result is plotted in Figure II.5a. We see that the ultimate temperature is achieved

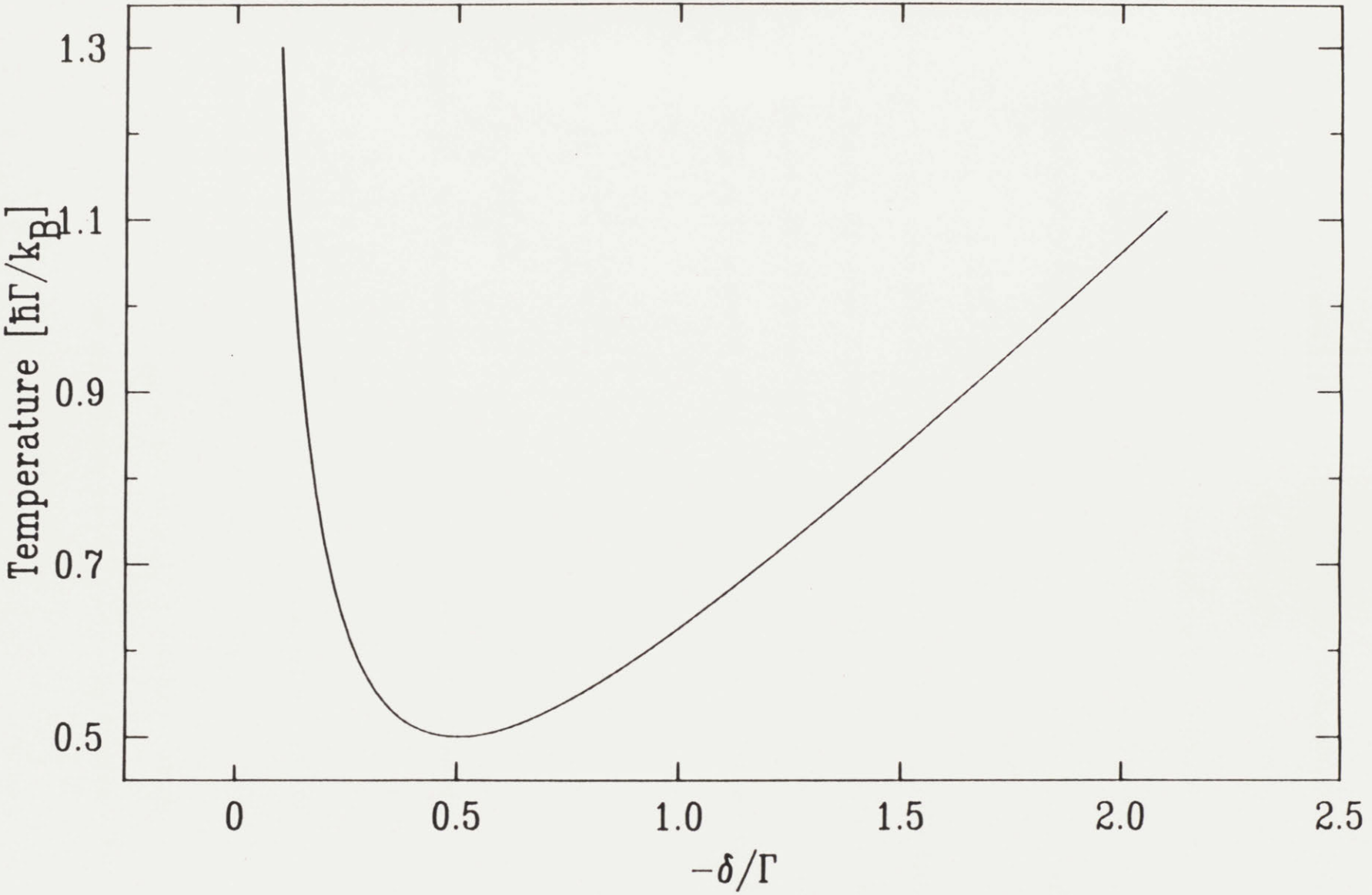

Figure II.5a: The minimum theoretical temperature attainable in a laser standing wave as $\Omega \to 0$. The laser must be tuned to the red to provide cooling. The ultimate temperature is $\hbar\Gamma/2k_B$ (~240μK for sodium), seen at $\delta = -\Gamma/2$.

at a detuning of $-\Gamma/2$, at which point $T_{\min} = \hbar\Gamma/2$. This configuration of lasers, therefore, can cool sodium to $240\,\mu K$; $T_{\min} = 140\mu K$ for lithium.

The second approach to finding the ultimate temperature is attributed to Cohen-Tannoudji, Cook, and others (COH86,COO80). We begin by writing the rate of change of kinetic energy along one axis as

$$\frac{dK_i}{dt} = F_i v_i + \frac{d}{dt}\frac{<(\Delta P - <\Delta P>)^2>}{2M} \quad . \tag{33}$$

The first term is the work done by the force directed along the i-axis, and the second term is the heating due to the random changes in momentum inherent to the cooling process. The force can be written as $F_i = -\alpha v_i$ when the velocity is small (usually compared to Γ); the latter term is often expressed in terms of the *diffusion coefficient* D, defined as

$$D \equiv \lim_{\Delta t \to 0} \frac{<(\Delta P - <\Delta P>)^2>}{2\Delta t} \tag{34}$$

$$= \lim_{\Delta t \to 0} \frac{<(\Delta P)^2>}{2\Delta t} \quad ,$$

since $<\Delta P> = 0$. We can then express Eq. (33) in terms of these definitions:

$$\frac{dK_i}{dt} = -\alpha v_i^2 + \frac{D}{M} \quad . \tag{35}$$

If $\alpha>0$ (i.e. F_i is a damping force), then given D and α, we can set (35) to 0 and solve for the ultimate temperature: $T_{\min} = D/k_B\,\alpha$.

We shall first solve for $T_{\min}$ at low intensity to compare with the result of Wineland and Itano. To find the diffusion coefficient, we may separate it into two

terms: $D = D_{dip} + D_{em}$, i.e. the diffusion caused by the dipole fluctuations plus that due to by spontaneous emission. At low intensities, D_{dip} can be viewed as the uncertainty in the absorption of photons (GOA80). The derivation of D_{dip} even at low intensities is beyond the scope of this work, so we will merely quote the result (COH86):

$$D_{dip} = \frac{\hbar^2 k^2 \Gamma}{4} \frac{s}{(s+1)} (1+Q) , \tag{36}$$

where

$$Q = \frac{8\Omega^2 (\delta^2 - 3\Gamma^2/4)}{[4\delta^2 + 2\Omega^2 + \Gamma^2]^2}$$

is the correction to the Poisson statistics of absorption due to photon anti-bunching. Under conditions of low intensity (or large detuning),

Q is much less than one and $\frac{s}{s+1} \rightarrow 2s_0$, implying that

$$D_{dip} \rightarrow \frac{\Gamma}{2} s_0 (\hbar k)^2 . \tag{37}$$

The contribution to diffusion from spontaneous emission D_{em} is readily calculated by noting that every spontaneously emitted photon gives the atom a momentum kick of $\hbar k$. Since this happens at the rate given in Eq. (16), we find (COH86)

$$D_{em} = \frac{\Gamma}{4} \frac{s}{s+1} (\hbar k)^2 ; \tag{38a}$$

note that we again use the full recoil momentum $\hbar k$ per event to treat the three-dimensional problem. At low intensities, Eq. (38a) becomes

$$D_{em} \rightarrow \frac{\Gamma}{2} s_0 (\hbar k)^2 , \tag{38b}$$

which equals D_{dip}. We thus obtain

$$D = \frac{(\hbar k)^2 \Gamma}{2} \frac{s}{s+1} \tag{39}$$

$$\approx (\hbar k)^2 \Gamma s_0 , \qquad (low\ intensity)$$

in agreement with the result of Gordon and Ashkin (GOA80).

To find the damping coefficient, we take the low intensity limit of Eq. (21) and obtain

$$\alpha \rightarrow -\frac{8\hbar k^2 \delta s_0}{\Gamma^2 + 4\delta^2} .$$

The ultimate temperature is therefore

$$T_{\min} = \frac{D}{k_B \alpha} \rightarrow \frac{\hbar}{k_B} \frac{\Gamma^2 + 4\delta^2}{8\delta} . \tag{40}$$

This is equal to the result calculated using the first approach (Eq. (32)).

Wineland and Itano cannot extend their formalism beyond this point, however, since their approach can account for neither the uncertainty in the dipole moment at high field intensities nor the effects of stimulated cooling. The advantage of the formalism using the diffusion coefficient is that it is more general; it can include the effects which Wineland and Itano must neglect, and thus obtain the correct result at any intensity.

When the intensity in the standing wave is high ($\Omega \gg \Gamma$), D_{dip} does not saturate,

even though absorption does; one can longer associate D_{dip} with fluctuations in *either* absorption *or* the dipole force, but must speak only in terms of the *total* induced diffusion. The contribution of dipole fluctuations to the total diffusion coefficient valid for all intensities can be found by solving the Fokker-Planck equation for the total phase-space distribution function of the atom (CHA43). The solution is analytic but complicated (COO80,GOA80); we shall only examine its limits. At *high intensities*, we find

$$D_{dip} = \frac{\hbar^2}{2\Gamma}\left[\left(\frac{\partial\Omega}{\partial z}\right)^2 + \Omega^2\left(\frac{\partial\theta}{\partial z}\right)^2\right]. \tag{41}$$

In a standing wave, $\partial\theta/\partial z = 0$, and with $\Omega(z) = 2\Omega_0\cos(kz)$, we may average the first term over a wavelength to get $\langle(\partial\Omega/\partial z)^2\rangle = 2\Omega_0^2k^2$. We thus obtain

$$D_{dip} = \frac{(\hbar k)^2\Omega_0^2}{\Gamma} \qquad (high\ intensity) \tag{42}$$

independent of the detuning. The total diffusion coefficient in strong fields is of course given by the sum of Eq. (42) with D_{em} (Eq. (38b)), though the effect of the recoil is completely negligible at even moderate intensities (Ω = several $\times\ \Gamma$).

The atomic motion will be damped in strong fields when the laser is tuned to the blue of resonance (cf. II.1.4), with the damping coefficient given by (21). In Figure II.5b we plot $T_{\min} = D/k_B\alpha$ for several laser tunings at high intensities. The lowest temperature is achieved when $\delta = 1.5\Gamma$, though it is still 50 times higher than the ultimate temperature at low intensities.

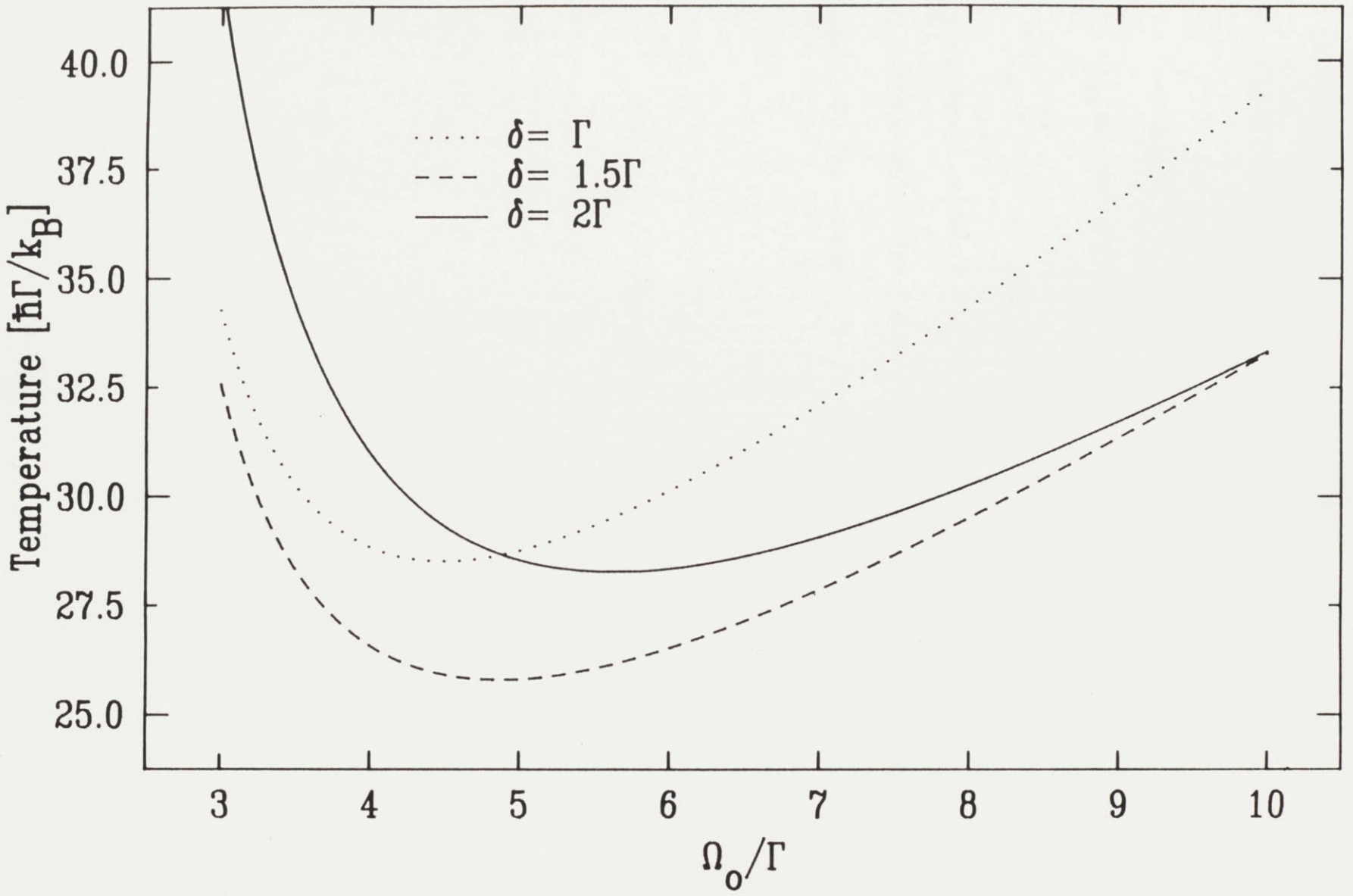

Figure II.5b: The minimum theoretical temperature attainable in a laser standing wave of *high* intensity. The laser must be tuned to the blue to provide cooling. The ultimate temperature is ~25$\hbar\Gamma/k_B$, seen at $\Omega = 5\Gamma$ and $\delta = 1.5\Gamma$.

As a check for consistency, we shall also take the low intensity limit of the Fokker-Planck result. In this limit, we find (COO80)

$$D_{dip} = \frac{\hbar^2\Gamma}{2[4(\delta - k\,\mathrm{v})^2 + \Gamma^2]} \left[\left[\frac{\partial\Omega}{\partial z} \right]^2 + \Omega^2 \left[\frac{\partial\theta}{\partial z} \right]^2 \right]. \tag{43}$$

Since $k\,\mathrm{v}_{\min} \ll \Gamma$, this reduces to

$$D_{dip} \approx \frac{\hbar^2\Gamma}{2(4\delta^2 + \Gamma^2)} (2\Omega_0^2 k^2) = \frac{\Gamma}{2} s_0 (\hbar k)^2 \tag{44}$$

at the optimum detuning $\delta = -\Gamma/2$. Comparing this with Eq. (37), we see that this indeed corresponds to the diffusion caused by the uncertainty in the absorption of photons in the low intensity limit.

II.2 Trapping Atoms Using the Spontaneous Force

II.2.1 Introduction

Obtaining a large number of cold atoms for experimental study has become almost a routine exercise. The basic method involves hitting a thermal atomic beam head on with a resonant laser beam; the atoms absorb the counter-propagating photons then radiate them nearly isotropically, resulting in a net loss of atomic momentum. (There is also a net loss of entropy in the atomic beam from this cooling process, the entropy being transferred to the newly accessible modes of the radiation field (CAB86)). The trick of all slowing methods involves keeping the laser resonant with the desired velocity group of atoms, since the Doppler effect will cause the absorption frequency to decrease as the atoms slow. One trick is to quickly increase ("chirp") the laser frequency as the atoms decelerate (EBH85); another is to use a solenoid magnet with a varying field to tune the atoms' internal resonance frequency using the Zeeman effect (PHM82,PPM82,BLM87). The latter method can slow as many as 10^{12} atoms/sec in a continuous fashion (cf. IV.6.3).

When a thermal distribution of atoms is slowed using these techniques, not only is the mean velocity $\overline{v}$ of the distribution decreased, but so is the *spread* in velocity. Since the squared deviation of the velocity from $\overline{v}$ is proportional to the temperature, we say that these atoms have been *cooled*. Effective temperatures of less than one kelvin have been attained using these processes. Devices such as the tapered solenoid

are therefore a rich source of cold atoms, and are a necessary tool in the investigation of atom traps.

A trap for atoms can be formed when lasers are configured such that the resulting force on the atoms satisfies two conditions: 1) it is restoring to some point in space, and 2) it damps the velocity. In the previous section we derived expressions, valid at low velocity, for the dynamics of an atom illuminated by a either a traveling or standing wave laser beam. Aside from the spontaneous and dipole forces which act on a stationary atom, we showed that these forces also had a velocity dependent term which under certain conditions opposes the atomic motion. Given the motivation for forming traps for cold atoms outlined in Chapter I, it was natural to try to envision ways to construct traps out of laser beams. Our treatment will continue to focus on the regime where $v \ll \Gamma/k$ ($T << 0.1$ K).

II.2.2 Dipole versus Spontaneous Force Traps

The general expression (II.3.15) for the total radiative force on an atom is usually separated into its two terms, spontaneous and dipole, when discussing schemes for radiatively trapping atoms. The reason is that each term performs in a qualitatively different fashion. A successful trapping scheme will typically operate in a regime where one term is much greater than the other. This simplifies the theoretical treatment of the trap and allows one to optimize the trap's performance in the regime of interest. Though hybrids do exist, both in theory (STW84) and experiment

(GOU87), most neutral atom traps are *either* "dipole traps" or "spontaneous force traps." It is therefore instructive to compare the assets and liabilities of these two types of forces in a number of applications pertaining to cooling and trapping:

1) Maximum restoring force: As shown in the previous section, dipole traps hold the clear edge in this category. The spontaneous force saturates at $\hbar k\Gamma/2$, which for the sodium corresponds to an acceleration of about 10^6 m/s. The dipole force, on the other hand does not saturate; as we showed in II.1.3, the maximum acceleration could be 10^3 times *greater* than the spontaneous force acceleration using readily attainable intensities (100mW focused to a 3μm waist). This has implications for slowing as well as for trapping neutral atoms.

2) Size: Dipole traps, their force being proportional to the gradient of the field intensity, generally require focused laser beams for best performance. (Very cold atoms may be "channeled" in the nodes or anti-nodes of a standing wave field (SDA87)). This limits the order of their size to that of a typical confocal waist: $V \leq$ several μm^3. A standard dye laser, on the other hand (or diode laser, for atoms such as cesium and rubidium), will saturate the spontaneous transition at very modest intensities — ~10 mW/cm^2 for the Na D2 line, for example. The beam can therefore be spread out over a relatively large volume, typically several cm^3.

3) Cooling ability: Dipole traps, since they generally require high laser intensities, have a relatively high ultimate temperature (cf. II.1.5). All practical traps

based on the dipole force must therefore alternate trapping with radiative cooling (typically "red molasses") (CBA86,GOU87). A trap which uses radiation pressure for both confining and cooling the atom's can approach the ultimate temperature for Doppler cooling ($T_{\min} \approx \hbar\Gamma/2k_B$) without using additional beams.

4) Depth: We shall define the depth of a trap as the maximum kinetic energy of a particle at the center of the trap that is still contained by the trap. (This is usually more energy than is required to extract the atom slowly, due to the velocity dependence of the damping forces). If we neglect damping, a radiation pressure trap could typically have 10^3 times less force but be 10^4 times bigger than a dipole trap, and thus $\int F \cdot dx$ is 10 times greater. The damping, however, is typically provided by the same red molasses in both types of traps. Radiation pressure traps, since they are bigger, will therefore be able to capture atoms having much greater initial velocity, and consequently are several orders of magnitude deeper (1K versus 1mK) than dipole traps.

We see, then, that spontaneous force traps hold several advantages over dipole force traps: they are several cm^3 in volume, can simultaneously provide cooling and restoring forces, and are potentially very deep. Dipole traps, on the other hand, are μm^3 sized, require additional red-tuned lasers to cool the trapped atoms, and are relatively shallow.

II.2.3 The "Optical Earnshaw Theorem"

As far back as 1962, laser beams were proposed as a means of trapping (or compressing) atoms using either the dipole (ASK62,DRC83,ASH78,YSH86,e.g.) or the spontaneous (MIN80,LMP76,LMP78,MIJ82,e.g) force. Dipole force traps were demonstrated first by Ashkin, when in 1970 he trapped micron-sized particles in the waist of a cw laser beam (ASH70). Proposals for spontaneous force traps continued to proliferate, however, because of their practical advantages over dipole traps as described above.

The spontaneous force trappers were led to reconsider some of their ideas when in 1983 Ashkin and Gordon published an "optical Earnshaw theorem," hereafter OET (ASG83). They proved that a "small dielectric particle could not be trapped using only the scattering force of radiation pressure." Gordon elaborated in a 1984 paper, stating that "in the case of a real atom such as sodium, a successful trap must involve at least three levels and three radiation fields of different frequencies." Their reason, in analogy to Earnshaw's theorem of electrostatics, was as follows: the scattering force, which is the first term in Eq. (II.1.15), points in the direction of propagation of the field, which in general is in the direction of the Poynting vector $\vec{S} = \frac{c}{4\pi}\vec{E}\times\vec{B}$. In order to satisfy the first condition for trapping, namely that the force be everywhere restoring to some point, the Poynting vector must have an inward component everywhere on some closed surface about that point. In the absence of current

sources, though, $\nabla \cdot \vec{S} = \partial U / \partial t$, implying that if such a field *could* be arranged, it would result in a net continuous flow of energy into the trap. Since this is clearly impossible, a necessary condition for trapping can never be satisfied.

The publication of this theorem naturally encouraged researchers to find a way around it. Ashkin himself had already proposed a method which alternated the trapping beams on and off to produce a net trapping force (ASH84). The principle was similar to RF Paul traps for ions (WSL59), or the strong focusing effect of a series of lenses or dipole magnets.

Recently, D.E. Pritchard and the author realized that the internal structure of an atom can be utilized to create a spatial dependence of the atom-laser interaction. By making the atom interact more strongly with a laser when it enters the trapping region than when it leaves, one can circumvent the O.E.T. Together with V. Bagnato, C. Wieman, and R. Watts, we published a paper (cf. Appendix A) which pointed out this fact and gave three examples of possible spontaneous force traps.

The general arrangement for a spontaneous force trap consists of two counter-propagating laser beams placed along the z-axis and focused just beyond the trap center, as shown in Figure II.6a. The radial restoring force for the trap is provided by the inward component of the beams for any ρ in the shaded area. To form a stable trap, we must make an atom at $z>0$ scatter more photons from the beam propagating toward $z<0$ ("laser L") even though it is less intense, and *vice versa* for a $z<0$ atom.

One way to accomplish this is to apply an external field to shift the resonant frequency of the atom, and tune the two lasers to different frequencies. Imagine, for example, that laser R is red-tuned and laser L is blue-tuned, and that we apply a positive magnetic field which increases with z. As the atom moves to the left, say, its resonant frequency decreases, bringing it closer to resonance with laser R. If B changes quickly enough, it will more than compensate for the intensity imbalance, and the atom will experience a restoring force to the origin. Similarly, it is clear that for z>0, the atom will absorb more from laser L than R, and again feel a restoring force. The trap is therefore stable in three dimensions, utilizing the scattering force in apparent violation of the O.E.T.

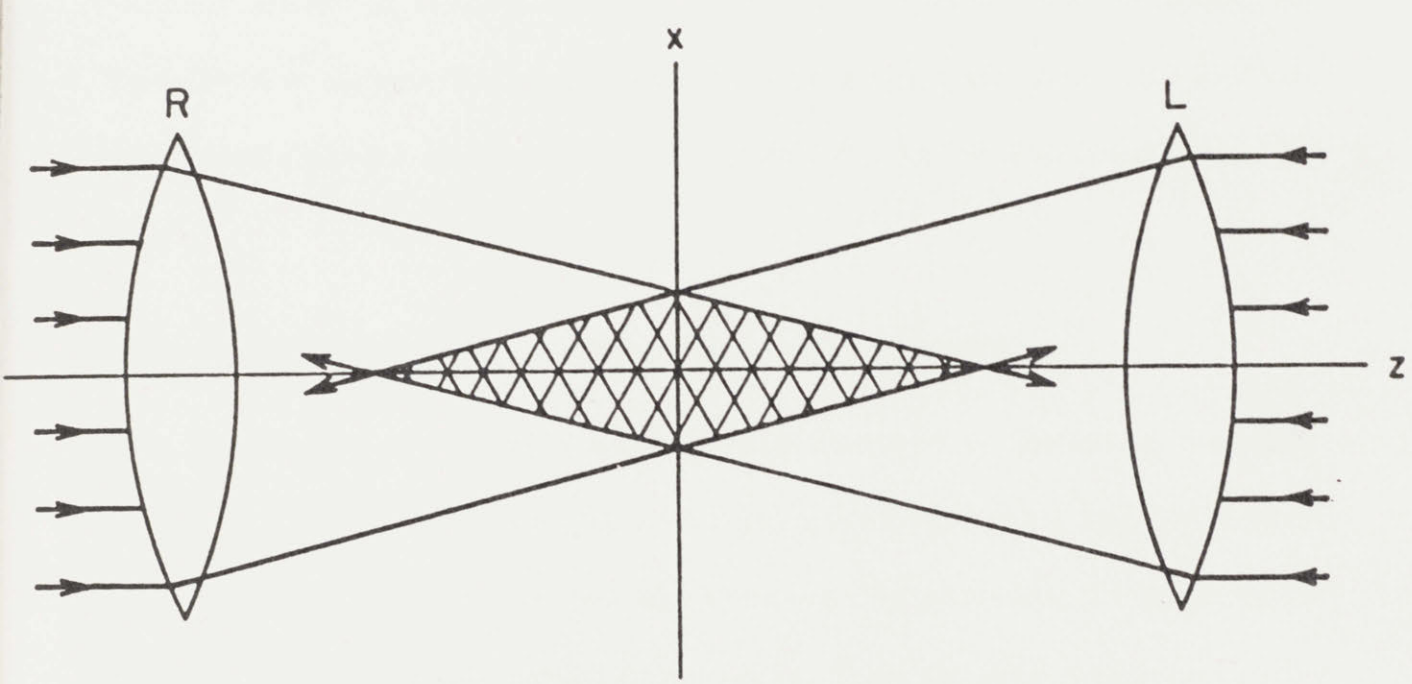

Figure II.6a: Basic configuration for two-laser spontaneous force trap. *f*/2 optics are shown.

Another possibility mentioned in the paper is to use the fact that transition rates depend upon the relative orientations of the atomic quantization axis with the electric field polarization vector. If we apply a field which has a constant magnitude but points in a different direction on the +z side of the origin as on the -z side, we can polarize the lasers differently in a manner which produces a stable trap. Yet a third possibility utilizes the different oscillator strengths between Zeeman sub-levels to optically pump certain atoms such as cesium to states where they will scatter more light from a weaker beam than a stronger one. Specific realizations of these ideas are given in the Appendix.

All these schemes were mentioned in talks given by Pritchard and Wieman in a "summer school" at Helsinki in July, 1986. After Pritchard's talk, he invited the participants to suggest other possibilities for spontaneous force traps. Jean Dalibard approached Pritchard afterward with the seminal idea for the trap described in this thesis.

II.2.4 The Dalibard Scheme for Trapping with Radiation Pressure

The essence of Dalibard's scheme can be illustrated by considering the z-axis motion of a hypothetical atom with a spin S=0 ground state and a spin S=1 excited state. Illuminate this atom with two counter-propagating monochromatic plane waves of equal intensity traveling parallel to the z-axis. Since the plane waves are equally intense, an atom will scatter equally from both of them and will not experience a net

spontaneous force.

To create a restoring force when the atom is displaced from the origin, apply a weak magnetic field gradient of the form $B_z(z) = bz$, and give the two traveling waves the opposite circular polarization (Figure II.6b). The left propagating beam (beam L) is polarized σ−, while the right propagating beam (beam R) is polarized σ+. As the atom moves toward z>0, e.g., the S=0 to -1 transition energy is decreased due to the Zeeman effect, while the S=0 to +1 transition energy is increased. If we tune both lasers slightly to the red of the zero field transition frequency, then laser L, which is σ− polarized and therefore excites only $\Delta S = -1$ transitions (SOB63), will be closer to the resonance frequency of its transition than the σ+ polarized laser R, causing the

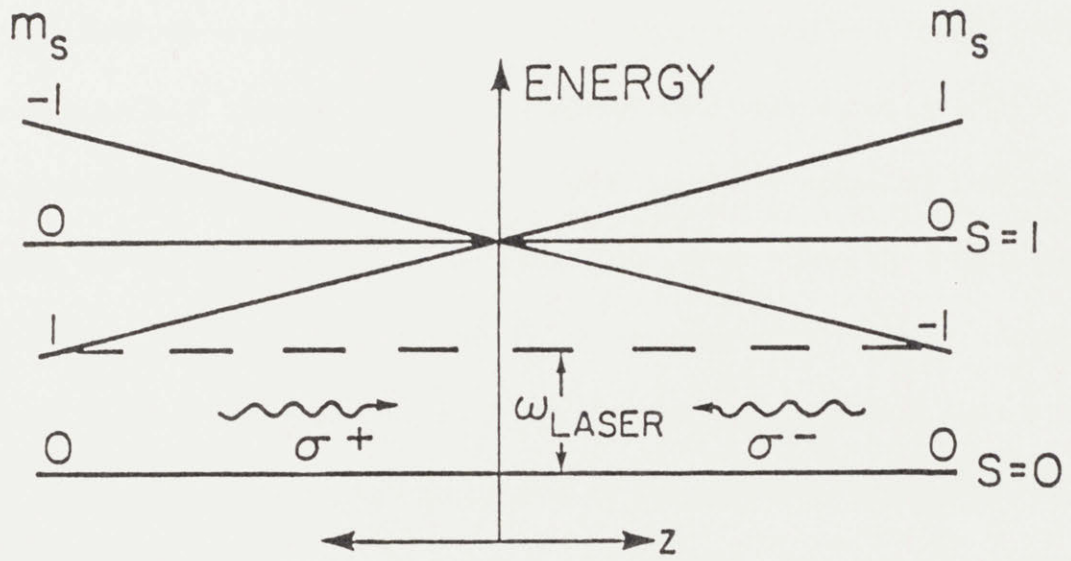

Figure II.6b: Energy level diagram of hypothetical atom having spin S=0 ground state and spin S=1 excited state, immersed in a magnetic field $B_z(z)=bz$. The frequency and polarization of the counter-propagating laser are chosen to produce damping and restoring forces for the atom's z-axis motion.

atom to scatter more photons from laser L than laser R. The atom therefore experiences a net force back to the origin. Similarly, when the atom ventures toward $z<0$, it will scatter preferentially from beam R, and again be restored.

Since the light frequency is tuned slightly to the red of the atomic transition, and the intensities are low (i.e. $\Omega \leq \Gamma$), the motion of the atom will be damped, since the beam opposing the atom's motion will be Doppler shifted closer to resonance than the co-propagating beam as described in II.1.4. This scheme therefore satisfies both the damping and restoring requirements for a stable trap.

II.2.5 Extending the Dalibard Trap to Three Dimensions

Generalizing this trapping scheme to three dimensions is straightforward. Orient three retro-reflected lasers along three mutually orthogonal axes, which will define a Cartesian coordinate system. Generate a magnetic field with a pair of coils having opposed current spaced about a radius apart, with the axis of symmetry along one of the lasers, say the z-axis beam (Figure II.6c). Close to the origin, the field along the z-axis will be $\vec{B}(\rho=0,z) = bz\hat{z}$ as required for one-dimensional trapping. Since the field must satisfy $\nabla\cdot\vec{B} = \nabla\times\vec{B} = 0$, it is easy to show that the field in the x-y plane will lie in this plane and have half the gradient of the z-axis field: $\vec{B}(\rho,z=0) = -\frac{1}{2} b\rho$. If we reverse the helicity of the $\sigma+$ and $\sigma-$ beams traveling along x and y with respect to the z beam, the conditions for one-dimensional trapping will be satisfied independently along each of the three Cartesian axes.

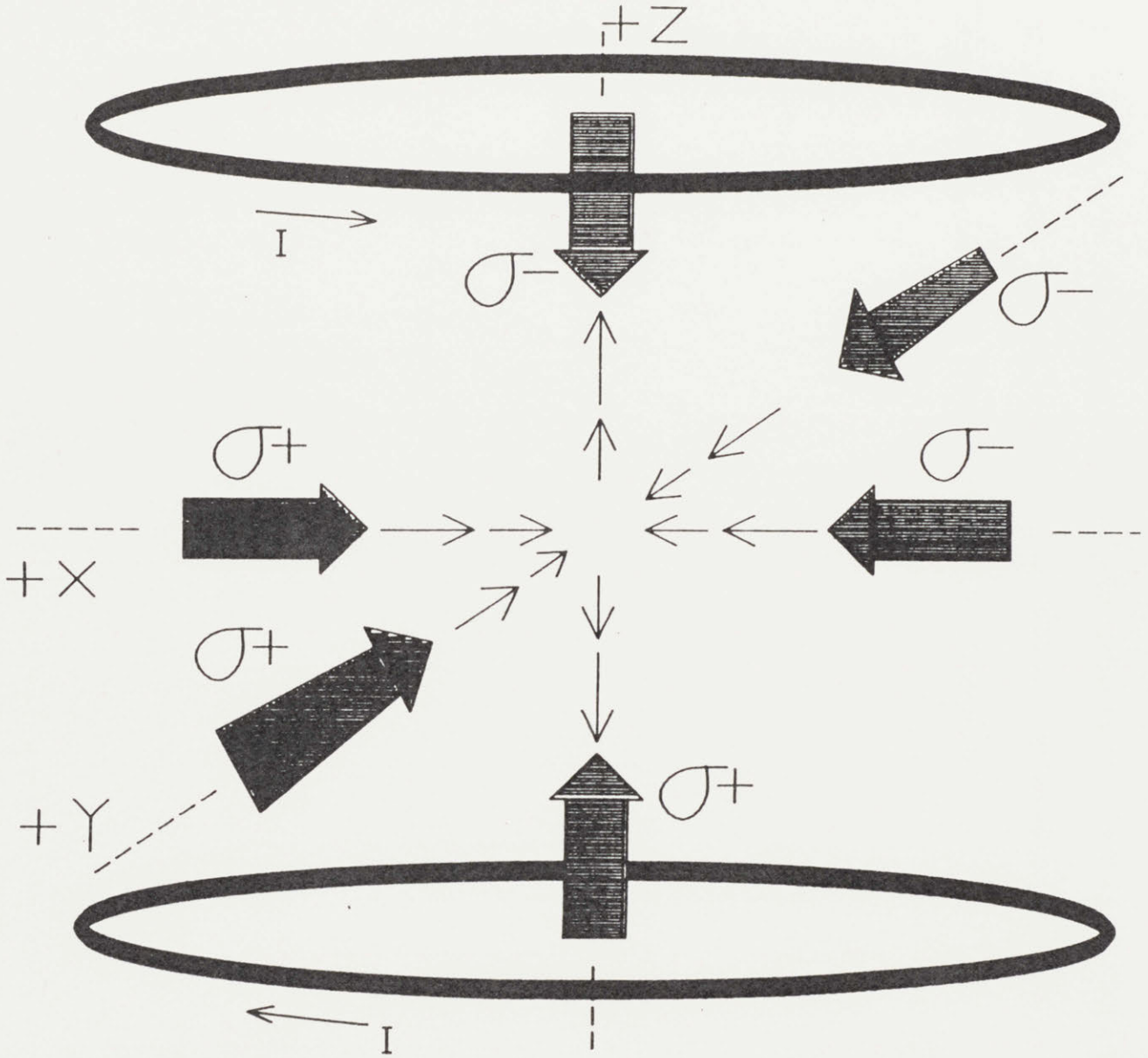

Figure II.6c: Trapping scheme in three dimensions. The "spherical quadrupole" field is generated by two coils of opposing current placed along the z-axis approximately as shown. The field along the axes, indicated by the light arrows,is parallel to its respective axis. Laser light, indicated by the heavy arrows, counter-propagates along x,y, and z and is polarized as shown with respect to the axis of propagation.

Although the atom is restored if it is displaced along x, y, or z, it is not evident that the trap will work under other conditions. When the atom ventures off-axis, complications arise because the magnetic field, and hence the atom's axis of quantization, forms oblique angles with the polarization vectors of the light. This can cause a $\sigma+$ beam, for example, to excite $\Delta M = 0 \text{ and } -1$ transitions. The effects of these complications will be dealt with in the following section.

II.3 Application: A Sodium Atom in the Spontaneous Force Trap

II.3.1 Introduction

In the previous section we showed qualitatively how a judicious arrangement of laser beams and magnetic fields can trap a hypothetical atom via the spontaneous force. The situation for a real atom, of course, is much more complicated. A real atom may have several levels in the ground and excited states which are close enough to be excited by a single laser. Each of these levels will in general have a different magnetic field dependence and different matrix elements which couple it to the various other levels. One is not able to simplify matters by cycling the atom between "stretched states," where the nuclear and electronic angular momentum vectors are aligned, since the trap relies on both $\Delta m = +1$ and -1 transitions to restore the atom to the origin. It is therefore difficult, if not impossible, to describe the trap dynamics for any atom possessing both nuclear and electronic spin without resorting to numerical methods.

In this section we will analyze the dynamics of the Dalibard trap for sodium, taking into account three dimensions as well as all the hyperfine structure. We will begin with a review of some atomic physics to describe some of the properties of sodium such as its energy levels, Zeeman splittings, and transition strengths. Our ultimate goal will be to find the forces on the sodium atom for various parameters which are likely to be tried in experiment. We will restrict our discussion to the

regimes which are likely to be of practical interest, namely weak magnetic fields and low optical intensities.

II.3.2 The Level Structure of Sodium — Fine and Hyperfine Structure

Neutral sodium is the third atom in the alkali series, with Z=11 and A=23. Since it has one valence electron, its spectrum resembles that of atomic hydrogen in some respects: its terms are all doublets, and its spectroscopic terms for n≥3 are the same. Differences arise from the shielding effects of the core electrons in sodium and the different nuclear spins, 3/2 in sodium versus 1/2 in hydrogen.

The hamiltonian for the sodium atom can be written

$$H = H_0 + H_{fs} + H_{hfs} + H_{ext} \tag{1}$$

where H_0 represents the unperturbed atom, H_{fs} is the fine structure caused by L-S coupling, H_{hfs} is the hyperfine structure due to I-J coupling (and small contributions from the nuclear electric quadrupole moment and other perturbations), and H_{ext} represents all externally applied perturbations such as electric or magnetic fields.

The unperturbed atom can be described by the quantum numbers n, L, m_L, S, m_S, I, and m_I, where n is the principle quantum number, L, S, I are the electron orbital, electron spin, and nuclear spin angular momenta, respectively, and m_Λ is the z-component of the angular momentum Λ. H_0 is diagonal in the basis $|n\ L\ S\ I\ F\ m_F\rangle$, where $F \equiv I + J \equiv I + L + S$ is the total angular momentum.

The principle optical transitions in sodium, the D1 and D2 lines, are between the $3\,^2S_{1/2}$ ground state and the two lowest-lying excited states which split by the fine structure, $3\,^2P_{1/2,3/2}$. The fine structure hamiltonian is given by $H_{fs} = \xi(r)\vec{L}\cdot\vec{S}$, where $\xi(r)$ is a function which depends only on the radial operator r. Since $\vec{J} = \vec{L}+\vec{S} \Rightarrow \vec{L}\cdot\vec{S} = (\vec{J}^2-\vec{L}^2-\vec{S}^2)/2$, we see that the fine structure splits terms with the same value for L and S but different J. The first excited states of sodium therefore consists of two terms, $3\,^2P_{1/2}$ and $3\,^2P_{3/2}$, as shown in Figure II.7. The magnitude of this splitting is ~17.19 cm^{-1}. In most applications of laser spectroscopy, this separation is large enough to allow one to ignore one of these levels while investigating the other. Hereafter we will deal exclusively with transitions between the $3\,^2S_{1/2}$ and the $3\,^2P_{3/2}$ levels, called the D2 line.

The ground and excited states of sodium are split to a smaller degree by interactions with the atomic nucleus, called the hyperfine structure. The hamiltonian for this interaction is (COR77)

$$H_{hfs} = A_J \vec{I}\cdot\vec{J} + \frac{B_J}{2I(2I-1)J(2J-1)}\left[3(\vec{I}\cdot\vec{J})^2 + \frac{3}{2}\vec{I}\cdot\vec{J} - \vec{I}^2\vec{J}^2\right] \qquad (2)$$

where A_J is the hyperfine constant and $B_J \equiv eQ\langle\partial^2 V/\partial z^2\rangle$ is the electric quadrupole interaction constant. The first term arises from the energy of the nuclear magnetic moment in the magnetic field of the orbiting (and spinning) valence electron, and the second term arises from the interaction of the electric field of the electron cloud with the electric quadrupole moment of the nucleus. Values for the constants A_J and B_J for

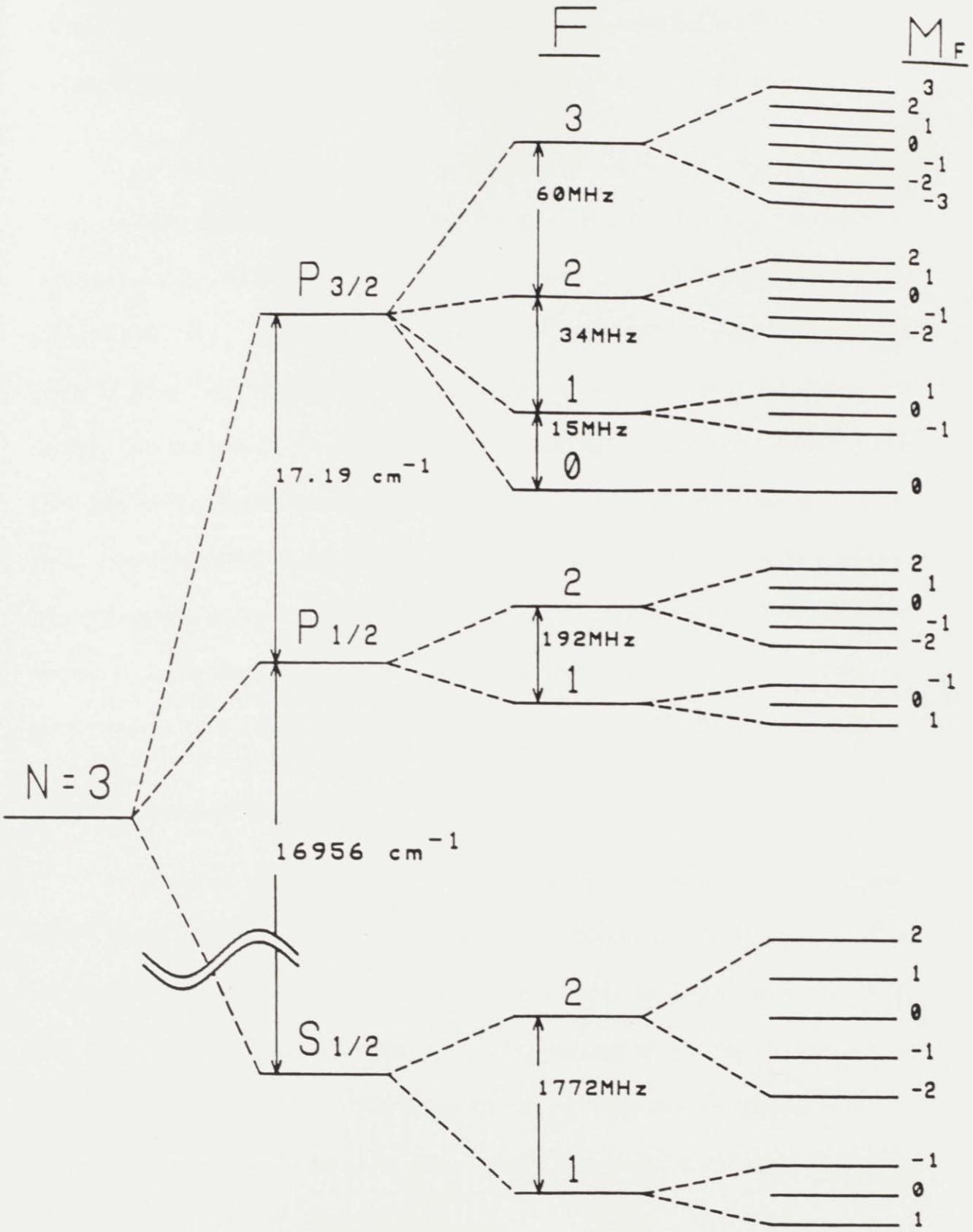

Figure II.7: Energy level structure of sodium. The ground state and first two excited states are shown. The Zeeman sub-levels, shown on the far right, are degenerate in zero magnetic field.

sodium can be found in COR77, p. 718. As above, we write $\vec{I}\cdot\vec{J} = (\vec{F}^2 - \vec{I}^2 - \vec{J}^2)/2$, and the hyperfine hamiltonian then becomes (COR77)

$$H_{hfs} = \frac{1}{2}A_J K + \frac{B_J}{8I(2I-1)J(2J-1)}[3K(K+1) - 4I(I+1)J(J+1)] \qquad (3)$$

where we have used the definition $K \equiv F(F+1) - I(I+1) - J(J+1)$. The splittings attributed to this interaction are shown in Figure II.7. Each hyperfine state is composed of $2F+1$ Zeeman sub-levels which are degenerate. If each of these sub-levels is given unit "weight," the "center-of-mass" of the levels is at the unperturbed energy. We see that in the excited state, the levels are spaced fairly close together compared to the natural linewidth of the transition (10 MHz). Also, an atom in the F=2,1, or 0 manifold of the excited state can decay to either of the ground state hyperfine levels; atoms excited by a single-frequency laser to one of these states will eventually accumulate in the non-resonant ground state hyperfine level. We therefore must consider *all* the hyperfine levels when dealing with the D2 transition.

II.3.3 The Zeeman Effect

We now shall examine the effect on the atom of an externally applied magnetic field. Recall that the trapping scheme requires applying a field strong enough to differentiate between the various Zeeman sublevels which are degenerate in zero field. The trap will work effectively when the splitting induced by the field is less than or equal to a linewidth; if the splitting is any greater, we must tune the trapping laser too far to the red to provide adequate damping near the center of the trap (cf. II.1.4).

Since the linewidth is less than or equal to the hyperfine separation in the states of interest, the applied magnetic field is considered "weak," in that it does not unduly perturb the atom.

The Zeeman hamiltonian is (COR77)

$$H_{ext} = g_J \mu_B \vec{B} \cdot \vec{J} - g_I \mu_N \vec{B} \cdot \vec{I} \tag{4}$$

where g_J, g_I are the electronic and nuclear g-factors, respectively, $\mu_B \equiv e\hbar/2m_e c$ is the Bohr magneton, and $\mu_I = \mu_B m_e/m_N$ is the nuclear magneton. By taking the electron spin moment to be exactly twice its orbital moment (valid to first order in α), we may write the electronic g-factor as

$$g_J \approx \frac{3J(J+1) + S(S+1) - L(L+1)}{2J(J+1)} . \tag{5}$$

The nuclear g-factor is determined by experiment to be 2.2176.

To determine the energy shift due to the magnetic field, we must diagonalize the total hamiltonian (1), including the perturbation H_{ext}. Since the magnetic field is weak, H will still be diagonal in the unperturbed basis of the total angular momentum $|F, m_F>$. Since the operators $\vec{J}$ and $\vec{I}$ which comprise H_{ext} are vector operators, by the Wigner-Eckhart theorem they must be proportional to $\vec{F}$ (CDL77, p. 1054). Specifically,

$$\vec{J} = \frac{<\vec{F} \cdot \vec{J}>}{F(F+1)} \vec{F} , \tag{6}$$

and

$$\vec{I} = \frac{\langle \vec{F} \cdot \vec{I} \rangle}{F(F+1)} \vec{F} ,$$

If the magnetic field direction defines the z-axis, the Zeeman splitting at low field may be written as

$$E_Z = g_F \mu_B B m_F \tag{7}$$

where the effective g-value is

$$g_F \equiv \left\{ \frac{3J(J+1) + S(S+1) - L(L+1)}{2J(J+1)} \right\} \left\{ \frac{F(F+1) + J(J+1) - I(I+1)}{2F(F+1)} \right\}$$
$$- 2.2176 \frac{m_e}{m_N} \left\{ \frac{F(F+1) + I(I+1) - J(J+1)}{2F(F+1)} \right\}.$$

The second term in the energy is smaller than the first by about the ratio $m_e/m_N \approx 1/1836$, and can usually be neglected. The Zeeman shift of the ground and excited states of the D2 line are shown in Figures II.8.

It is instructive to see whether or not our trapping scheme will work for an atom as complicated as sodium. The relative *transition frequencies* between Zeeman sub-levels in the two primary hyperfine manifolds in the D2 line are plotted in Figures II.9. We see that for the $F=2 \rightarrow F'=3$ transitions, all the $\Delta M_F = +1$ transition frequencies increase with increasing field, and the $\Delta M_F = -1$ frequencies decrease. For the $F=1 \rightarrow F'=2$ transitions, the transition frequency from a *given ground state* will again be shifted appropriately by the field. Though we cannot account for optical pumping effects at this point, we see why the scheme *might* work for a real sodium atom.

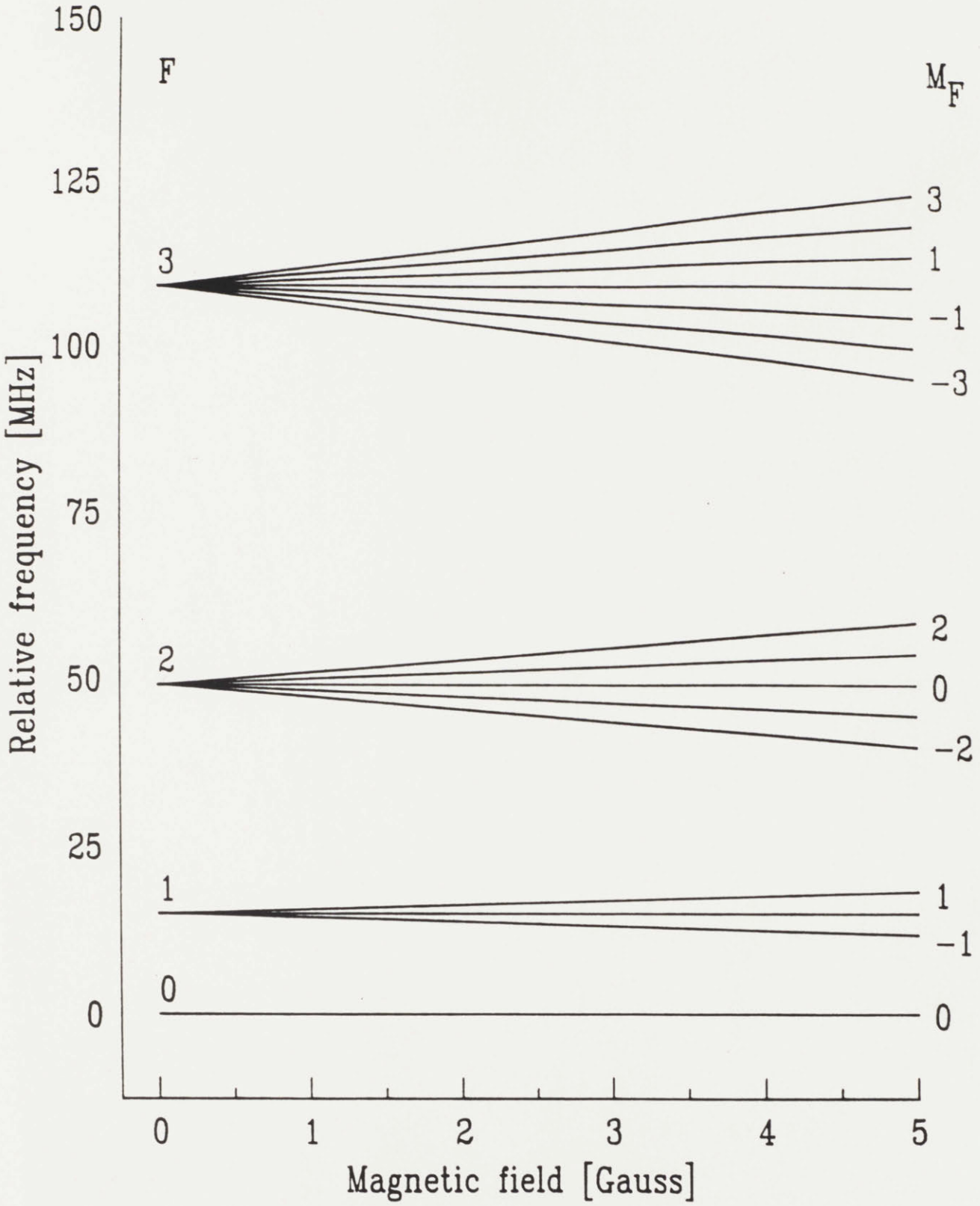

Figure II.8a: Energy shifts due to Zeeman effect in sodium $3P_{3/2}$ manifold. The M_F degeneracy is removed by the magnetic field.

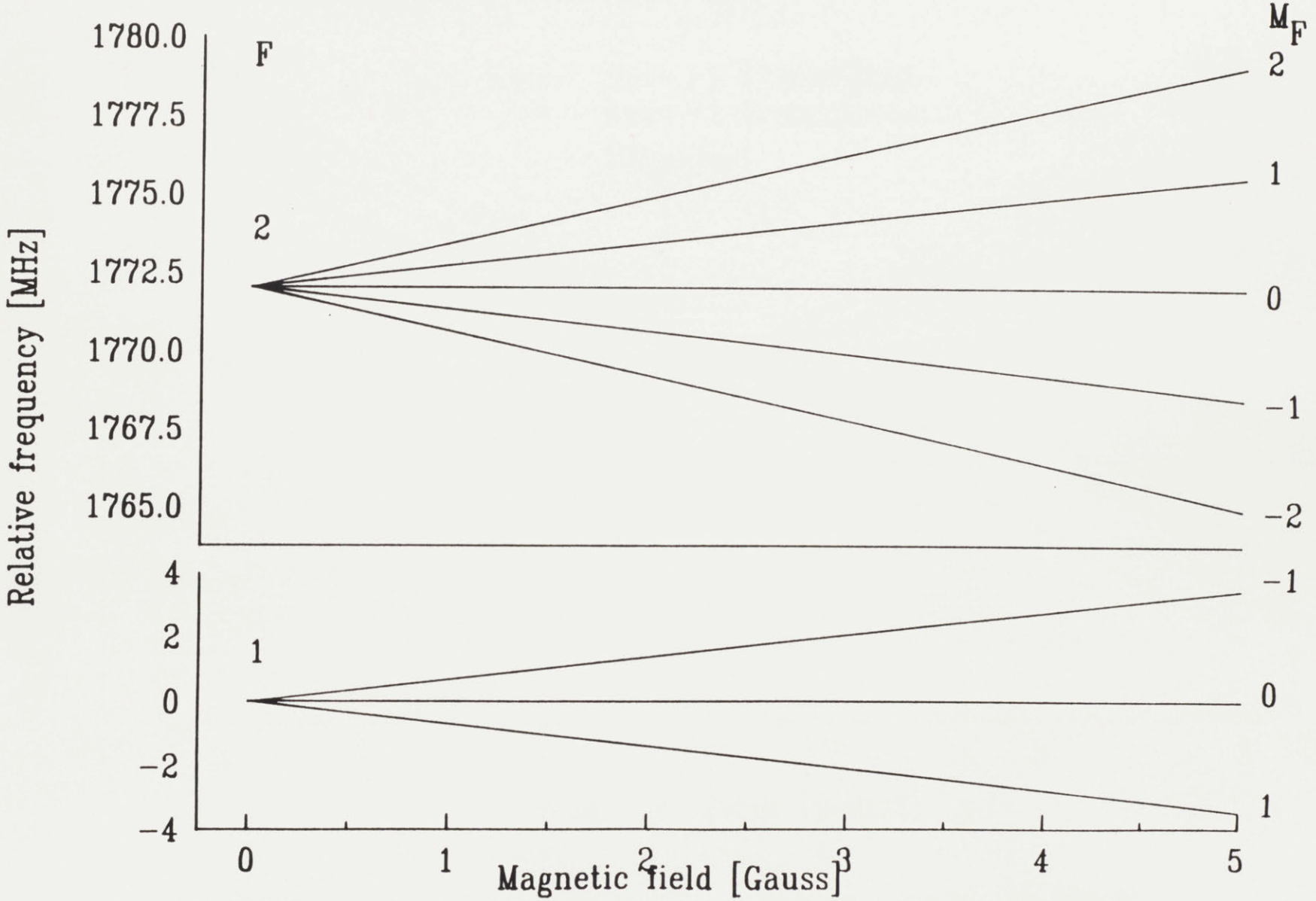

Figure II.8b: Energy shifts due to Zeeman effect in sodium ground state. Note the F=1 sub-levels shift with the sign opposite that of F=2.

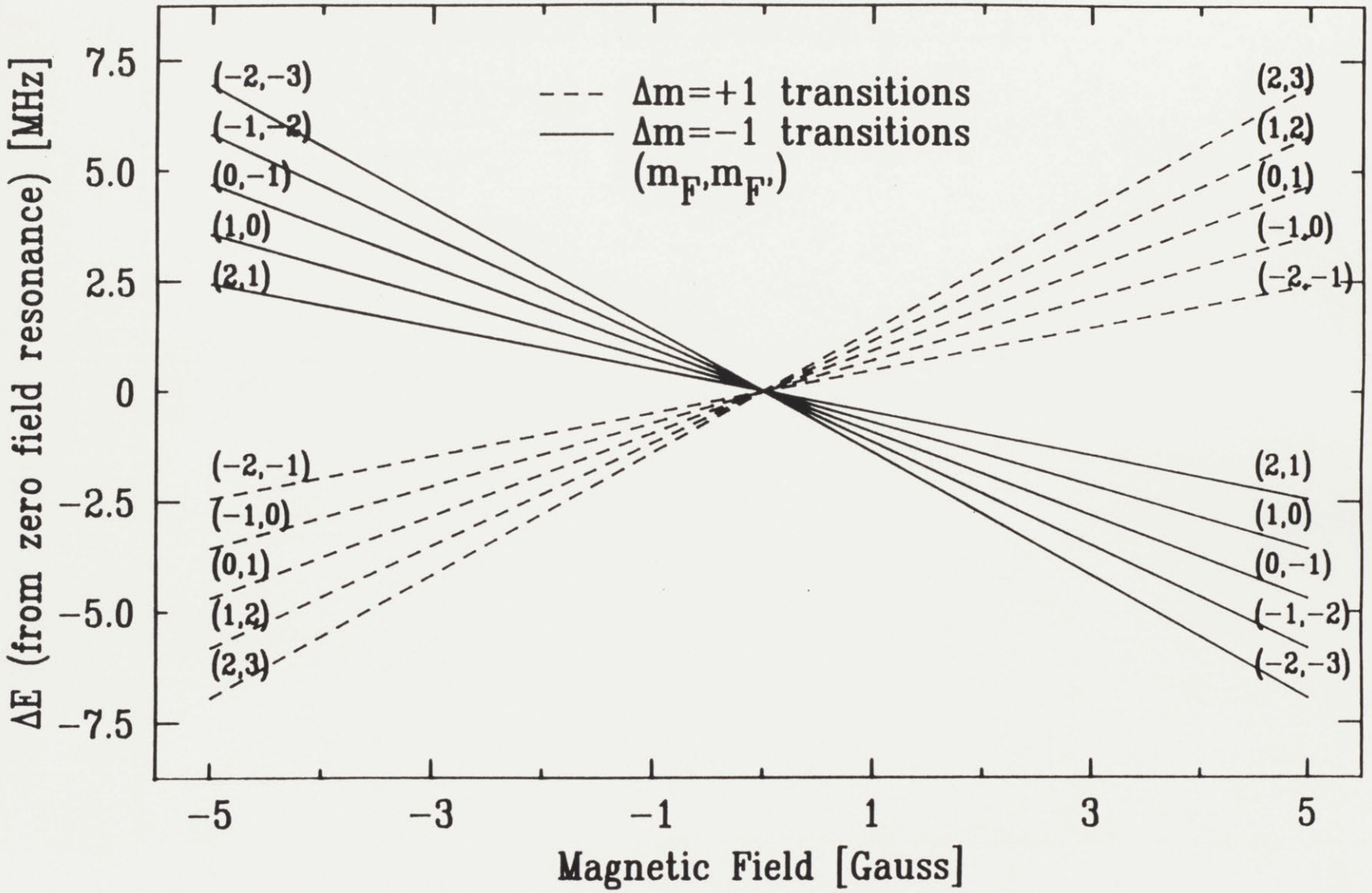

Figure II.9a: Field dependence of the $F=2 \rightarrow F'=3$ transition frequencies in the sodium D2 line. Note the all the $\Delta M=+1$ frequencies increase with field, while the $\Delta M=-1$ frequencies decrease with field. The M_F and $M_{F'}$ quantum numbers are indicated in parenthesis.

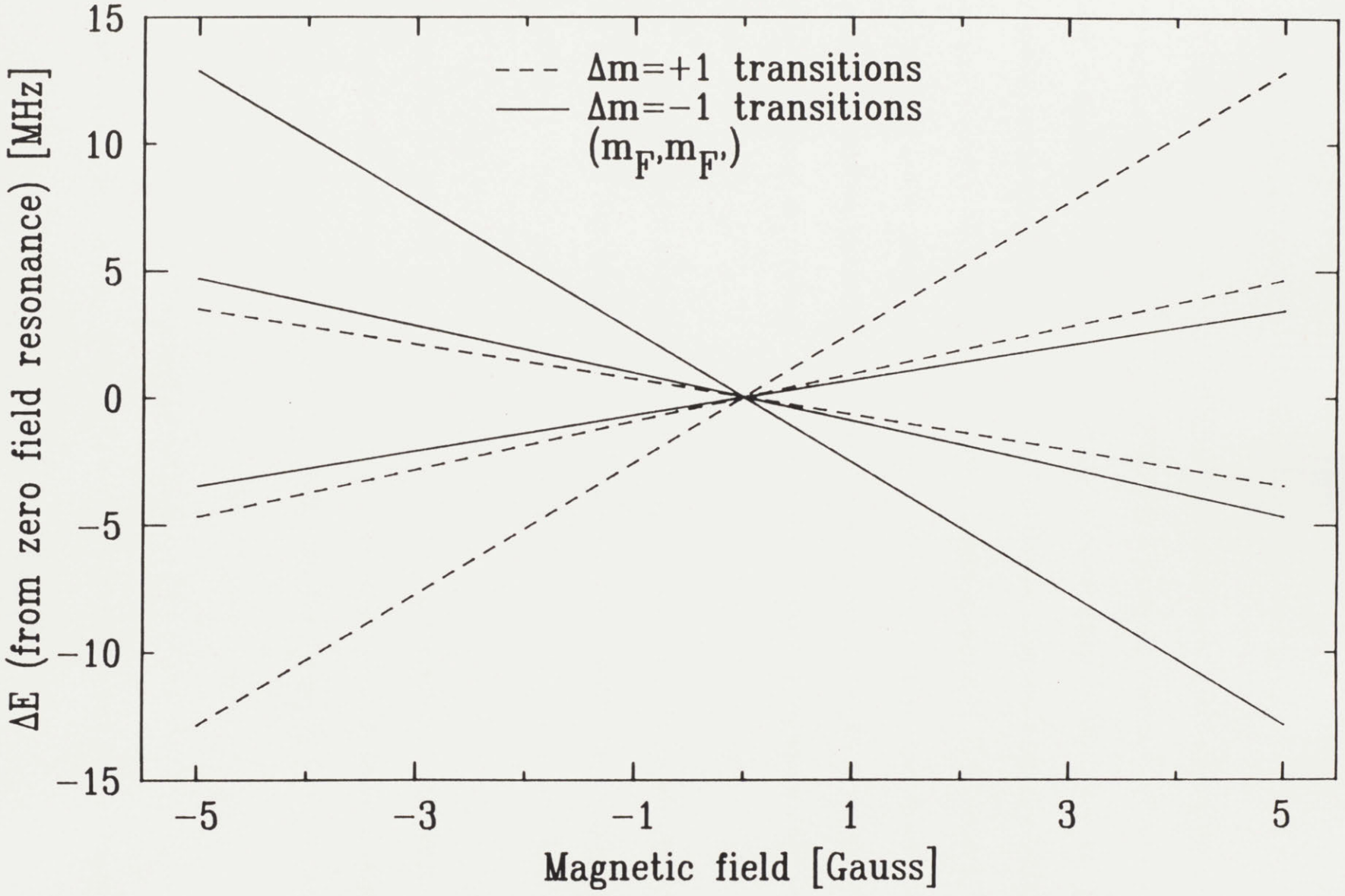

Figure II.9b: The $F=1 \rightarrow F'=2$ ($P_{3/2}$) field dependence. For a given initial M_F, the $\Delta M=+1$ transition frequency has a more positive shift than the $\Delta M=-1$ transition, even though they both have the same sign (e.g. $1 \rightarrow 2$ and $1 \rightarrow 0$).

II.3.4: Optical Transitions Between Zeeman Sub-levels

Now that we know the energy levels of the sodium atom at any point in the trap, we want to be able to calculate the transition rates between the various levels when the atom is immersed in laser light. In Section II.1.3 we found an expression for the transition rate at low intensity where we assumed that the atom was a simple two-level system. In reality, the atom has three coupled angular momenta $(\vec{S},\vec{L},\vec{I})$ which split our two-level system into the multi-level system discussed in the previous section. In order to connect the results of Section II.1.3 with the real sodium atom, we must be able to compare the transition rates between the all the field-dependent hyperfine levels.

The transition rate implicit in Eq. (II.1.16b) is related to a particular transition by the square of the Rabi frequency, $\Omega^2 \propto \mu_\varepsilon^2$. μ_ε is the dipole matrix element given by (SOB63)

$$\mu_\varepsilon = \hat{\varepsilon}\cdot\langle\gamma' J' I' F' M_{F'}|\vec{\mu}|\gamma J\, I\, F\, M_F\rangle \tag{8}$$

where $\hat{\varepsilon}$ is the polarization of the light, $\vec{\mu}\equiv e\vec{x}$ is the dipole operator, γ represents all other quantum numbers, and the primes denote the excited states. In order to utilize standard angular momentum algebra, we shall write the vectors in terms of their spherical components:

$$\mu_\varepsilon = \sum_{q=-1}^{1} e_q^*\langle\gamma' J' I' F' M_{F'}|\mu_q|\gamma J\, I\, F\, M_F\rangle \tag{9}$$

where $\mu_{\pm1} = \mu_x \pm \mu_y$, $\mu_0 = \mu_z$. Since μ_q is a tensor operator, we may use the Wigner-

Eckhart theorem to remove the M-dependence from the matrix element:

$$\begin{aligned}&\langle \gamma' J' I' F' M_{F'} | \mu_q | \gamma J\, I\, F\, M_F \rangle \\ &\quad = (-1)^{F'-M_{F'}} \langle \gamma' J' I' F' | | \mu_q | | \gamma J\, I\, F \rangle \begin{pmatrix} J' & 1 & J \\ -M_{F'} & q & M_F \end{pmatrix}. \end{aligned} \tag{10}$$

The double bars remind us that it is a reduced matrix element. The expression in parenthesis is a *3-j symbol;* it equals zero unless its elements fulfill certain conditions. This gives us *selection rules* for dipole transitions:

$$\Delta J \equiv J' - J = 0, \pm 1; \qquad J' + J \geq 1, \tag{11}$$

and

$$\Delta M_F \equiv M_{F'} - M_F = 0, \pm 1.$$

The selection rule for M_F depends on the value of q. $q = \pm 1$ corresponds to light with $\sigma\pm$ polarization, and consequently $\Delta M_F = \pm 1$; $q = 0$ corresponds to linearly polarized light, which yields the selection rule $\Delta M_F = 0$.

We can further reduce the matrix element in (9) by noting that $\vec{I}$ and $\vec{J}$ commute. This allows us to use the *6-j symbol* so that (9) becomes

$$\begin{aligned}&(-1)^{F'+F-M_F+I+J'+1} (\gamma' | | \mu_q | | \gamma) \\ &\qquad \times \sqrt{(2F+1)(2F'+1)} \begin{pmatrix} J' & 1 & J \\ -M_{F'} & q & M_F \end{pmatrix} \begin{Bmatrix} J' & F' & I \\ F & J & 1 \end{Bmatrix} \end{aligned} \tag{12}$$

where $(\gamma' | | \mu_q | | \gamma)$ is the *totally reduced* matrix element and is the same for all transitions in the D2 line. In fact, the method used here to factor out the angular momentum dependence is totally general, and can be used for any atom which can be described by a similar basis.

The relative strengths S of all the field-dependent hyperfine transitions within the D2 line can now be determined from the relation

$$S \propto | \sum_{q=-1}^{q=1} \varepsilon_q \langle \gamma J' I' F' M_{F'} | \mu_q | \gamma J I F M_F \rangle |^2 \qquad (13)$$

These relative strengths are tabulated in GOU86. It should be noted that the sum is taken *within* the absolute value sign, suggesting the possibility of interference terms (and quantum beats (LEV84)). These terms are not significant, however, because the light is circularly polarized (i.e. composed of only a single spherical component ε_q). Even when the quantization axis (determined by the direction of the magnetic field) is not orthogonal to the optical polarization vectors, each laser will still drive mostly one transition, and the cross terms between transitions will be negligible.

II.3.5 Calculating the Spontaneous Force for a Multi-Level Atom

We shall now calculate the average force on a sodium atom in the light trap described in Section II.2.4. We will assume that the light intensity is low enough to allow us to neglect dipole forces. In addition, we will neglect diffusion, because it does not contribute to the average force.

The experimental arrangement for our model is as follows: Retro-reflected, collimated laser beams of the correct polarization and equal intensity are situated along the x,y, and z axes (see II.2.4 and Figure II.6c). Each beam has two frequency components in order to drive the two ground state hyperfine levels. They are tuned slightly to the red of the $F=2 \rightarrow F'=3$ and $F=1 \rightarrow F'=2$ transitions. The necessary

magnetic field is assumed to be generated by two coils of opposed current placed about a radius apart.

We will first restrict our attention to the z-axis motion of an atom with velocity v_z, though we will account for the presence of all six beams. Consider a given laser beam incident on the atom, which is in a particular ground state F, m_F. At low intensities, this laser will excite the atom to an excited state $F', m_{F'}$ with a rate

$$R(F, m_F \rightarrow F', m_{F'}) = \frac{\Gamma \Omega^2}{\Gamma^2 + 2\Omega_T^2 + 4(\delta - \vec{k}\cdot\vec{v})^2} \tag{14}$$

where $\Omega_T = \sum_{all\ beams} <\gamma' F' M_{F'} | \mu | \gamma F M_F > E/\hbar$. Once in the excited state, the atom will decay to a particular ground state with a rate (SOB63)

$$R(F', m_{F'} \rightarrow F, m_F) = \frac{2\omega_0^3}{3\hbar c^3} | \sum_{all\ pol.} \hat{\varepsilon} \cdot <\gamma F\ M | \vec{\mu} | \gamma' F' M_{F'} > |^2 . \tag{15}$$

Define Π_{F, M_F} to be the population of the state (F, M_F) (the diagonal elements of the density matrix ρ). Since the total population must be constant, we have $\sum_{all\ states} \Pi_{F, M_F} = 1$. The rate of change of a given population is simply the rate in minus the rate out:

$$\dot{\Pi}_{F, M_F} = \sum_{F', M_{F'}} \left[R(F', M_{F'} \rightarrow F, M_F)\, \Pi_{F', M_{F'}} - R(F, M_F \rightarrow F', M_{F'}) \Pi_{F, M_F} \right]. \tag{16}$$

There is one such rate equation for each Zeeman sub-level in the system; for the sodium D2 line, there are 8 ground state sub-levels and 16 excited state sublevels. After a short time, the populations will assume steady state values Π^{st}. For a given set

of experimental parameters, we may solve for these values by setting the time derivative in (16) to zero and solving the resulting set of 24 coupled equations. This is done numerically by computer; it takes about 10 seconds to complete the process on an IBM AT with a 10 MHz math co-processor.

Once the steady state populations have been found, we can calculate the force in a straightforward manner. If the atom is constrained to move along the z-axis, the force will be the net result from the absorption of photons from the two z-axis beams beams, labeled R (+z) and L (-z):

$$F_z = \hbar k \sum_{F,M_F} \Pi_{F,M_F} \left[\sum_{F',M_{F'}} R^R(F,M_F \rightarrow F',M_{F'}) - R^L(F,M_F \rightarrow F',M_{F'}) \right] \qquad (17)$$

Since the decay from the excited to the ground states emits a photon in a random direction, it does not contribute to the net force.

Some results obtained using this method are plotted in Figures II.10. We note that both restoring and damping forces are present. The restoring and damping coefficients k and β defined by the relation $F = -kz - \beta v$ can be obtained in this fashion for a variety of experimental parameters. For a laser intensity of I=4 mW/cm^2 per beam, for example, we obtain $\kappa = 5.76\times10^{-17}$ dynes/Gauss, and $\beta = 1.29\times10^{-18}$ dynes/(cm/s). This will be compared with experiment in Chapter III. Note that the restoring and damping coefficients are non-linear in intensity; when we double the intensity from 2mW/cm^2 to 4mW/cm^2 , the force increases by less than a factor of two. This is a consequence of saturation effects.

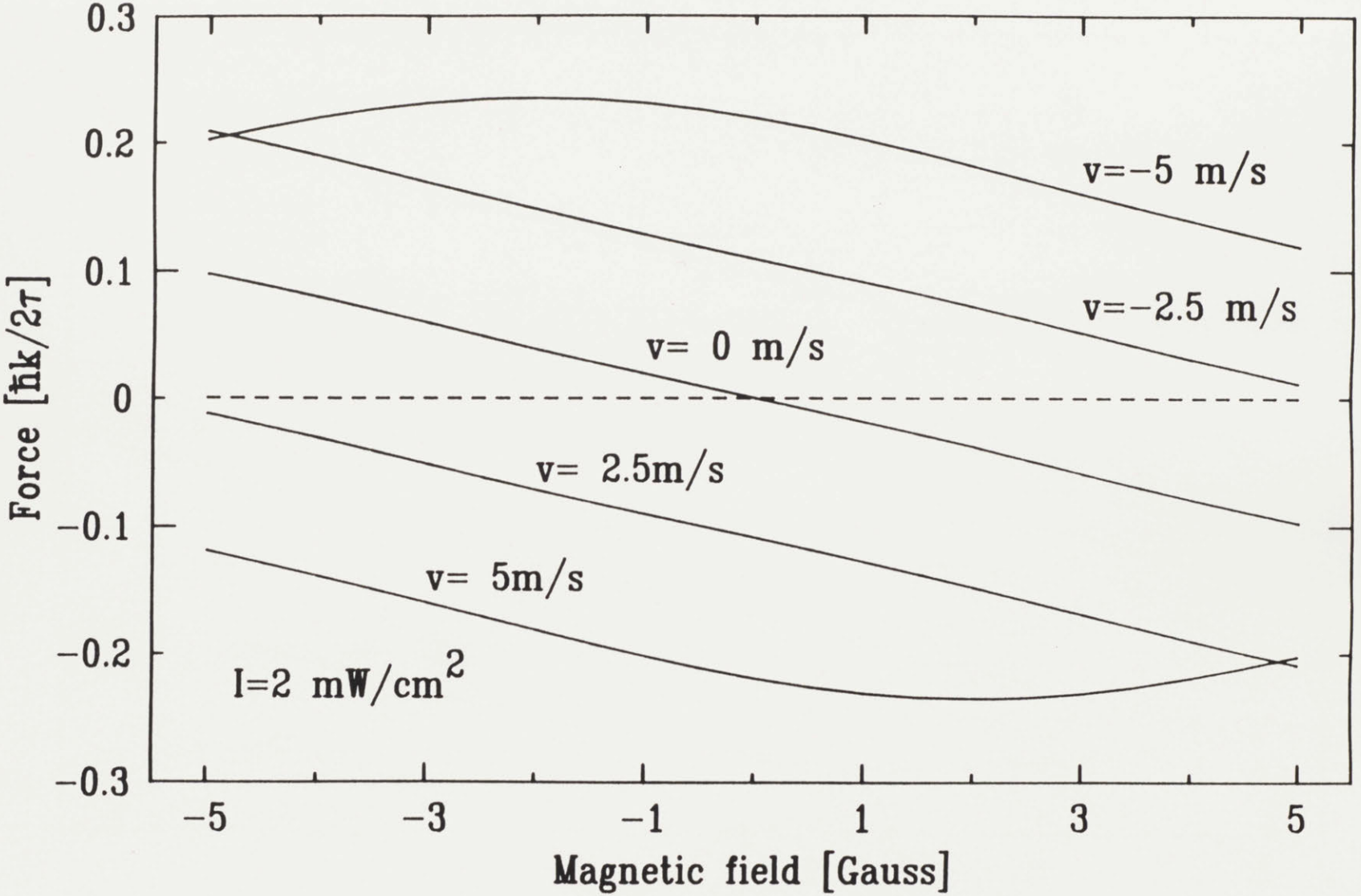

Figure II.10a: Results of a computer calculation for the simulated forces on a sodium atom in the proposed light trap. The laser frequencies are tuned 10 MHz to the red of the $2 \rightarrow 3$ and $1 \rightarrow 2$ transitions, and all the beams have an intensity of 2 mW/cm^2. Though the atom's motion is restricted to one dimension, the model accounts for all six laser beams. The maximum possible spontaneous force for an atom, $\hbar k/2\tau$, is 1 in these units. The force peaks when the Doppler plus the Zeeman effects shift the atom into resonance with the laser.

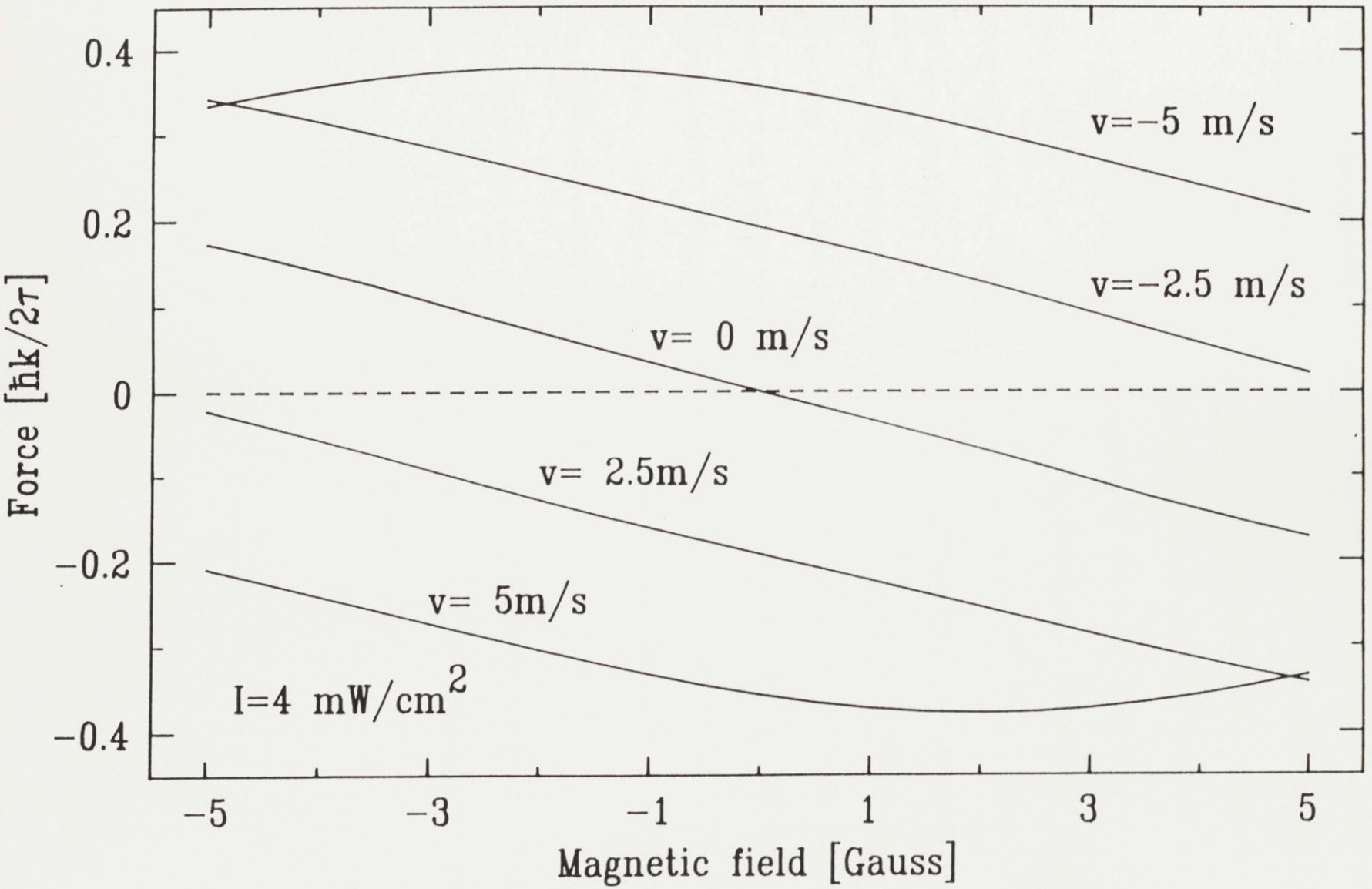

Figure II.10b: Same as II.10a, but with 4 mW/cm^2 in each beam. The forces are not twice what we obtained with 2 mW/cm^2 per beam, evidence of saturation effects.

If we allow the atom to venture away from the axes, additional complications arise. The axis of quantization is locally defined by the direction of the magnetic field vector. The field can now make an oblique angle with the polarization vectors of the light, allowing for the possibility of $\Delta M_F = 0$ transitions. These transitions may not have the proper field dependence to provide a net restoring force, so for the same total laser intensity, the trapping force may be diminished. Figure II.11 plots the components of the force for various positions along the (1,1,1) diagonal for two different intensities. (Note that the force is plotted versus total magnetic field to permit easy comparison with the one-dimensional model). We see that each component of the force still restores the atom to the origin; however, the total force does not point radially inward. This may affect the size of the trap . In addition, all other parameters being equal, the total force along the diagonal is slightly less than it is on axis. This is a consequence of the allowed $\Delta M_F = 0$ transitions. We again see the non-linearity of the force with intensity.

The theory and modeling of this section indicate the spontaneous force trap *should* work for sodium, and has potential for trapping some other alkalis as well. In the next section, we present the experimental results.

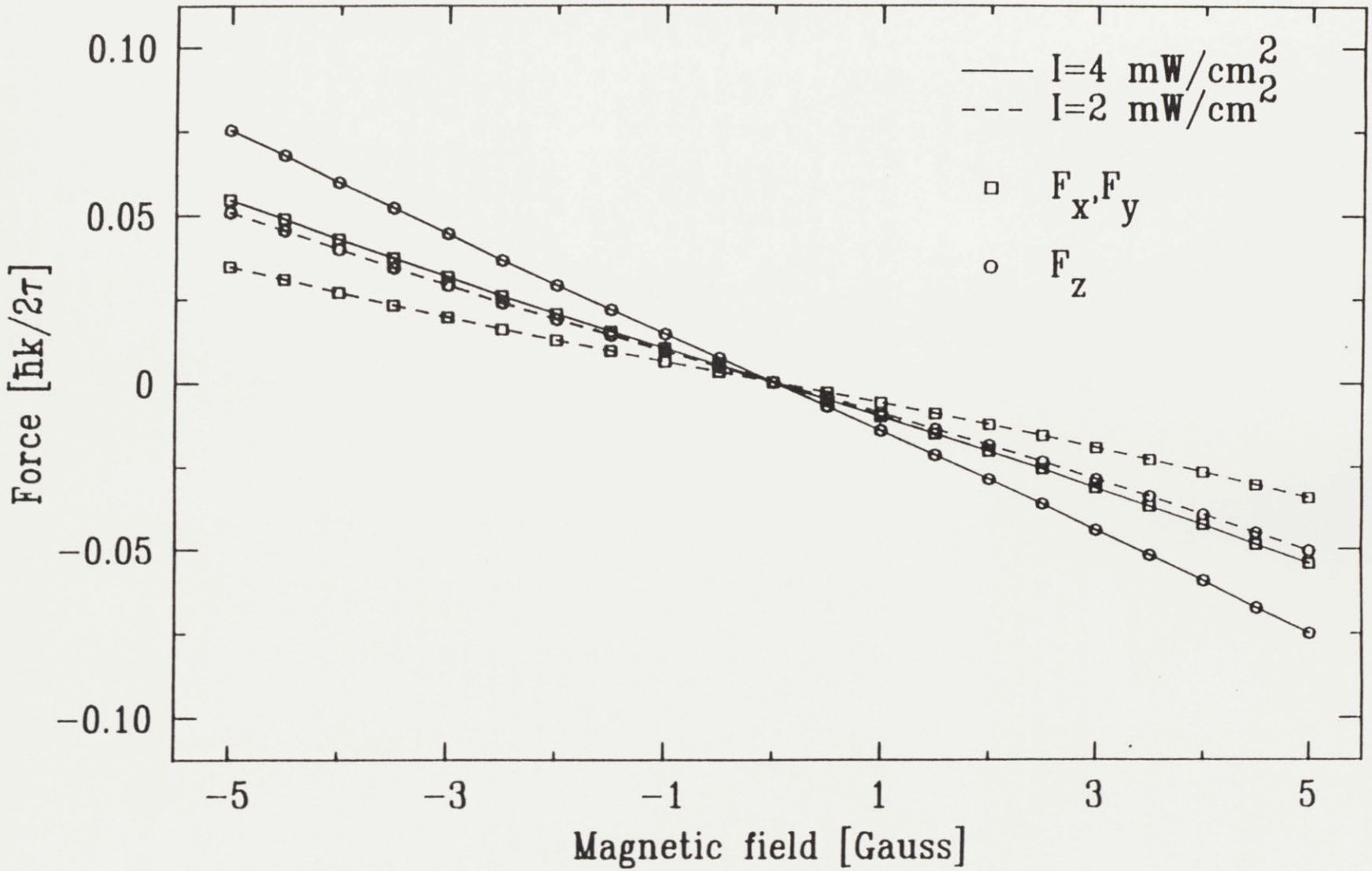

Figure II.11: Calculation of the forces on the atom for various points along the (1,1,1) diagonal. The atom is stationary. All experimental parameters are otherwise identical to those used in the calculation in Figures 10. Note that the total force is not directed toward the origin and also that its magnitude is only about 60% of the z-restoring force.

VOLUME 57, NUMBER 3 PHYSICAL REVIEW LETTERS 21 JULY 1986

Light Traps Using Spontaneous Forces

D. E. Pritchard, E. L. Raab, and V. Bagnato[a]

Physics Department and Research Laboratory of Electronics, Massachusetts Institute of Technology, Cambridge, Massachusetts 02139

and

C. E. Wieman and R. N. Watts

Joint Institute for Laboratory Astrophysics, University of Colorado and National Bureau of Standards, Department of Physics, University of Colorado, Boulder, Colorado 80309

(Received 28 March 1986)

We show that the optical Earnshaw theorem does not always apply to atoms and that it is possible to confine atoms by spontaneous light forces produced by static laser beams. A necessary condition for such traps is that the atomic transition rate cannot depend only on the light intensity. We give several general approaches by which this condition can be met and present a number of specific trap designs illustrating these approaches. These traps have depths on the order of a kelvin and volumes of several cubic centimeters.

PACS numbers: 32.80.Pj

Since the optical Earnshaw theorem (OET) was proven,[1] it has been widely believed that it is impossible to confine atoms with static configurations of laser beams by use of only light forces associated with spontaneous emission. In this Letter we show that this theorem does not necessarily apply to atom traps and suggest general approaches for making stable "spontaneous-force" light traps for atoms. We also present several examples of possible traps which have cubic-centimeter volumes and depths on the order of a kelvin. These numbers are orders of magnitude larger than those predicted for other static-light-force traps and thereby open up an entirely new range of possible applications.

There are two types of radiation forces that can be used to trap neutral particles.[2] The first is the gradient force arising from the interaction of the induced dipole moment with the field-intensity gradient. The second is the scattering force associated with the transfer of momentum from photons to particles by the scattering of light. This latter force was used to cool beams of thermal atoms[3-5] and to viscously damp a collection of already cold atoms.[6] Minogin[7] and Minogin and Javainen[8] proposed that a trap could be constructed using only the scattering force. However, Ashkin and Gordon showed that, in analogy with the Earnshaw theorem of electrostatics, such traps are fundamentally unstable,[1] thereby discrediting these proposals and discouraging any others. The current avenues of investigation have therefore been restricted to ac spontaneous-force light traps and the relatively shallow gradient-force traps. The former type was first proposed by Ashkin[9] and uses time-varying light intensities and/or frequencies to circumvent the OET in much the same way that rf ion traps overcome the traditional Earnshaw's theorem.

The key idea underlying the OET is that, in the absence of sources or sinks of radiation, the divergence of the Poynting vector of a static laser beam must be zero. Hence, if the force is proportional to the laser intensity, the force must also be divergenceless, thus ruling out the possibility of having an inward force everywhere on a closed surface. An example is shown in Fig. 1 where the Poynting vector is inward in the x-y plane at $z=0$, but outward along the z axis. On axis there is no Poynting vector at $z=0$ if the intensities of the right- and left-moving laser beams (R and L) are equal. However, the outward Poynting vector, and hence the force, increases in proportion to $|z|$ due to the focusing and consequent increase in intensity of the laser beam traveling away from the origin.

Ashkin and Gordon proved the OET for the scattering force on particles with "scalar polarizability" whose "dipole is linearly related to the field."[1] [These conditions assure that the scattering force is proportional to the Poynting vector but the word "dipole" does not imply that the gradient (also known as dipole or induced) force is involved in the present discussion.] They applied the theorem to atoms and atom traps without considering the internal degrees of freedom of the atoms. This was appropriate for traps of

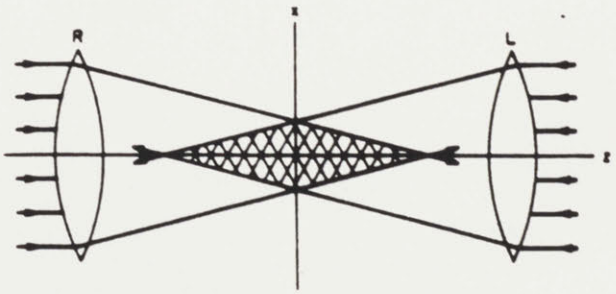

FIG. 1. Basic trap configuration. $f/2$ optics are used.

the Minogin type. However, the OET does not generally apply to the spontaneous force in atoms because this force is not always proportional to the intensity, and therefore the corollary that "the scattering force by itself cannot form a trap"[1] does not rule out atom traps based on spontaneous force. Note our use of the terms "scattering force" to apply to light forces that obey the OET and "spontaneous force" for the analogous forces in atoms (which do not). These two terms have been used interchangeably by previous authors.

The basic point of this paper is that the internal degrees of freedom of the atom can change the proportionality constant between force and Poynting vector in a position-dependent way, and thus allow static spontaneous-force traps. Such a change can result, for example, from external fields which shift the resonant frequency or orientation of an atom, or optical pumping which changes the state of the atom. These and other ideas can be exploited to violate strict proportionality and create stable optical traps using spontaneous forces, especially if one uses multibeam arrangements.

In the remainder of this paper we give three specific examples of how the sources of disproportionality mentioned above can be used to produce stable traps. For this purpose we shall restrict out attention to the simple two-beam configuration shown in Fig. 1. While this is almost certainly not the best practical design for a trap, it will serve to illustrate the general principles. The configuration shown in Fig. 1 is already stable in the x-y plane. For it to be stable along the z axis and hence form a trap, we must make an atom at $z > 0$ absorb more strongly from the left-moving laser beam (L) than from the right-moving beam (R) even though the left-moving beam is less intense.

We first show how this can be done by use of a static external field to shift the resonant frequency of the atoms. Consider a two-level atom and imagine that R is tuned below its resonant frequency while L is tuned above it. Assume also that the intensities are adjusted so that there is no force at $z = 0$ and that there is a magnetic field gradient in the $\hat{\mathbf{z}}$ direction, $dB_z/dz > 0$. As the atom moves toward positive z, its transition frequency will be Zeeman tuned toward the blue, bringing it closer into resonance with L and farther from resonance with R. Obviously if dB_z/dz is sufficiently large, the increased absorption of photons from L will more than offset its decreased intensity, resulting in a net spontaneous force back toward $z = 0$ and consequent stability along $\hat{\mathbf{z}}$. Since this configuration is already stable along $\hat{\mathbf{x}}$ and $\hat{\mathbf{y}}$, it is a spontaneous light-force trap in violation of the OET. To achieve damping of the velocity (a useful trap must have cooling in addition to stability), R should be detuned slightly below resonance ($\sim -\Gamma/2$ for maximum damping where Γ is the natural linewidth) and L should be tuned either close to resonance or several Γ above it. The velocity dependence of the force from R, which provides damping, is much greater than that from L and hence dominates and cools. For either tuning, to make the center of the trap an equilibrium point, the powers in the two beams must be different.

Although real atoms have more than two levels, a spin-polarized alkali atom, such as sodium in the $F,M = 2,2$ level excited with circularly polarized ($\sigma+$) light, is a sufficiently good approximation to this two-level case. A plot of acceleration versus longitudinal position and velocity for sodium in such a trap is shown in Fig. 2. Stability results from the fact that the spatial derivative of the force is negative near $z = 0$ (and for zero velocity the sign of the force changes). Damping occurs because the higher the velocity of the atom, the larger is the force which is opposing it.

In the second example we demonstrate how a static field which changes the orientation of the atoms can be used to produce a stable trap. In this case the laser beams have different linear polarizations, say R polarized along $\hat{\mathbf{x}}$ and L along $\hat{\mathbf{y}}$. Application of a magnetic field of constant amplitude but changing direction can cause atoms to interact differently with the two beams provided that the atoms follow the field adiabatically. In particular, for Na atoms in the $F,M = 2,2$ state, transitions to $F,M = 3,3$ are not excited by light polarized parallel to the axis of quantization (the local magnetic field). Consequently, if the B field is a helix that twists toward $\hat{\mathbf{x}}$ for $z > 0$ and toward $\hat{\mathbf{y}}$ for $z < 0$, the configuration can be made stable. If the atom moves

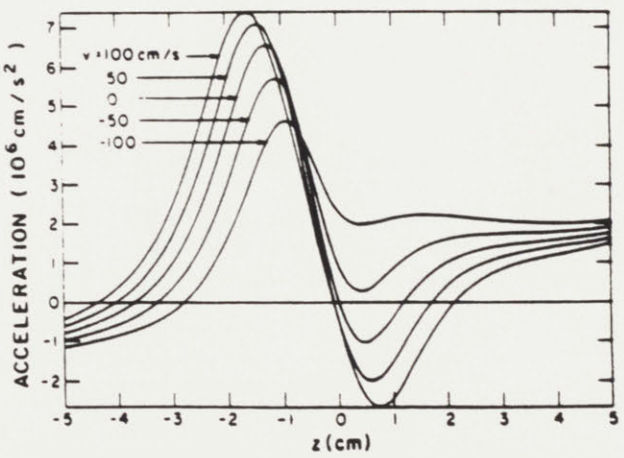

FIG. 2. Accelerations felt by sodium atoms with various velocities in a light trap having frequency-discriminated counter-propagating beams and a magnetic field gradient of 4 G/cm. At $z = 0$, beam L, tuned $\Gamma/2$ to the red side of resonance, has an intensity $I_L = 0.8 I_{sat}$; beam R, tuned $\Gamma/10$ to the blue side of resonance, $I_R = 0.15 I_{sat}$. Both L and R are right-circularly polarized and use $f/2$ optics.

sufficiently far in the $+\hat{z}$ direction, B will be parallel to $\hat{y}$ and the atom will absorb photons only from the (weaker) L beam. Motion in the $-\hat{z}$ direction will produce a similar restoring force from the R beam. Moreover, both beams can be tuned on the red side of the resonance to provide viscous damping of the velocity. Since the light is not circularly polarized, transitions to $F=3$, $M=2$ or 1, which destroy the polarization, may also occur unless the magnetic field causes sufficient Zeeman splitting. Approximate modeling shows that a high fraction of population can be maintained in the $F,M=2,2$ state for appropriate B fields and laser detunings.

Our final example demonstrates how optical pumping of the atoms can be used to obtain a stable trap. Assume now that the laser beams have opposite angular momentum (e.g., σ^+ for L and σ^- for R). Consider a transition where the F quantum number of the excited state is less than that of the ground state but not equal to zero (e.g., Cs, $F=3 \rightarrow F'=2$, which must decay back to $F=3$). If atoms are exposed to two beams of different intensity, the atoms become optically pumped so that they absorb more photons from the weaker beam than from the stronger. This can be understood from the transition probabilities shown in Fig. 3. An atom in the $M=0$ state, for $z>0$ will be quickly pumped into the $M=2$ or 3 sublevel by the stronger σ^+ beam. At that point, the atom can *only* absorb σ^- photons from the other beam which is directed toward the center of the trap. In addition, since the matrix elements strongly favor $M=+1$ decays, the atom will continue to absorb mostly σ^- photons, thus generating an average longitudinal restoring force. This peculiar intensity dependence makes it necessary to tune the laser *above* resonance to provide longitudinal velocity damping. This weakly heats the atoms in the transverse direction. Thus in a real trap it would be necessary to provide additional transverse damping, for example, by use of an asymmetric trap geometry or adding weak "optical molasses"[6] beams along $\hat{x}$ and $\hat{y}$. Phase-space trajectories for an atom in this trap with such additional cooling beams are shown in Fig. 4. These show that the atoms quickly are compressed into a region which is a fraction of a millimeter in size and have residual random velocities on the order of several centimeters per second corresponding to T. A weaker version of this trap results from use of orthogonal linear polarizations.

We have calculated the performance of the above traps and variations on them. While it is not the purpose of this paper to give detailed results, it seems worthwhile to give the general scale to stimulate consideration of optical traps based on the concepts of this paper. With available dye-laser powers, spontaneous-

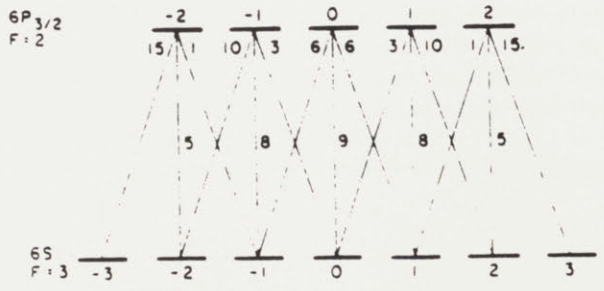

FIG. 3. Relative transition probabilities for the $6S(F=3)$-$6P_{3/2}(F=2)$ transition in cesium.

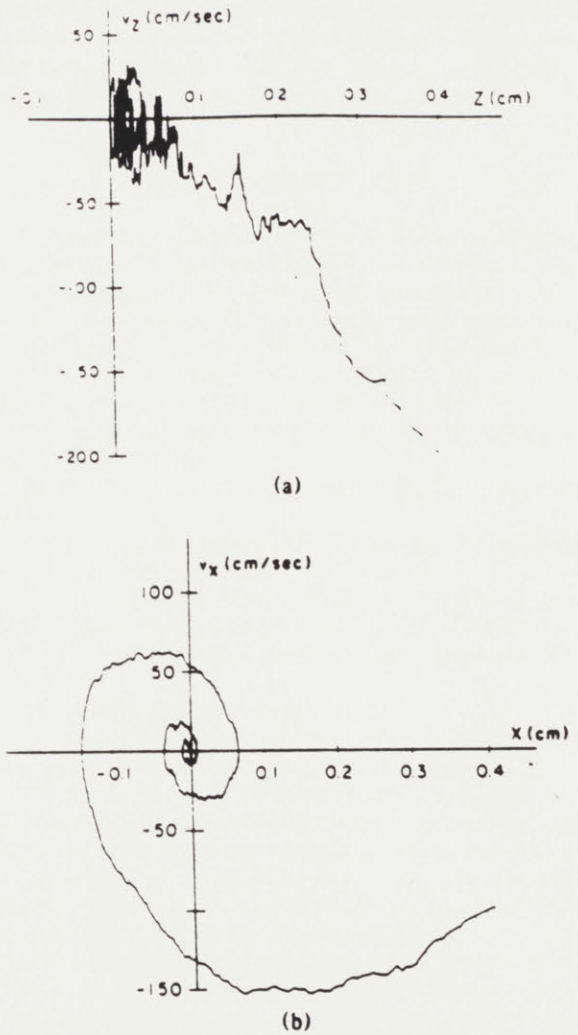

FIG. 4. Phase space plots in z and x for a cesium atom of particular initial position and velocity in a light trap having polarization discriminated (σ^+ and σ^-) counterpropagating beams along the z axis and weak optical "molasses" in the x-y plane. At $z=0$ the trap beam characteristics are area 1 cm^2, intensity 0.5 mW/cm^2, $f/2$, and detuning $\Gamma/2$. The "optical-molasses" beams are plane waves with an intensity of 0.025 mW/cm^2 and detuning of $-\Gamma/2$.

force traps such as those we have described can be constructed with ~ 10-cm dimensions, but 1 cm is more practical with inexpensive optics. The 1-cm size has confinement forces that are a fraction ($< \frac{1}{4}$) of the unidirectional spontaneous force. Integration of this force over the size of the trap gives a depth of several kelvins. However, a particle of this energy will not necessarily be confined in the trap since Doppler shifts can cause the forces to be significantly smaller for atoms with this much energy. For example, a 1-K Cs atom has a Doppler shift of $\sim 6\Gamma$ and will interact much more weakly with the radiation than the above calculation of the depth assumes. This trap depth is nearly 100 times deeper and 10^{15} times larger than that obtained for gradient-force traps of the type recently demonstrated by Chu *et al.*[10]

The spontaneous-force optical traps we have proposed are relatively simple ones designed to illustrate general ways in which the optical Earnshaw theorem can be circumvented. More complicated geometries can probably exploit these approaches more fully, particularly ones which provide more direct cooling and confining in the x-y plane. As a simple example, the addition of weak optical molasses along $\hat{x}$ and $\hat{y}$, mentioned above, will make any of these traps perform better. Also, additional beams may be needed to ensure that trapped atoms do not escape to untrapped hyperfine ground states such as exist in all alkali atoms.

The particular examples we have chosen illustrate three ways the internal degrees of freedom of the atom can be exploited to trap atoms, but there are many additional possibilities. Other types of optical pumping exist, such as pumping between two different hyperfine levels. Also, external static or oscillating fields can be used in a variety of ways to affect how an atom absorbs radiation.[11] Probably all of these can be used to produce light-force traps. Finally, it may be possible to avoid the restrictions of the optical Earnshaw theorem by use of saturation[1] or absorption. The latter is particularly attractive: An optically dense cloud of Na will experience a maximum spontaneous radiative pressure of $\sim 10^{-7}$ N/m^2 (corresponding to 5 mW/cm^2), enough to contain an atom density of 5×10^{13}/cm^3 at $T = 0.25$ mK according to the perfect-gas law. Indeed, gas pressure limits the confinement density of a spontaneous-force trap, but this limit may be increased by using a weaker transition with a correspondingly lower ultimate temperature.

We have pointed out ways in which spontaneous light forces may be used to make traps for atoms or ions. The advantages of this spontaneous-force approach as compared to other proposed neutral-particle light traps include large physical extent, reasonably deep wells, and experimental simplicity. Time-varying laser intensity or frequency is not required and the simple designs proposed are quite forgiving to optical misalignment or intensity mismatch. We hope our suggestions will remove the optical Earnshaw theorem as a practical barrier to the design of spontaneous-force light traps and will open the way to the realization of successful traps of different types.

We acknowledge useful conversations with S. L. Gilbert, C. E. Tanner, and D. Z. Anderson. This work was supported by the National Science Foundation and the Office of Naval Research. One of us (C.E.W.) is an A.P. Sloan Foundation fellow.

---

[a]Permanent address: Instituto de Física e Química de São Carlos da Universidad de São Carlos, São Carlos, Brazil.

[1]A. Ashkin and J. P. Gordon, Opt. Lett. **8**, 511 (1983).

[2]See, for example, the feature issue on the mechanical effects of light, J. Opt. Soc. Am. B **2**, 1707–1860 (1985).

[3]J. Prodan, A. Migdall, W. D. Phillips, I. So, H. Metcalf, and J. Dalibard, Phys. Rev. Lett. **54**, 992 (1985).

[4]W. Ertmer, R. Blatt, J. L. Hall, and M. Zhu, Phys. Rev. Lett. **54**, 996 (1985).

[5]R. N. Watts and C. E. Wieman, Opt. Lett. (to be published).

[6]S. Chu, L. Hollberg, J. E. Bjorkholm, A. Cable, and A. Ashkin, Phys. Rev. Lett. **55**, 48 (1985).

[7]V. G. Minogin, Kvant. Elektron. (Moscow) **9**, 505 (1982) [Sov. J. Quantum Electron. **12**, 299 (1982)].

[8]V. G. Minogin and J. Javainen, Opt. Commun. **43**, 119 (1982).

[9]A. Ashkin, Opt. Lett. **9**, 454 (1984).

[10]S. Chu, J. Bjorkholm, and A. Ashkin, and A. Cable, following Letter [Phys. Rev. Lett. **57**, 314 (1986].

[11]While these fields do exert forces themselves on the atoms, here we are limiting our discussions to cases, such as the magnetic fields mentioned above, where such forces are many orders of magnitude weaker than the spontaneous force. Hence it is most useful to think of the fields as merely providing a control for the spontaneous force. It is possible to have hybrid traps which are produced by a combination of forces from large static fields and radiation pressure. An interesting possibility for such a trap which employs a large magnetic field for confinement and detuning has been pointed out to us by P. Gould, private communication.

CHAPTER III — THE BELL EXPERIMENT

III.1 Introduction

Shortly after the idea for the spontaneous force light trap described in Chapter II was conceived, we were presented with an opportunity to test it. Dr. Steven Chu and his colleagues at AT&T Bell Laboratories in Holmdel, New Jersey had succeeded in cooling sodium atoms to less than one milliKelvin using "optical molasses" (CHB85) in late 1984. It was evident that by making a few small additions to their apparatus, the "molasses" would become a spontaneous force trap. A letter was sent to Dr. Chu in July, 1986 outlining the trapping scheme and proposing a collaboration to try it in his apparatus. He agreed to join forces with us; and in January, 1987, the author went to Holmdel to attempt the experiment. This chapter describes the work performed and the results obtained during the ~4 weeks spent at Bell.

III.2 Additions to the Bell Apparatus

III.2.1 Optical System

The apparatus used in the "optical molasses" experiment is sketchily described in the appropriate references (CHB85,CBA86). I shall elaborate here on the parts of the setup that are especially pertinent to the requirements of the light trap experiment. I will assume that the reader is already familiar with the descriptions given in the above references.

A schematic of the apparatus is shown in Figure III.1. The laser light was generated by a computer-controlled Coherent Model 699-29 ring dye laser pumped by an Innova 100 argon ion laser. A portion of the light was picked off and sent to a sodium reference cell, which was used to actively lock the laser frequency to one of the crossover resonances of the D2 transition. The crossovers are halfway between resonances of the F=1 and F=2 hyperfine levels of the ground state with the various excited state hyperfine levels.

The balance of the laser output was first sent through an electro-optic modulator driven at 856.2 MHz, which is half the difference between the $F=1 \rightarrow F'=2$ and $F=2 \rightarrow F'=3$ transitions in the D2 line. The modulator consisted of a 1mm×1mm×25mm $LiTaO_3$ crystal enclosed in a resonant cavity (Q~50) tuned to the driving frequency. A small piece of glass, anti-reflection coated on one side, was placed next to both the optical entrance and exit faces of the crystal with the coated side facing outward. A drop of index-matching fluid was placed between the glass and the crystal to minimize reflective losses.

The light was next passed through a series of two acousto-optic modulators (Isomet 1205C-2). This arrangement served two purposes: one, it deviated part of the trapping beam for the frequency-chirped atomic beam slower; and two, it served as a fast shutter for the trapping beams, whose frequency and duty cycle could be electronically controlled.

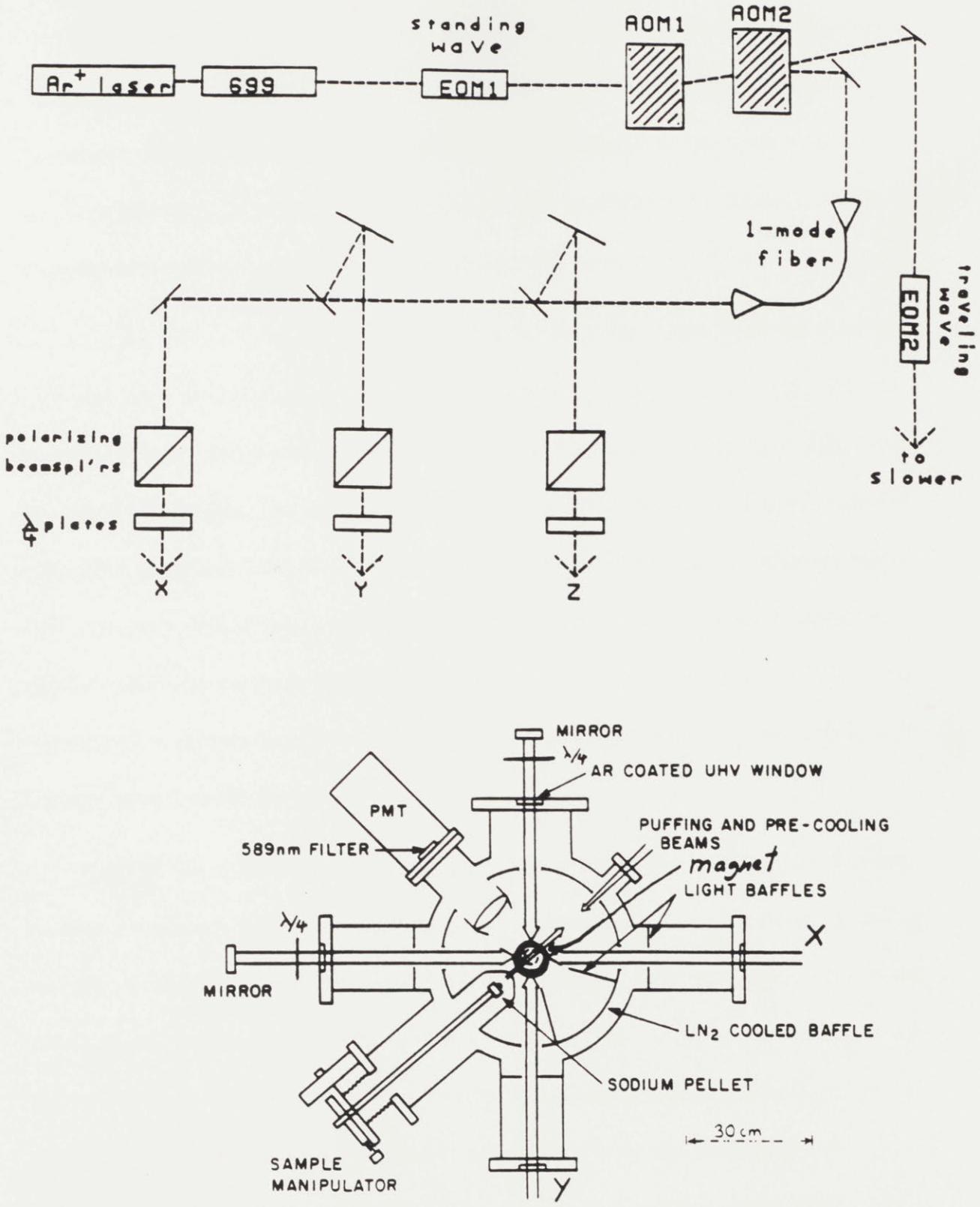

Figure III.1: Schematic of the optical system used in the Bell experiment.

A single-mode optical fiber was used as a spatial filter for the trapping beam. This had the advantage of effectively dividing the optical system into upstream and downstream sections which could be aligned independently. If the beam direction in the upstream section changed for some reason, one needed only to readjust the input coupling of the fiber to restore the overall system alignment.

On the downstream section of the optical system, the output from the fiber was split into three beams of approximately equal power by a pair of multi-layer dielectric bandpass filters. The transmission through (and the reflection from) each filter could be varied by changing the angle of the filter. The three beams were then expanded, collimated, and sent into the vacuum system through three "input" windows placed along the +x,y, and z axes. After passing out of the vacuum system through "exit" windows opposite the input windows, the x and y-axis beams were reflected back upon themselves by mirrors facing the exit windows. The z-axis beam was retroreflected by a mirror placed inside the vacuum chamber.

One of the additions required for the light trap was that each pair of the three counter-propagating trapping beams was given opposite circular polarization. Each leg was first linearly polarized by a polarizing beamsplitting cube (2" edge, A.R. coated faces) placed before the entrance window for each axis. A zero-order quarter wave plate (CVI Laser Optics Co., 25mm aperture, A.R. coated) was mounted in a rotatable stage (Newport Corp. RSA-1) just before each of the three entrance windows in order to circularly polarize the input beams. The sense of circular polarization of the x and y

return beams was reversed with respect to that of the input beam by placing another quarter wave plate between the exit window and the retroreflecting mirror. Since the retro mirror for the z beam was enclosed in the vacuum chamber, however, a mount for the necessary quarter-wave plate was fashioned out of black anodized aluminum and supported just above the retro mirror by a rod and clamp assembly. A flexible cable connected this mount to a rotatable vacuum "feed-thru," allowing us to adjust the orientation of the optic axis from outside the chamber.

With the quarter-wave plates in place, we were able to check the polarization of the trapping beams by monitoring the reflection of the retro beams off the polarizing beamsplitter. A reflection maximum with one retarder in place indicated that the beam was circularly polarized; a reflection null with both retarders in the beam then indicated that the retro beam had the opposite circular polarization of the incident beam.

III.2.2 Vacuum System

The main vacuum chamber was a custom designed cylinder approximately 12" in diameter and 9" high. Several ports extended from the chamber for windows, feed-thrus, measurement devices, etc. Two turbo-molecular pumps were used to evacuate the chamber to a pressure of $\sim 10^{-10}$ torr. A copper jacket lining the inside of the chamber could be cooled with liquid nitrogen to produce ultimate pressures as low as $\sim 10^{-11}$ torr.

The second addition was to place a pair of opposed current coils inside the vacuum system to generate the necessary magnetic field (as described in II.2.4). The coils were fashioned by winding a single piece of 1/8" O.D. copper refrigerator tubing around a 2" diameter cylinder. Three turns were made for the top, and three in the opposite direction for the bottom, with about 1" clearance between them. A fiberglass sheath was slipped over the copper tube for insulation, then painted black with Aquadag to reduce light scattering.

A Hall probe ("Gaussmeter") was used to measure the field produced by this magnet prior to its insertion into the vacuum system. It was found that a current of 20 amps yielded a gradient of 5 Gauss/cm along the z-axis (axis of symmetry), and about 2.5 Gauss/cm in the x-y plane. The field was zero approximately midway between the coils along the z-axis. This agrees with our expectation for the axial field of two coils of opposing currents I having radii and separation a:

$$B_z(z,\rho=0) = \frac{\mu_0 I a_2}{2}\left[\frac{1}{[a^2+(z+a/2)^2]^{3/2}} - \frac{1}{[a^2+(z-a/2)^2]^{3/2}}\right] \qquad (1)$$

$$\Rightarrow B_z'(z,\rho=0) = \frac{-3\mu_0 I a_2}{2}\left[\frac{z+a/2}{[a^2+(z+a/2)^2]^{5/2}} - \frac{z-a/2}{[a^2+(z-a/2)^2]^{3/2}}\right]$$

$$\Rightarrow B_z'(z=0,\rho=0) = -\frac{3\mu_0 I}{2a^2}\left[\frac{4}{5}\right]^{5/2} \approx \frac{1.11 I}{a^2}\,.$$

The ends of the copper tube were joined to an MDC water-cooled high-current feed-thru via a pair of Swagelock connectors. The feed-thru was mounted on a 2-3/4" Conflat flange and bolted to the top of the vacuum chamber. The coils could thus be

positioned in the vacuum chamber with an adjustable mounting bracket, then connected to the feed-thru via the VCR's. The magnets were able to dissipate ≥100 amps continuously, using ~1 liter/min of water for cooling.

Current was supplied to the magnets via a Hewlett-Packard power supply. The maximum current rating was 100 amps, though it was rarely pushed to the limit. The output could be varied conveniently by the application of an external voltage to a control terminal on the rear of the supply.

III.3 Results

III.3.1 Trapping the Atoms

The first step in running the experiment was to generate a cloud of cold atoms in the usual "optical molasses." The current supply to the magnet was turned off, and the quarter-wave plates were oriented with their optical axes parallel to the polarization vector of the light so that they did not induce any rotation. A YAG laser pulsed at ~10 Hz evaporated a puff of sodium, which subsequently was slowed to <20m/s by the chirped cooling laser. These slow atoms would then drift into the "molasses" region at the intersection of the six laser beams.

The accumulation of atoms in the "molasses" region was monitored by imaging this region onto the cathode of a photomultiplier tube using a lens inside the vacuum system (see Figure III.1). Various experimental parameters, such as beam alignment,

chirp range, and YAG timing, could be adjusted as the signal was monitored in an effort to maximize the hold time of the "molasses." In order to determine later if the atoms were being trapped, it was important that the atoms in the "molasses" be visible to the naked eye, because the detector was sensitive only to the *number* of fluorescing atoms and not to their density or position. It was therefore essential to get the hold time to be ~100 msec (the repetition period of the YAG laser) in order to allow the atoms to accumulate to the point where they were visible.

Once a visible cloud of cold atoms was obtained, the quarter-wave plate by the input window of one of the axes was rotated 45°, causing the beams along that axis to be circularly polarized with the same helicity. The current in the magnets was then slowly turned up to ~20 amps. If the sign of the polarization was correct, the cloud of atoms would be compressed along the axis with the counter-polarized beams. If the sign of the polarization was reversed, the cloud would be dispersed. All three axes were counter-polarized in this fashion until a small sphere of trapped atoms was formed.

Trapping was observed under a wide range of conditions. With a fixed separation of 1712.4 MHz between the first order sidebands of the modulated light, the laser could be tuned to the red of the $F = 2 \rightarrow 3$ and $1 \rightarrow 2$ or the $F = 2 \rightarrow 2$ and $1 \rightarrow 0$ transitions. The former tuning produced a much more compact and regular ball of atoms than the latter, due possibly to the higher oscillator strength and the existence of a cycling transition in the $F = 2 \rightarrow 3$ manifold. The detuning from resonance could

vary from as much as ~30 MHz to as little as ~2 MHz to the red of the transitions, with the optimum signal occurring at ~-15 MHz. The current could be turned down to ~5 amps, corresponding to a field gradient of ~0.6 Gauss/cm in the x-y plane. The intensity in each trapping beam could be as low as ~0.4 mW/cm^2 per sideband, and as high as we were able to make it (~30 mW/cm^2 per sideband). The trap seemed to be fairly insensitive to the purity of the circular polarization — the quarter-wave plates by the input windows could be rotated as much as 20° from the optimum position before having any adverse effects on the trap's appearance. A neutral density filter of 0.2 could be inserted before a retro mirror without destroying the trap, creating a beam intensity imbalance of ~2.5:1. There where a sufficient number of slow atoms in the tail of the pulsed atomic beam to load the trap without having to use the chirped slower; however, the highest overall number and density of trapped atoms was obtained by optimizing the loading procedure.

There were many interesting qualitative features of the trapped atoms which we observed by eye and recorded with a video camera. When the laser beams were slightly misaligned, the atoms would sometimes form a ring-shaped pattern, whose orientation could be changed by altering the angle of the retro mirrors. Moving the retro mirrors could also effect the gross position of the trap; we were able to move it as much as 1 cm. Under certain conditions two distinct regions of trapped atoms would be formed, their edges separated by less than 1 mm but clearly delineated; the atoms would appear to slosh back and forth between the two regions. Under weak

trapping conditions (tuning far from resonance, low current and laser intensity) atoms could be seen escaping along the diagonals of the trap in the x-y plane. The general procedure for running the experiment, however, was to "tweak" the optics to eliminate these anomolous phenomena in order to optimize the performance of the trap.

III.3.2 Lifetime of the Trapped Atoms

The first quantitative measurement was the lifetime of the trapped atoms. We define the lifetime to be the mean time τ an atom remains trapped before being expelled. If we assume that the atoms leave the trap region independently and stochastically, then the decay of the trap will be governed by the equation

$$\frac{dN(t)}{dt} = -\frac{N(t)}{\tau} , \tag{2}$$

where $N(t)$ is the instantaneous number of trapped atoms. This has the simple solution

$$=>N(t) = N(0)\, e^{-t/\tau} . \tag{3}$$

The existence of non-linear terms reflecting collisions will be discussed later in Section III.3.3; they contribute negligibly to the decay at low densities ($<10^9 cm^{-3}$).

The number of trapped atoms, N, was determined by

$$N = \frac{4\pi \times (PMT\ \ signal) \times R_L}{\Omega \times (Q.E.) \times G \times (1-L) \times \rho_{ee} \times R} .$$

R_L is the load across the output of the photomultiplier tube (PMT), $(Q.E.)$ its quantum efficiency and G its current gain. L is the reflective and transmissive losses in the

collection optics (estimated to be ~20%) which subtend the solid angle Ω; we used a 6.5cm diameter collection lens ~15cm from the trap region => Ω ~ .15 sterradians. ρ_{ee} is the fraction of atoms in the excited state, and $R = \rho_{ee}\Gamma/2$ is the rate of fluorescence from each trapped atom.

We determined the lifetime τ by measuring the decay of the total fluorescence from the trap. We assumed that N is proportional to the total trap fluorescence, i.e. that the excited state population ρ_{ee} has reached equilibrium with the laser excitation. The measurement procedure was first to load the trap in the manner described in III.3.1 until either the fluorescence was maximized or we obtained a satisfactory signal from the trapped atoms. The loading process was then terminated by shutting off the YAG and slowing lasers; if the YAG only was shut, the slowing laser would generate sufficient heat to evaporate some sodium from the source and load more atoms in the trap. The fluorescence was then monitored until τ could be accurately determined.

A plot of our data taken at a pressure of $\sim 3\times10^{-11}$ torr is reproduced in Figure III.2. After the first few seconds (when collisions accelerate the decay — cf. next section), the fluorescence decreases exponentially with a time constant τ~60 sec. We found that the trap lifetime increased with decreasing background pressure, implying that atoms were being knocked out of the trap by collisions with the relatively hot atoms of the background gas. We recorded decay time constants as long as 150 sec, at pressures of $\sim 10^{-11}$ torr (measured by two ion gauges).

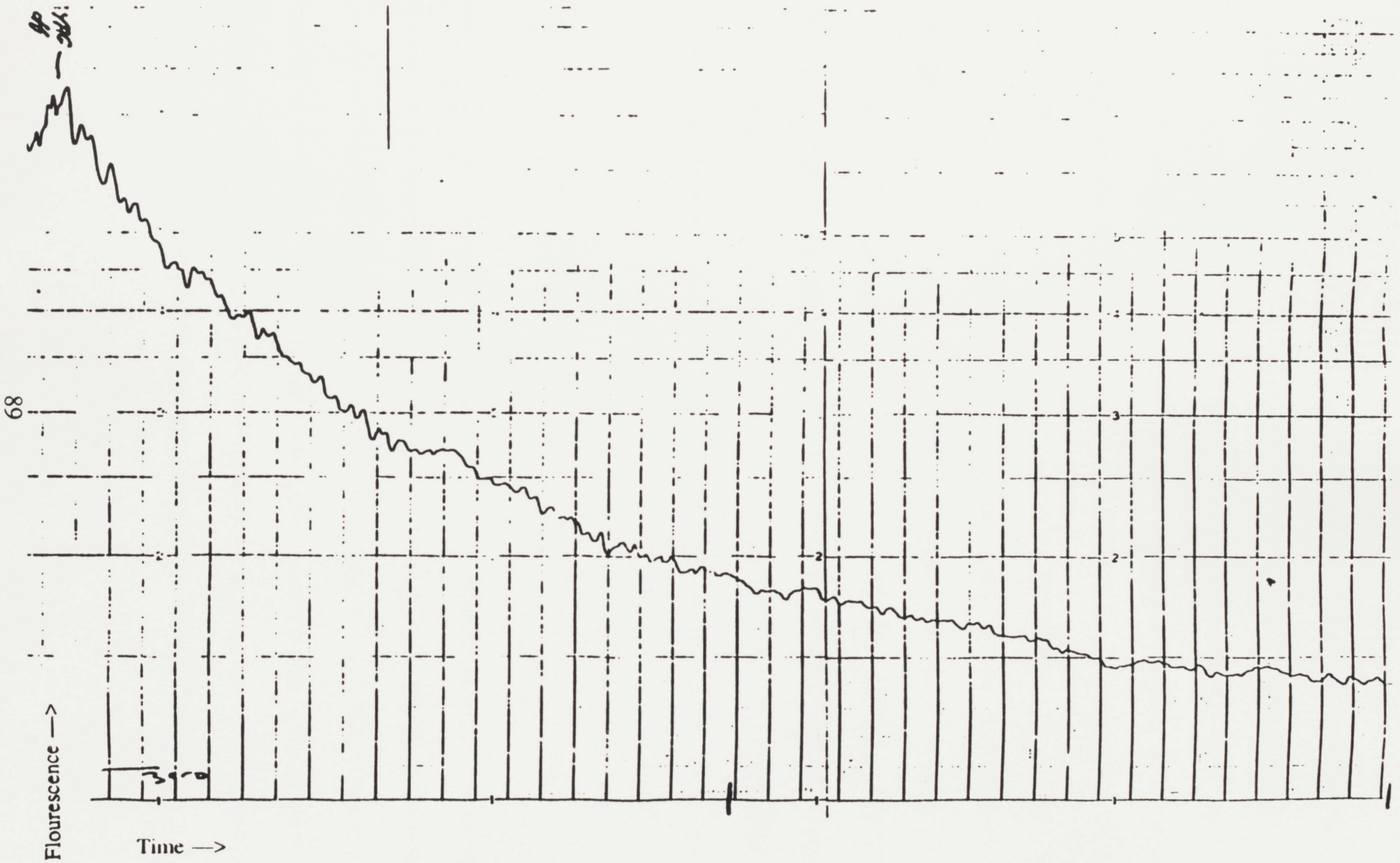

Figure III.2: Fluorescence of the trapped atoms versus time. Tick marks are placed along the abscissa every minute. The loading was stopped at the point labeled "YAG off." The pressure was ~3×10^{-11} torr.

We can use our measure of the trap lifetime to make a crude estimate of the cross-section for collisions with the background gas atoms in terms of their mass. From the kinetic theory of gases we obtain the relationship for the cross-section (RAM56) $\sigma = 1/\tau n \bar{v}$, where n is the density of the trapped sodium (assumed to be stationary) and $\bar{v}$ the mean relative velocity of the colliding atoms (and hence the mean velocity of the background atom). For a gas at temperature T, we may write $n = P/kT$, and $\bar{v} = \sqrt{8kT/\pi m}$, where m is the mass of the background atom (RAM56). We thus obtain $\sigma = (\pi mkT/8)^{1/2}/\tau P$, which for T=77K, P=$10^{-11}$$torr$, and τ=150s becomes $\sigma = 4.2\times10^{-14}\sqrt{m}\ cm^2$ where m is the molecular weight of the background collider. If helium were the primary constituent of the background gas, for example, we would obtain $\sigma = 8.4\times10^{-14}cm^2 = 8.4\times10^2\text{Å}^2$. This can be compared to the theoretical total cross-section for a C_s/r^s potential (MAS71) given by

$$\sigma = \gamma(s)\left[\frac{C_s}{\hbar v_{rel}}\right]^{\frac{2}{s-1}}, \tag{4}$$

where $\gamma(s)$ is a numerical coefficient and v_{rel} is the relative velocity of the colliding partners in the center-of-mass reference frame. Assuming a van der Waals interaction, an independently measured value for $C_6 \approx 20\times10^{-60}erg\cdot cm^6$ (RAM56) yields a cross-section of $\sigma \approx 200\text{Å}^2$. Our measured cross-section is about four times as large; this could be a consequence of collisions with different background gas atoms having much stronger interactions with sodium (e.g. argon has a $C_6 \approx 200\times10^{-60}erg\cdot cm^6$

(RAM56)), or possibly collisions with excited-state sodium, which would present a much larger cross-section.

To measure the total number of atoms in the trap, we needed to determine the excited-state fraction ρ_{ee}. We showed in II.1.3 that $\rho_{ee} = s/2(1+s)$, where s is the saturation parameter; we may write this as $s = \frac{I}{I_{sat}} \frac{2\Gamma^2}{\Gamma^2+4\delta^2}$, where $I_{sat} \sim 12 mW/cm^2$ for the sodium D2 transition. ρ_{ee} is difficult to calculate because there are several frequencies of light present, each driving different transitions at different rates. We were able to measure ρ_{ee}, however, by using an acousto-optic modulator to attenuate the trapping beams for time sufficiently short so that no atoms would leave the trap (~10 ms). Since the detuning was known (the atoms were contained in a region within a few mm of the center, so the induced Zeeman shift was much less than the natural linewidth), we were able to obtain an effective value for I_{sat} by plotting the fluorescence versus intensity for varying I. We were able to contain as many as $\sim 10^7$ atoms at one time.

III.3.3 Binary Collisions

When the density in the trap was high ($>10^9 cm^{-3}$) we observed non-linear effects in the decay of the atoms. If we assume that the volume occupied by the trapped atoms is independent of their number, then the density $n(t)$ will satisfy

$$\frac{dn(t)}{dt} = -\frac{n(t)}{\tau} - \beta n(t)^2, \tag{5}$$

where β is the rate for second-order processes. Evidence of non-linear decay can be seen in Figure III.3, where the fluorescence departs from a simple exponential fall-off at early times (t<4s), i.e. when the density is the highest.

The solution for equation (3) is

$$n(t) = \frac{n(0)\, e^{-t/\tau}}{1 + \beta\tau n(0)(1 - e^{-t/\tau})} \tag{6}$$

The data in Fig. III.3 were fitted by A. Cable (CAB87) using τ and β as free parameters; he obtained $\tau = 55s$, and $\beta = 2.2\times10^{-13} cm^3 s^{-1}$.

Non-linear decay will result most probably from two-body collisions between atoms in the trap which cause one or both of the atoms to be expelled. Possible processes include:

1) $Na(3P) + Na(3S) \rightarrow Na(3S) + Na(3S) + \Delta E$
2) $Na(3P) + Na(3P) \rightarrow Na(5S) + Na(3S) + \Delta E$ $(\Delta E \sim 600\ cm^{-1})$
3) $Na(3P) + Na(3P) \rightarrow Na_2^+ + e^- + \Delta E$

Process 1 involves the collision of a ground state atom with one in the excited state. Since the inter-atomic potential for this system goes as $\pm 1/R^3$, the two atoms will be drawn together from a relatively large distance (when the potential is attractive); each will gain momentum as it rolls down the potential "slope" (though of course the center-of-mass momentum is conserved). When the excited atom then decays to the ground state, the interaction becomes a much weaker $1/R^6$; the momentum gained while the one atom is excited may be enough to eject one or both

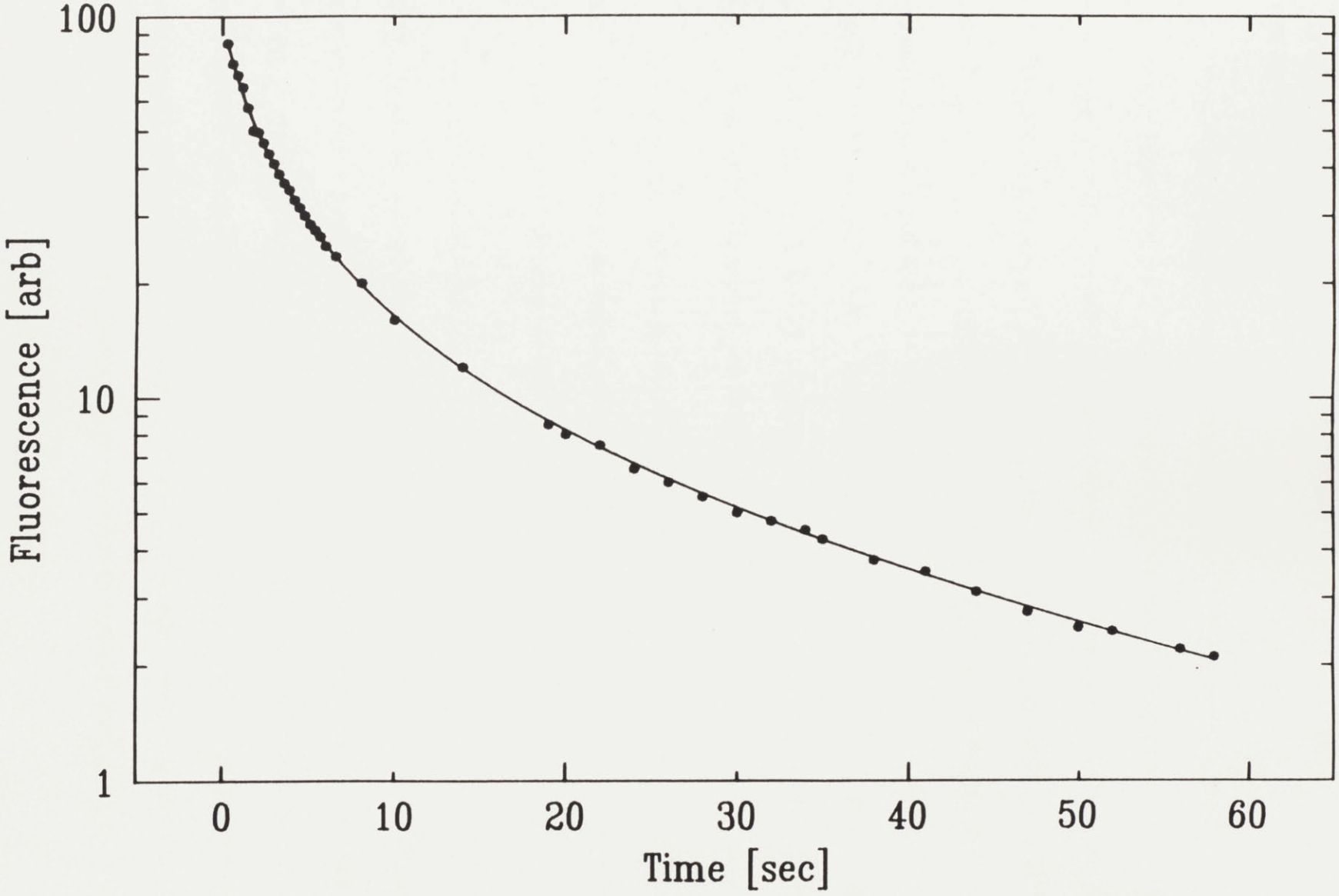

Figure III.3: Decay of the fluorescence from the trapped atoms when the initial density was high. We see that at early times, the decay deviates from a simple exponential, indicating the presence of non-linear decay. The solid line represents a fit of Eq. (5) to the data.

from the trap.

We can find an upper bound to the loss rate from this process by first estimating the effective interaction length R_{int} (Figure III.4). We note that a pair of atoms will absorb a photon only if $|V(R_{abs})| < \hbar\Gamma$ (otherwise its resonance is shifted too far from the laser frequency) and will be ejected from the trap only if $|V(R_{em})| > 2kT$, where T is the depth of the trap. Hence $R_{int} = R_{abs} - R_{em}$; for sodium, we take the potential to be the weighted average of the attractive Π and Σ branches of the inter-atomic 3S-3P potential: $V(R) \approx 6.3\times10^5 cm^{-1}/R^3$, with R in units of Bohr radii $a_0 = .53$ Å (PRI78, p. IX-B-3.4). We thus obtain $R_{abs} \approx 50$ Å and $R_{em} \approx 640$ Å (for a trap depth of 0.5 K) implying $R_{int} \approx 590$ Å.

The maximum loss rate due to this process can now be estimated if we assume that the atomic trajectories are not affected by the presence of the excited-state atoms (quasi-static approximation) (GAP88). We obtain a rate per atom of

$$R_l \leq \tfrac{1}{2}\Gamma\,\varepsilon\, n\,(1-\varepsilon)\,\frac{4\pi}{3}R_{em}^3\,, \tag{7}$$

where ε is the excited state fraction, n the density, and $n(1-\varepsilon)(4\pi R_{em}^3/3)$ the probability that a ground state atom will be close enough to the excited atom when it decays to cause both atoms to be ejected; the preceding factor of 1/2 is because half of all collisions will occur on the repulsive potential. If we assume saturation intensity, then $\varepsilon = 0.3$ and we get a loss rate of $R_l = 3.5\times10^{-12}\, n\ sec^{-1}$, with n given in cm^{-3}. This is about an order of magnitude greater than the rate obtained from the fit to the

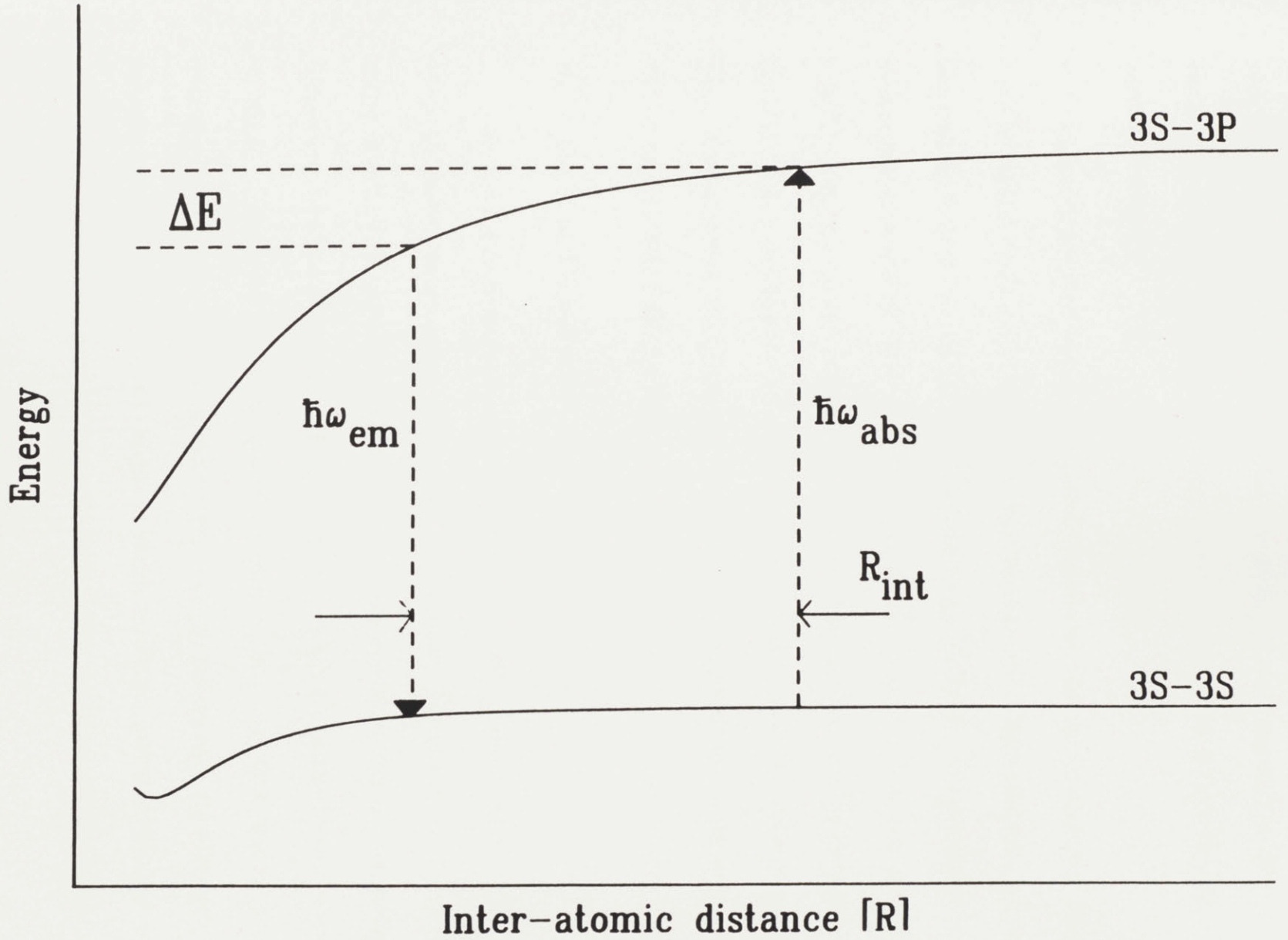

Figure III.4: Collision process 1. The pair of atoms gains kinetic energy $\Delta E = \hbar(\omega_{abs} - \omega_{em})$.

data; aside from the simplifications made in obtaining our estimate, the discrepancy may also be a consequence of forces from other excited state atoms and the effects of stimulated emission.

Process 2 is a near-resonant collision; it could be verified by observing the red $5S \rightarrow 3P$ photon (~610 nm). Process 3, the formation of a molecular ion, has been observed by the trapping group at NBS Gaithersberg (GOU87). They report a cross-section (unpublished) of ~840 $\mathring{A}^2$ at 240 μK, which implies a loss rate of $\sim 10^{-12}$ $n\ sec^{-1}$. This is ~1 order of magnitude greater than the rate seen in our trap, and therefore is also an important process to consider. A detailed study of the many-body phenomena occurring in a light trap will be one of the objectives of the new super-conducting light trap (Chapter IV).

III.3.4 Size of the Trapped Atom Cloud

We were able to measure the size of the trapped atomic cloud using a black and white television camera and a video waveform analyzer. The camera viewed the trap along the (1,1,1) diagonal through a window on the outside of the vacuum chamber. The output from the camera was sent through the waveform analyzer, which was able to "grab" a horizontal line from the video picture. We were thus able to get the intensity profile of the trap for various "slices" through the image. By calibrating this system with an object of known length (a ruler), we could determine the size of the cloud of trapped atoms under various conditions. The resolution of the camera was

better than $100\,\mu m$.

To avoid confusion, we must be careful to distinguish between the phrases "trap size" and "size of the trapped atom cloud." The "trap size" refers to the volume over which free atoms will be captured by the trap; it is synonymous with "capture volume." Once the atoms are captured, however, the effect of the trap is to compress them into a much smaller volume; the dimensions of this cloud of trapped atoms is the topic of the present discussion.

One item of fundamental interest was the variation of the size of the trapped cloud as a function of the current through the coils. If we model the trap as a harmonic potential $U = \frac{1}{2}\kappa r^2$, then an atom with total energy E will have a maximum excursion $r_{max} = \sqrt{2E/\kappa}$. The size of the cloud formed by an ensemble of atoms having a distribution of energies will be defined by the atoms in the ensemble possessing the greatest energy. By using an independent measure of this maximum energy, we can compare the measured diameter of the cloud with that predicted by our model (cf. III.2.2) for any given value of the current. In addition, if we assume that the atom's energy is independent of the field gradient, then the measured variation of the diameter versus the current can be used to confirm our qualitative understanding of the trap dynamics. The models show that the force on a stationary atom is proportional to the magnetic field B, implying that κ should be proportional to B'. Since $B' \propto I$ (Eq. (1)), we therefore expect $\kappa \propto I$, and the diameter of the cloud to vary as $I^{-1/2}$.

Some of the results are shown in Figure III.5. We see that for the laser tunings shown, $r_{max} \sim I^{-1/2}$ as expected. It is encouraging that the size of the trapped cloud maintained its $I^{-1/2}$ character for currents up to 100 amps. This suggests that still greater currents will compact the atoms even more.

To relate the measured r_{max} to the modeled force constant κ, we shall use the independently measured energy of the hottest atoms $E = 7 \pm 1 \times 10^{-4}$ eV (cf. III.3.5). For the "primary" trap tuning of ~8 MHz to the red of the $F = 2 \rightarrow 3$ and $1 \rightarrow 2$ transitions (indicated by the filled circles), the diameter $2r_{max} = 0.5 \pm .05$mm at a current of 20 amps; the experimental error is predominantly from the limited resolution of the video camera — we have used the measurement taken at the smallest current to minimize the relative uncertainty. The model, under the same conditions, yields a force of $1.60 \times 10^{-16} dynes/gauss$ along the (1,1,1) diagonal (the direction of observation); using $B' = 3.5 gauss/cm$ at this current, we obtain $\kappa = 5.6 \times 10^{-16} dynes/cm$. The predicted diameter is then $2\sqrt{2E/\kappa} = 0.3 \pm .1$ mm, 60% smaller than the measured value. This discrepancy may point to the inadequacy of the model at higher intensities, where it does not completely account for the saturating effects of the beams which induce transitions but do not contribute to the net force. This causes the model to yield a larger value for the force, and consequently to predict a diameter which is too small. We unfortunately did not have the opportunity to measure the diameter at lower intensities for a more consistent comparison to the theory.

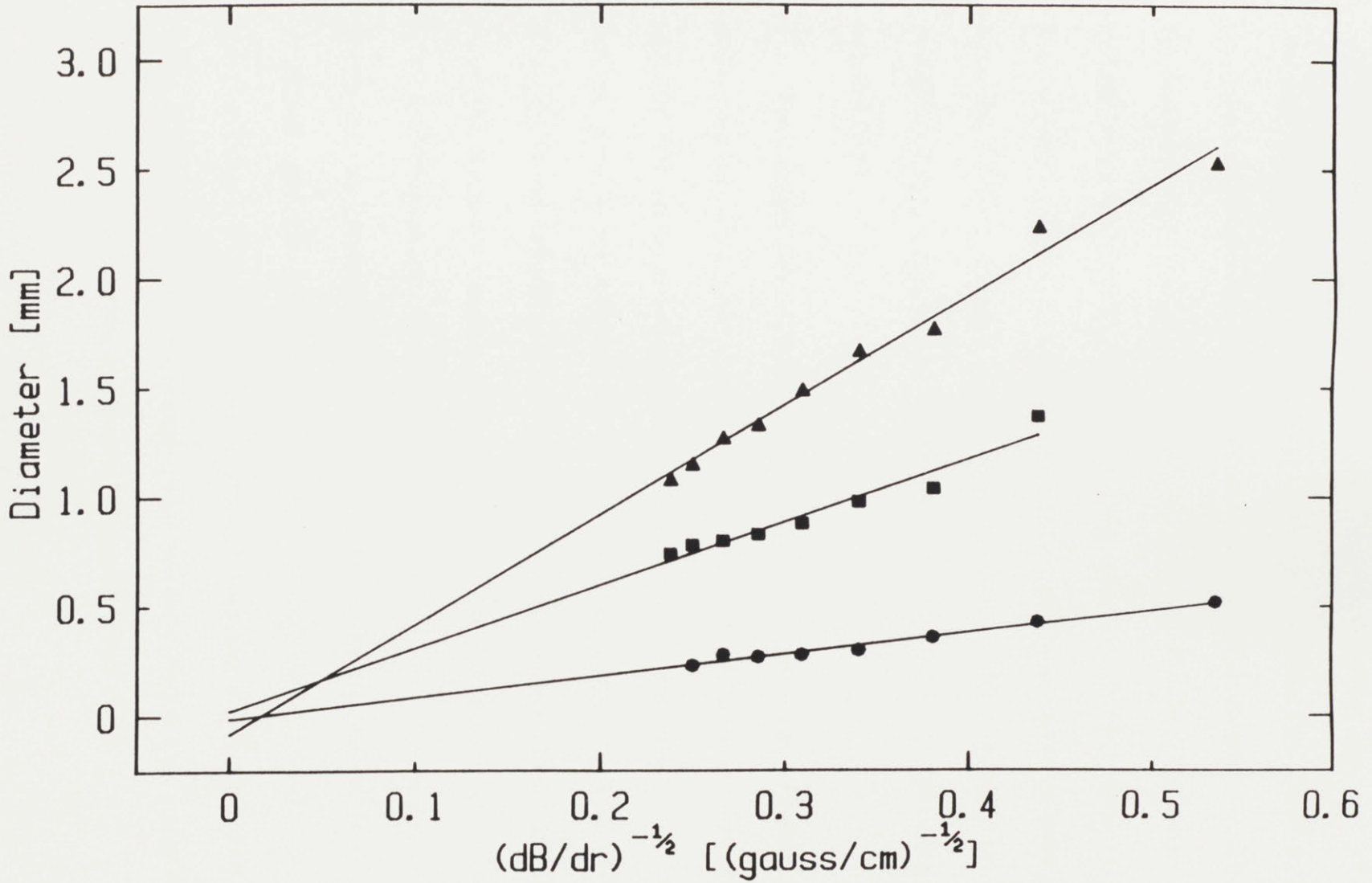

Figure III.5: The diameter of the trapped atom cloud (FWHM) as a function of the field gradient in the direction of measurement *dB/dr*. various laser tunings. The filled circles indicate tuning 8 MHz to the red of the F=2 to 3 and 1 to 2 transitions, with an intensity of 13 mW/cm^2 per sideband. The squares and triangles represent tuning 8 MHz and 20 MHz respectively to the red of the F=2 to 2 and 1 to 0 transitions, with an intensity of 15 mW/cm^2.

The diameters measured at the "secondary" trap tuning (red of the $F=1 \rightarrow 0$ and $F=2 \rightarrow 2$ transitions) were many times greater than those obtained for the "primary" tuning. There are a number of possible explanations for this: for one, the oscillator strength for $F=2 \rightarrow 2$ is less than the $F=2 \rightarrow 3$ by a ratio of 5:14. Perhaps more significantly, there are cycling transitions having $\Delta M_F = \pm 1$ in the $F=2 \rightarrow 3$ manifold which allow for efficient use of the circularly polarized trapping light; the $F=2 \rightarrow 2$ manifold has no such transitions. The latter also has a higher probability for decaying to the $F=1$ ground state, resulting in an even greater loss of trapping force.

Even though these effects were accounted for by our model, the agreement with experiment was not as good as it was for trapping with the "primary" transition. For a tuning 8 MHz to the red of resonance (indicated by the filled squares in Figure III.5) and an intensity per sideband of 15 mW/cm^2, we obtain $2r_{max} = 1.3 \pm 0.5$mm at $B' = 5\ gauss/cm$, assuming the same maximum temperature as above. The theoretical value for the force constant using our model with the appropriate parameters is $\kappa = 3.6 \times 10^{-18}\ dynes/cm$, which predicts a diameter of 4.6 ± 1.5 mm; this is ~3 times greater than the measured size. This discrepancy may point to the failure of the model to properly deal with a system that has several excited states relatively close together; the $F = 3, M_F = 1$ hyperfine level is separated from the $F = 3, M_F = 2$ by only 15 MHz. Stimulated effects and possibly "blue molasses" might play a significant role under these conditions. Our results are summarized in Table III.1.

Tuning	dB/dr (G/cm)	r_{pred} (mm)	r_{meas} (mm)
-8MHz from 2→3, 1→2	3.5	.15 ±.05	.25 ±.03
-8MHz from 2→2, 1→0	5	2.3 ±1.5	.69 ±.03
-20MHz from 2→2, 1→0	3.5	2.3 ±1.5	+1.27 ±.03

Table III.1: Comparison of model predictions of the trap radius r_{pred} with experimental measurement r_{meas}. The size of the trapped cloud is assumed to be defined by atoms with a temperature of 1 mK. Possible explanations for the discrepancies are given in the text.

By simultaneously measuring the size of the trapped cloud and the number of trapped atoms (cf. III.3.3), we can determine the density of the gas. The highest measured density was ~10^{11} atoms/cm^3. Such a density could be achieved only by optimizing the loading procedure: the solid angle subtended by the slowing laser was increased, and the fraction of light diverted from the trapping beams for the slower was decreased. Due to losses quadratic in the density, however, very high densities could not be maintained for longer than ~.1 sec. These density measurements were later corroborated by Cable and Prentiss by measuring the absorption of a weak, resonant probe beam by the trapped atoms (PRC87); this marked the first absorption measurement performed on trapped neutral atoms.

III.3.5 Trapping with the Quadrupole Magnet Exclusively

The magnetic field configuration used in this experiment to allow the lasers to form a light trap can also be used to confine cold "spin-up" atoms when the light is off. This fact is evident from the energy of atoms with magnetic dipole moment $\vec{\mu}_B$ in a static magnetic field $\vec{B}$: $U = -\vec{\mu}_B \cdot \vec{B}$. Atoms whose magnetic moments are aligned with the field will be drawn to the field minimum; atoms with anti-aligned moments will be expelled. In fact, it is impossible to create a static magnetic field with a local maximum (WIN84), so strong-field-seekers cannot be trapped magnetically. Our field configuration is identical to the "spherical quadrupole" used by Migdall *et al.* to confine a gas of spin-polarized sodium atoms (MPP85), though the maximum field

they used was ~100 times greater than ours.

Even though our trap was much shallower than the Migdall trap, it was deep enough to contain atoms that has already been captured and cooled by the optical trap. We showed in II.1.5 that the minimum temperature of sodium in a weak 3-dimensional standing wave tuned slightly to the red of resonance is ~0.3 mK. With a current through the magnets of ~60 amps, the field at the edge of the coils was ~30 *gauss*, corresponding to a depth of 2 mK. We therefore expect that most of the atoms whose spins are aligned with the field will remain trapped when the light is shut off.

The numerical model in II.3.5 was used to calculate the expected fraction of spin-aligned atoms for various values of the magnetic field. Figure III.6 shows the expected population distribution close to the center of the trap. We note that even at zero field, optical pumping forces most of the population into the $F=2, M_F=\pm 2$ "stretched states," so called because all the spins are aligned and "stretched" out along the quantization axis. Those atoms in the $M_F=2$ state (and some in $M_F=1$) will be trapped by the magnetic field; all others will either be anti-trapped, or too weakly bound to overcome their kinetic energy. Since virtually all of the atoms see a field less than 1 *gauss* (with the light on), we estimate that roughly 35% of all the optically trapped atoms will relax to the $F=2, M_F=2$ ground state after excitation.

Data were taken by first trapping the atoms in the light trap and measuring their initial fluorescent brightness. The trapping laser beams then were shut off for an

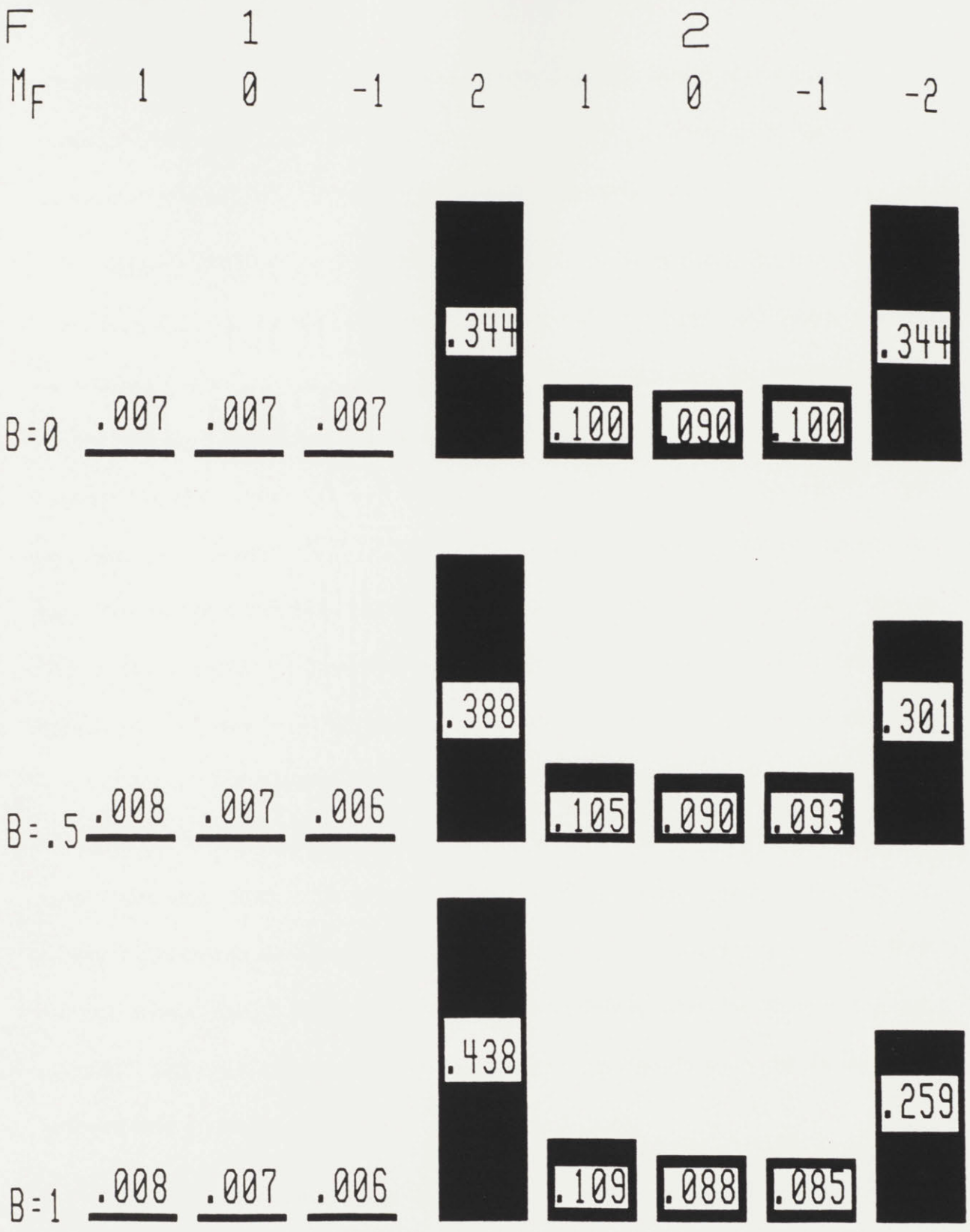

Figure III.6: Populations of the ground state Zeeman levels as a function of magnetic field (given in gauss). Even when B=0, ~69% of the population resides in the F=2, $M_F = \pm 2$ "stretch states." As the field increases, the population is driven to the states which are Zeeman shifted closest to resonance with the lasers. For negative values of the field (not shown here), the populations are reversed with respect to $\pm M_F$.

adjustable amount of time by momentarily stopping the RF to one of the acousto-optic modulators upstream. The light was then turned back on, and we again measured the fluorescence from the trap to compare with the initial level.

Some of our results are shown in Figure III.7. At early times, the loss of atoms is dominated by those atoms which are not confined by the magnet and therefore leave the trapping region (nearly) ballistically. (Some are actually *expelled* by the magnet, but the velocity gained from this is small compared to their initial velocity). We can estimate the mean velocity $\overline{v}$ of the trapped atoms by noting that about half of the untrapped atoms leave within ~15 ms. If we assume a capture radius of ~1±0.1 cm, we obtain a $\overline{v}$ of 65±5 cm/s, corresponding to a temperature of 0.5-0.7 mK. This is slightly greater than the theoretical minimum temperature of .5 mK for a two-level system as calculated in II.1.5 for our experimental conditions of low intensity and $\delta = -10$ MHz. The elevated temperature might be a consequence of optical pumping which causes a moving atom to absorb some photons from the wrong (non-damping) beam. For later times, it is evident that some of the atoms remain trapped by the spherical quadrupole field exclusively. They display a time constant of ~0.3s for both currents shown, though more atoms appear to be confined when the magnet has *less* current. This is probably an indication of the increased capture radius of the light trap at lower field gradients.

The actual time constant for decay might be many times larger than this value, however. If we simply blocked the laser beams with a card instead of chopping them

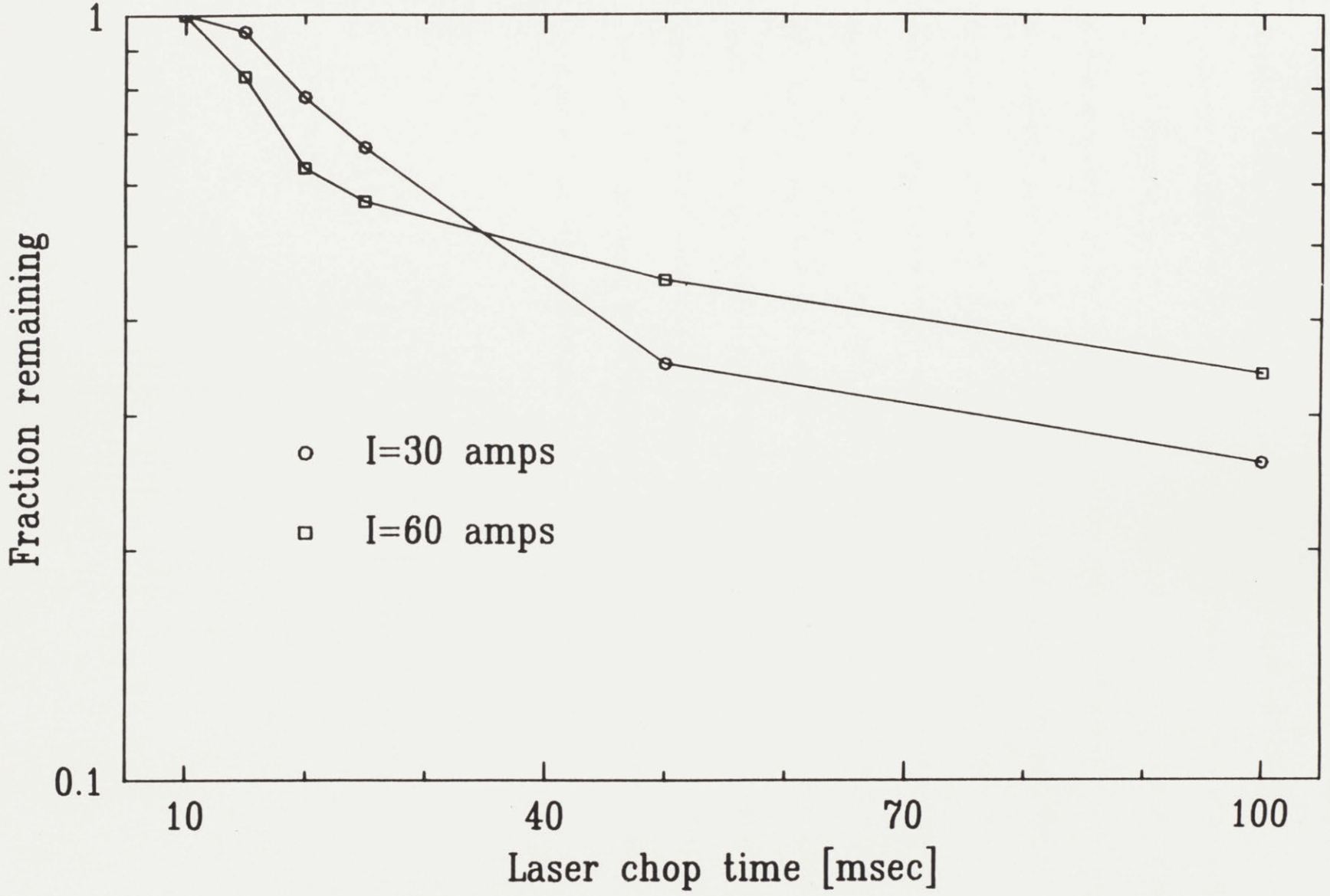

Figure III.7: Relative fraction of the atoms remaining in the trap after the lasers were shut off for various lengths of time ("chop time"). There is a hint of two decay times: one for the atoms not confined by the magnetic field exclusively, and a longer one for the spin-aligned atoms which are confined. Data were taken with A-O shutters which may not have had sufficient extinction.

by turning off the acousto-optics modulator, we would record significantly longer lifetimes. Figure III.8 shows a reproduction of data taken by the latter method. Because of the imprecise nature of chopping the beams manually, we were not able to extract a value for the 1/e time of decay in the magnetic trap; atoms were visible for a manual chop time as long as 10 seconds, however, compared to less than 1 second for the modulator chopped beam. A plausible explanation for the discrepancy is that some of the light was leaking through the acousto-optic modulator even when the RF was off. If we assume an extinction ratio of 10^8 (as quoted by the manufacturer, for two modulators in series), then light which would get through would be too weak to provide any confinement force, yet would still be able to induce 1 transition every few seconds. Since this transition may take the atom from a trapped state to an untrapped one, the apparent lifetime of the magnetically trapped atoms would be diminished. Unfortunately, the timing of the collaboration prevented a more careful study of this phenomena from being undertaken.

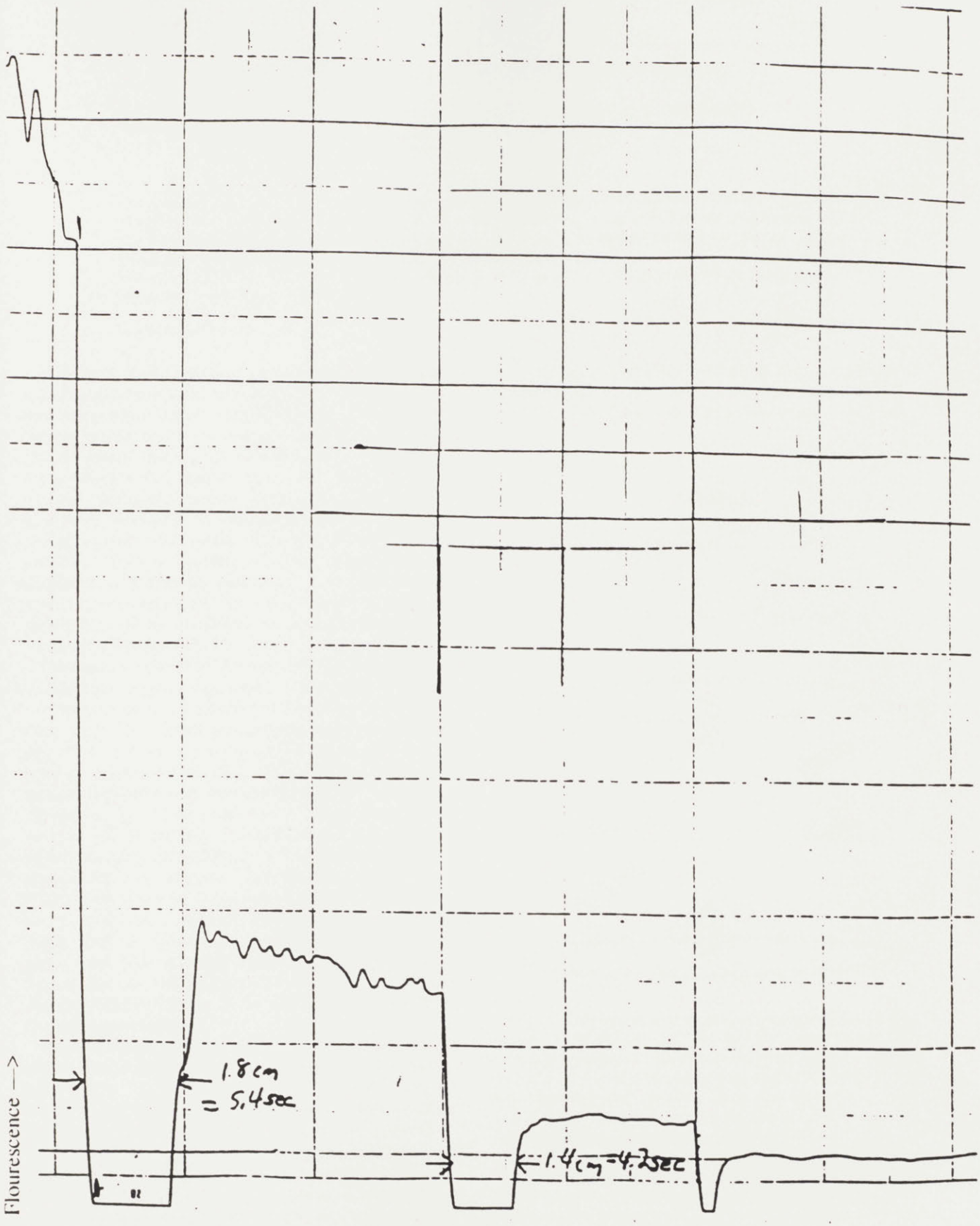

Figure III.8: Manual chop data. A sizable fraction of atoms rmained in the trap after the laser beams were blocked with a card for several seconds.

VOLUME 59, NUMBER 23 PHYSICAL REVIEW LETTERS 7 DECEMBER 1987

Trapping of Neutral Sodium Atoms with Radiation Pressure

E. L. Raab,[a] M. Prentiss, Alex Cable, Steven Chu,[b] and D. E. Pritchard[a]
AT&T Bell Laboratories, Holmdel, New Jersey 07733
(Received 16 July 1987)

We report the confinement and cooling of an optically dense cloud of neutral sodium atoms by radiation pressure. The trapping and damping forces were provided by three retroreflected laser beams propagating along orthogonal axes, with a weak magnetic field used to distinguish between the beams. We have trapped as many as 10^7 atoms for 2 min at densities exceeding 10^{11} atoms cm^{-3}. The trap was $\approx$0.4 K deep and the atoms, once trapped, were cooled to less than a millikelvin and compacted into a region less than 0.5 mm in diameter.

PACS numbers: 32.80.Pj

The ability to cool and trap neutral atoms has recently been demonstrated by several groups.[1-3] Their traps utilized the intrinsic atomic magnetic dipole moment or the induced oscillating electric dipole moment to confine sodium atoms about a local-field strength extremum. We report the first optical trap which relies on near-resonant radiation pressure (also called *spontaneous* light force, in contrast to *induced* light forces[4]) to both confine and cool the atoms. The trap has an effective depth of about 0.4 K, about 10 times deeper than the deepest traps previously reported.[3] It is the first trap which exploits an atom's internal structure to induce a greater absorption probability for light moving toward the center of confinement.[4,5]

The basic principle of the trap can be illustrated by considering a hypothetical atom with a spin $S=0$ ($m_s=0$) ground state and a spin $S=1$ ($m_s=-1,0,+1$) excited state. In a weak inhomogeneous magnetic field $B_z(z)=bz$, the energy levels are Zeeman split by an amount $\Delta E=\mu m_s B=\mu b m_s z$ [Fig. 1(a)]. Now illuminate the atom with weak, collimated σ^- light propagating in the $-\hat{z}$ direction and σ^+ light propagating towards $+\hat{z}$. If the laser is tuned below the $B=0$ resonance frequency, the atom at $z>0$ will absorb more σ^- photons than σ^+ photons (since the laser frequency is closer to the $\Delta m=-1$ transition frequency) and consequently will feel a net time-averaged force toward the origin. For an atom at $z<0$, the Zeeman shift is reversed, and the force will again be directed to $z=0$. Tuning the low-intensity laser to the red of resonance also provides damping, as in the "optical molasses" demonstrated previously.[6]

The scheme is readily extended to three dimensions by adding counterpropagating beams along the x and y axes, and a "spherical quadrupole" magnetic field as shown in Fig. 1(b). The field is of the type used by Migdall *et al.* to confine spin polarized atoms magnetically,[1] though the field magnitudes in the light trap are about 100 times smaller and contribute negligibly to the confining force. If the x and y axis beams are polarized as shown, the conditions for confinement will be satisfied independently along each of the three axes.

The method can also work for atoms with a more complicated hyperfine structure. In the case of the sodium $3S_{1/2}$-$3P_{3/2}$ transition, e.g., the ground states have total

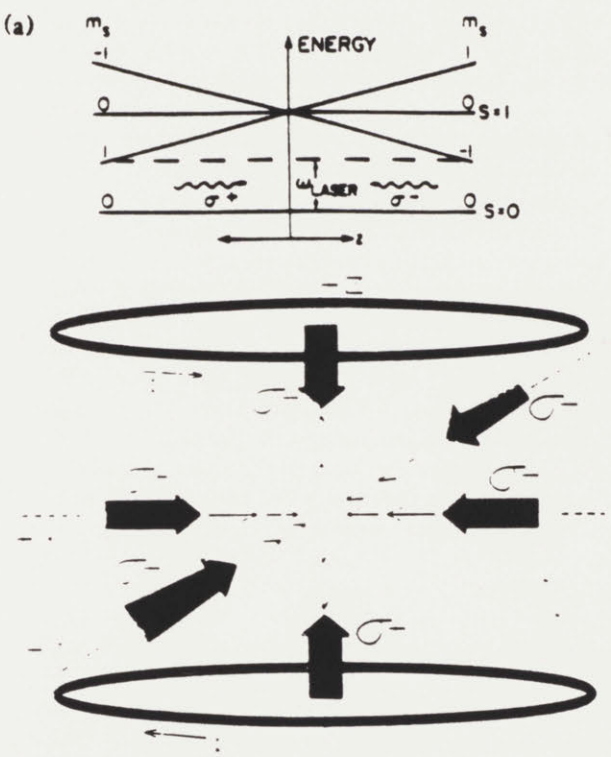

FIG. 1. (a) Energy-level diagram of hypothetical atom having spin $S=0$ ground state and spin $S=1$ excited state, immersed in a magnetic field $B_z(z)=bz$. The frequency and polarization of the counterpropagating laser are chosen to produce damping and restoring forces for the atom's z-axis motion. (b) Trapping scheme in three dimensions. The "spherical quadrupole" field is generated by two coils of opposing current placed along the z axis approximately as shown. The field along the axes, indicated by the light arrows, is parallel to its respective axis. Laser light, indicated by the heavy arrows, counterpropagates along x, y, and z, and is polarized as shown with respect to the axis of propagation.

angular momentum $F=2,1$ and the excited states have $F'=3,2,1,0$. Figure 2 shows the results of a computer model of the trap where the average force in one dimension was calculated for several magnetic field strengths and atomic velocities. Two laser frequencies are used in the model to avoid optically pumping the atom into an inaccessible ground hyperfine state. The results show the presence of both restoring and damping elements of the force. If we consider small displacements and velocities, we may write $F \approx -\kappa x - \alpha \dot{x}$; the model in this regime gives $\kappa = (dB/dz)2.67\times10^{-16}$ dynes cm^{-1}, and $\alpha = 6.07\times10^{-18}$ dynes/cm s^{-1}. The equation of motion for small oscillations about the origin is simply that of a damped harmonic oscillator: $\ddot{x}+2\beta\dot{x}+\omega_0^2 x=0$, where $\omega_0^2 \equiv \kappa/m$, $\beta \equiv \alpha/2m$, and m is the mass of the atom. If we assume a nominal field gradient of 5 G/cm, we obtain $\omega_0 \approx 6\times10^3$ s^{-1}, and $\beta \approx 8\times10^4$ s^{-1}. Thus, the motion is strongly overdamped; the relaxation to the origin (at this gradient) is governed by a time constant $\tau_{\text{simul}} \approx 2\beta/\omega_0^2 \approx 4$ ms. The model was also used to examine the case when the atom ventures off from the principal axes, where the additional complication of $\Delta m = 0$ transitions arises. It was found that the trap was indeed restoring for small displacements in any direction.[7]

The spontaneous-light-force trap described above was demonstrated in the same apparatus previously used to generate optical molasses,[6] with only a few modifications. Six antireflection-coated quarter wave plates were placed adjacent to the six windows to generate circularly polarized light and to reverse the polarization of the reflected beams. Also, a pair of coils with opposing current was positioned within the vacuum chamber to generate the desired magnetic field. Each 5-cm-diam coil consisted of three turns of $\frac{1}{4}$-in.-o.d. copper refrigerator tubing sheathed in fiberglass insulation. Water was passed through the coils for cooling.

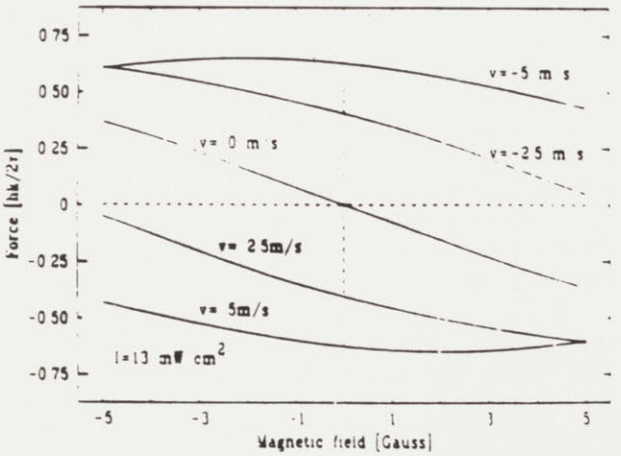

FIG. 2. Result of computer model for the forces felt by a sodium atom along the z axis in the light trap. The lasers are tuned 10 MHz to the red of the $F=2$ to 3 and 1 to 2 transitions in the $D2$ line, with an intensity of 13 mW/cm^2 per sideband. $k=2\pi/\lambda$, $\tau=16$ ns is the natural lifetime for the sodium $D2$ line; $\hbar k/2\tau = F_{\max} = 3.5\times10^{-15}$ dynes, the maximum theoretical spontaneous force attainable with this transition.

Improvements were made in the remaining apparatus to increase its reliability and repeatability. The ring dye laser was actively locked to a crossover resonance of the Na $3S_{1/2}$-$3P_{3/2}$ transition in a saturated absorption cell. This allowed us to determine the laser frequency accurately and to provide the frequency stability necessary to observe atoms that remain in the trap for half an hour or more. A 5-m single-mode optical fiber was used as a spatial filter for the trapping beams; this also improved their pointing stability (and day to day alignment) since spatial drift of the dye laser output could be compensated by minor changes in the input coupling of the fiber. We used a larger $1\times1\times20$-mm^3 $LiTaO_3$ crystal as an electro-optic modulator to provide optical sidebands with a minimum of beam distortion. The crystal was driven by a resonant circuit tuned to 856 MHz with $Q\simeq100$, allowing us to maximize the fraction of light in the two first-order sidebands ($\simeq70\%$ total) with an rf drive power of less than 0.5 W.

The trap was loaded with atoms evaporated by a pulsed yttrium-aluminum-garnet laser and cooled by a frequency-swept laser beam as previously described.[6] Once slowed to velocities less than 2×10^3 cm s^{-1}, the atoms drifted into the molasses region and were trapped. The combination of restoring and damping forces compressed the trapped atoms into a small bright ball. Since the storage time of the atoms in the trap was considerably longer than the 10-Hz rate of the pulsed atomic beam, many ($\simeq100$) pulses of atoms could be injected into the trap before an equilibrium density was achieved.

Trapping was observed over a wide range of conditions. With a fixed 1712.4-MHz optical sideband splitting, the laser frequencies were tuned to the red of the $F=2\rightarrow3$ and $1\rightarrow2$ transitions or the $F=2\rightarrow2$ and $1\rightarrow0$ transitions. The former tuning produced a much more compact ball of atoms than the latter. For a fixed light intensity and a variety of laser detunings and magnetic field strengths, the size of the atom cloud, measured with a video camera and video wave-form analyzer, is shown in Fig. 3. The resolution of the camera system was better than 200 μm. We found that the diameter of the trapped atom cloud varies inversely as the square root of the current, consistent with our model of a harmonic trap potential and an atomic temperature independent of the current. Using a independent measure of the temperature (described below), we obtain a force constant of $8.8B'\times10^{-17}$ dynes cm^{-1}; When $B'=5$ G cm^{-1}, this implies an oscillation frequency $\omega_0=3.4\times10^3$ s^{-1} when trapping with the stronger transition. The results are thus in accord with the predictions of the model.

The restoring and damping forces were studied by

VOLUME 59, NUMBER 23 PHYSICAL REVIEW LETTERS 7 DECEMBER 1987

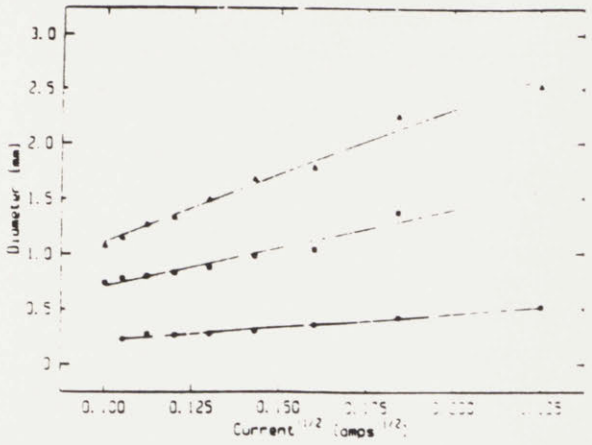

FIG. 3. The trap size (FWHM) as a function of the current through the magnets, for various laser tunings. The circles represent tuning 8 MHz to the red of the $F=2$ to 3 and 1 to 2 transitions, with an intensity of 13 mW/cm^2 per sideband. The squares and triangles represent tuning 8 and 20 MHz to the red of the $F=2$ to 2 and 1 to 0 transitions, respectively, with an intensity of 15 mW/cm^2.

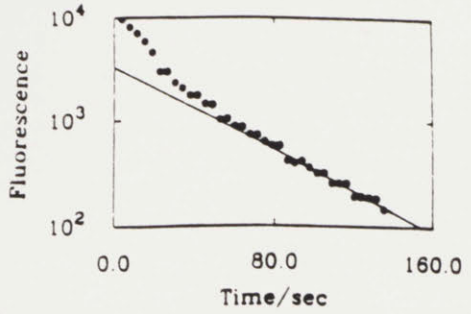

FIG. 4. Decay of atoms from the trap. The magnetic field gradient was $\simeq 12$ G cm^{-1}, and the laser intensity was $\simeq 20$ mW/cm^2 per sideband. The pressure was $\simeq 5\times10^{-11}$ Torr. The line indicates an exponential decay having a time constant of 95 s, which we observed at lower densities.

pushing the atoms from the center of the trap, then releasing them and allowing them to reequilibrate. Their relaxation to the origin was detected by placing an aperture around the image of the trap at equilibrium. Light passing through the aperture was detected by a photomultiplier tube; when the atoms were displaced from equilibrium, the signal from the photomultiplier tube would decrease. Two methods were used to displace the atoms: Either a neutral density filter was placed in one of the retroreflected beams (the trap was stable for a total attenuation of 0.6), or a cw probe laser was introduced (stability was destroyed for $I > 0.1 I_{sat}$). The maximum displacement was $\simeq 1$ mm. With a field gradient of 5 G cm^{-1}, both measurements yielded a restoring force of $\simeq 10^{-14}$ dynes cm^{-1} when $I = 10$ mW/cm^2 per beam (in each sideband) and $\delta = -10$ MHz, giving an oscillation frequency of $\omega_0 = 1.5\times10^4$ s^{-1}. This is approximately 2 times larger than ω_0 obtained from the model results at the higher intensity, which is fair agreement considering the experimental uncertainty and theoretical simplifications.

Once the trap was fully loaded, the yttrium-aluminum-garnet laser and chirped laser pulses were turned off, and the decay of the trap fluorescence was recorded as shown in Fig. 4. The longest lifetimes ($1/e$ $\simeq 2$ min) were recorded at pressures of 5×10^{-11} Torr, achieved by cooling a cooper shroud inside the vacuum chamber to liquid-nitrogen temperatures. For low densities or later times ($t > 5$ s), the decay curve approached a simple exponential whose time constant decreased with increasing background pressure. This indicates that atoms were being expelled from the trap by collisions with the background gas. The initial decay for higher densities was dominated by a loss which can be fitted to the square of the density of the trapped atoms. A detailed study of this loss mechanism will be presented in a future publication.

By measuring the absorption of a weak, resonant probe beam with the trapping light both on and off, we determined the ratio of the average excited-state population to the average ground-state population under various experimental conditions. With a magnet current of 50 A (corresponding to $B' \simeq 10$ g cm^{-1} along z) and tuning to the red of the stronger ($F=2\rightarrow3$, $1\rightarrow2$) transitions, e.g., we found this ratio to be $\simeq 3{:}4$. Measurements of the absolute fluorescence from the trapped atoms with a calibrated photomultiplier tube and lens assembly then implied that 3×10^6 atoms could be confined to a region $\simeq 320$ μm in diameter (FWHM). Thus the atomic density is 1.8×10^{11} atoms cm^{-3}. When the laser was tuned to the red of the $F=2\rightarrow2$ transition, the number of atoms trapped was $\simeq 1.2\times10^7$ with a trap diameter of 1 mm, giving a density of $\simeq 2\times10^{10}$ atoms cm^{-3}. The absorption of the probe beam was also used as an independent measure of the density. The peak absorption observed was 80% through $\simeq 300$-μm path which, with the assumption of a simple two-level atom, corresponds to a density of roughly 5×10^{10} atoms cm^{-3}. It is important to note that the rapid nonexponential loss mechanism seen at higher densities is responsible for keeping the atomic densities below 10^{12} atoms cm^{-3} under the present loading conditions. By adjustment of experimental parameters to limit the density of atoms (misalignment of the trapping beams, the tuning to the weaker transition, and the use of weak light intensities and field gradients), up to 10^8 atoms have been contained.

The effective depth of the trap was measured by giving the trapped atoms an impulse from an additional beam while the trapping lasers were momentarily off. We find that with an intensity per side band of 30 mW/cm^2, a

light pulse of 18 μs was necessary to eject $\simeq$80% of the atoms from the trap. Thus, atoms at the center of the trap require a velocity of $\simeq$1600 cm s^{-1} to escape, implying a trap depth of $\simeq$0.4 K.

We have also measured the fraction of atoms that remain in the trap after the molasses beams have been shut off for various times. At early times, the loss is dominated by atoms that leave the trapping region ballistically before the light is turned back on. We can estimate the mean atomic velocity $\bar{v}$ by observing that half the atoms are lost in the first 15 ms of darkness; if we assume a capture radius of 1 cm, we obtain a $\bar{v}$ of 45 to 85 cm s^{-1}, corresponding to a temperature of 300 to 1000 μK. Trapping with the $2 \rightarrow 2$ transition produced a gas 2 orders of magnitude hotter than trapping on the $2 \rightarrow 3$ transition.

The trap is very robust and does not critically depend on balanced light beams, purity of the circular polarization, or laser frequency (the trap worked over a 25-MHz tuning range). Trapping was observed for peak magnetic fields as low as 5 G and laser intensities ranging from 30 to 0.4 mW/cm^2. We were able to load the trap without the use of the chirped slowing laser by capturing atoms in the slow velocity tail of the pulsed atomic beam. When the laser beams were slightly misaligned, the potential well was no longer simply harmonic, causing the atoms to swirl around in rings or form irregular shapes. The atoms would sometimes settle into one of several local potential minima, and could be made to oscillate between them.

To summarize, we have trapped over 10^7 neutral atoms for over 2 min. We utilized a magnetic field to tune the atomic resonance, enabling radiation pressure to provide both cooling and damping forces. The confinement volume is several cubic centimeters and the effective depth is $\simeq$0.4 K. The density of atoms is $\simeq 2 \times 10^{11}$ atoms cm^{-3} at a temperature of $\simeq$600 μK.

We are extremely grateful to Jean Dalibard for giving us the seminal idea for this trapping scheme. This work was partially supported by the U.S. Office of Naval Research, Grant No. N00014-83-K-0695.

---

[a]Permanent address: Department of Physics and Research Laboratory of Electronics, Massachusetts Institute of Technology, Cambridge, MA 02139.

[b]Current address: Physics Department, Stanford University, Palo Alto, CA 94305.

[1]A. Migdall, J. Prodan, W. Phillips, T. Bergeman, and H. Metcalf, Phys. Rev. Lett. 54, 2596 (1985).

[2]S. Chu, J. Bjorkholm, A. Ashkin, and A. Cable, Phys. Rev. Lett. 57, 314 (1986).

[3]V. Bagnato, G. Lafyatis, A. Martin, E. Raab, and D. Pritchard, Phys. Rev. Lett. 58, 2194 (1987).

[4]D. E. Pritchard, E. L. Raab, V. Bagnato, C. E. Wieman, and R. N. Watts, Phys. Rev. Lett. 57, 310 (1986).

[5]S. Chu, M. Prentiss, J. Bjorkholm, and A. Cable, in *Laser Spectroscopy VIII*, edited by S. Swanberg and W. Pearson (Springer-Verlag, Berlin, 1987).

[6]S. Chu, L. Hollberg, J. Bjorkholm, A. Cable, and A. Ashkin, Phys. Rev. Lett. 55, 48 (1985).

[7]Proceedings of International Laser Science Conference II, October, 1986 (to be published).

CHAPTER IV — THE M.I.T. APPARATUS

IV.1 Introduction

Following the success of the spontaneous force light trap at Bell Labs, we decided to build a similar but improved trap at M.I.T. The M.I.T. trap design has two fundamental differences from the design of the Bell trap. One, it is contained in a cryogenic dewar cooled to 4.2K with liquid helium. This allows us to use superconducting magnets for the trapping coils, which are capable of field gradients ~200 times greater than the gradients achieved in the Bell device. This in theory would yield a trap with ~200 times the restoring force. The presence of liquid helium also guarantees an excellent vacuum in the experimental region, due to the high-speed "cryopumping" by the ultra-cold surfaces. The second difference of the M.I.T. design is that it will load the atoms into the trap continuously, instead of the pulsed loading scheme used at Bell. This has the potential to fill the trap ~10 times faster, netting a corresponding increase in the density of the trapped atoms, or in the rate of collisions which limit the density.

In this chapter we will present the design of the M.I.T. apparatus. We will discuss the physical dimensions, theory of operation, and expected performance of each component as appropriate.

IV.2 Overview

A schematic of the apparatus is shown in Figure IV.1. Its basic elements are, from bottom to top: an atomic source, a differentially pumped connection region, a LHe dewar, and horizontal and vertical optics tables.

The dewar is supported by a frame constructed mostly of 3"×5" cross-section aluminum I-beams (Ryerson Corp.). The frame is isolated from the vibrations of the floor by a 2" stack of rubber (Greene Rubber Co.) and wood. The distance from the floor to the top of the upper optics table is about 11 feet.

The general experimental procedure is as follows: A thermal atomic beam is created and collimated in the source region. The atoms enter the dewar through the port on the bottom flange and are illuminated head-on by a focused, single-frequency laser beam which shines through the window at the top. The atoms are shifted into resonance with the laser by the superconducting magnets in the atom-slower region, begin to absorb light, and slow down. As they slow, their resonance frequency is tuned by the spatially varying magnetic field so that they remain resonant and continue to scatter light and decelerate (PPM82). They will ultimately be brought to rest in the trapping region.

The trapping region is illuminated by three pairs of counter-propagating laser beams. One beam enters the dewar through the top window, passes through the trap region, and comes to a focus just to the side of the source channel where it is

Overall view

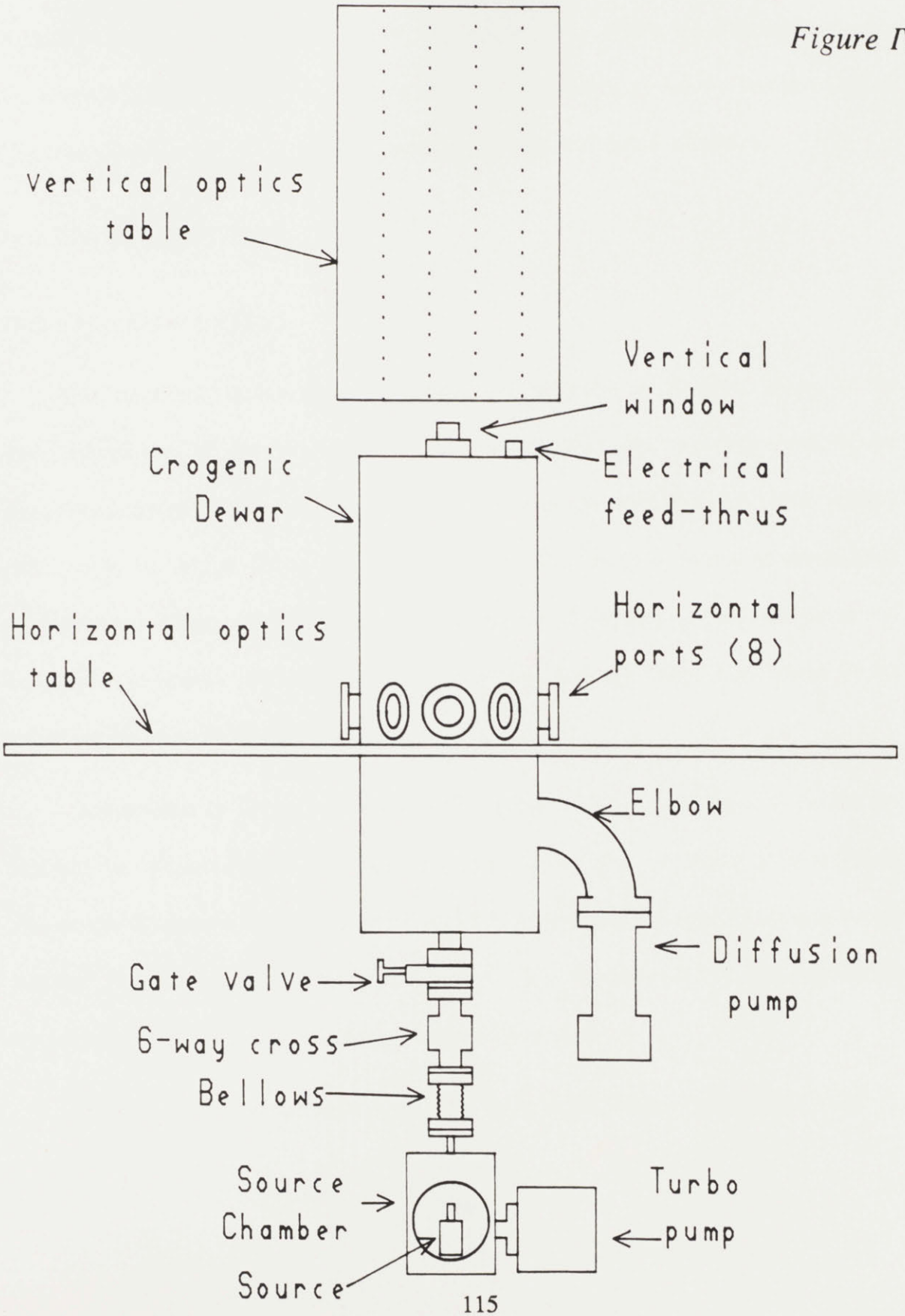

Figure IV.1

retroreflected by an adjustable mirror. The other two pairs enter the dewar through horizontal windows in the plane of the trapping region. When the trapping magnets are energized, these beams will create a radiation pressure trap for the stopped atoms. The atoms can be viewed through the remaining three horizontal windows.

IV.3 The Cryogenic Dewar

IV.3.1 Physical Description

The cryogenic dewar, built by Andonian Cryogenics of Newton, Mass., is the main component of the experiment. Andonian supplied the standard parts of the dewar, and designed and constructed custom parts to our specifications. The guiding principle in the design of this and most cryogenic systems is to minimize the boil-off of expensive liquid helium while maximizing its flexibility within the scope of intended experiments. We shall describe the dewar in rough detail, elaborating on the techniques used to fulfill this principle.

A schematic of the dewar is shown in Figure IV.2. It consists of three distinct regions: the vacuum region, the liquid nitrogen dewar, and the liquid helium dewar. The design is unusual in that it allows optical access along five axes to helium-cooled surfaces in roughly the center of the dewar. This is essential for our application because that is the location of the spontaneous force trap.

The outermost tube is made of stainless steel, 8-5/8" O.D., ~3/16" wall, 64.5"

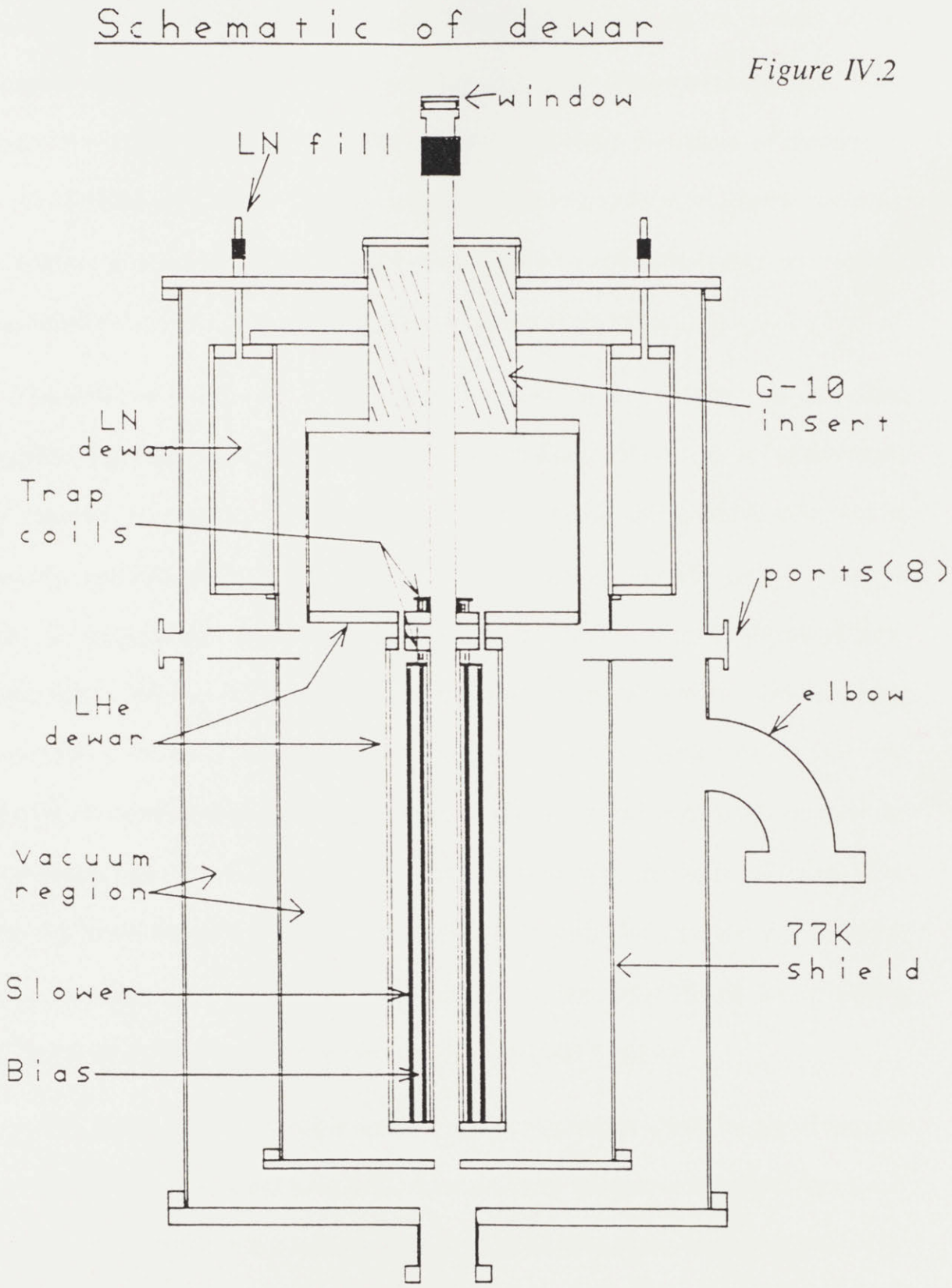
Schematic of dewar
window
LN fill
G-10 insert
LN dewar
Trap coils
ports(8)
elbow
LHe dewar
Vacuum region
77K shield
Slower
Bias

Figure IV.2

length. There is a steel band on the inside just underneath the windows for reinforcement, to prevent the tube from buckling under atmospheric pressure. The centers of the windows are 40" from the bottom of the tube. The inside of the tube, as are *all* the major surfaces in the vacuum, is plated with gold to reduce the radiative emissivity. An intermediate heat shield between the LN_2 and LHe dewars was omitted because of Andonian's experience that they save very little LHe.

A diffusion pump (Varian HS-2) is connected to the chamber via an elbow extending from the outer wall just beneath the windows. The pump is isolated from the vacuum chamber by a water-cooled baffle (Varian 0332-F9453-302) and a manually operated gate valve (Varian 1298-K9938-332). The pump is used when we warm the liquid helium dewar from 4.2K to 77K but want to keep the liquid nitrogen dewar filled. Without the pump, this process would allow the gasses which had been condensed on the 4.2K walls, but now begin to evaporate, to significantly increase the pressure of the vacuum chamber and cause undesirable thermal conduction between the room-temperature and 77K surfaces, causing a large loss of liquid nitrogen. The pumping speed for helium is $\sim 340 l/s$, sufficient to keep the pressure at a desirable level. The gate valve is normally kept closed to prevent the pump oil (Dow-Corning DC704) from fouling the low-emissivity surfaces and the windows.

The liquid nitrogen dewar extends from the top of the dewar to just above the trap region. It has a capacity of $5.5 l$. Connected to the bottom of this dewar is an aluminum heat shield, which extends almost to the bottom of the vacuum region. The

shield has eight holes to permit observation of the trap region from the outside. If unabated, the radiative load from the 300K windows to the liquid helium region would be substantial; each window, approximately a blackbody in the infrared, emits ~¼*W*. To reduce this load, horizontal tubes are secured to the through holes, cutting down on the solid angle of the windows and hence the total room temperature radiation visible from the cold surface. Most of the heat, in fact, will radiate straight through to the opposite window.

The liquid helium dewar is composed of upper and lower sections. The upper section is primarily a storage reservoir for the LHe; it has a capacity of ~7*l*. The outer seal of its lower flange is made with 50:50 Pb:Sn solder, so the outer and inner parts of the upper section can be completely separated. This permits one to service the magnet, switches, and other components in the reservoir. The top part of the upper section has a smaller O.D. than the bottom part, and is connected to the LN_2 dewar with a high-conductivity aluminum flange ~2" from the top. This reduced diameter lessens the cross-section of conductive material between the 77K aluminum flange and the LHe, thus minimizing LHe boil-off.

An insert composed of fiberglass-impregnated epoxy (G-10) fills the region of reduced diameter; it has a thread helixing around the outside to serve as a heat exchanger between cold helium vapor boiling up from the reservoir and current-carrying wires running down to the superconducting magnets. The benefit of this arrangement is two-fold: it increases the thermal path length of the wires, and

decreases ohmic losses (since the copper wires are less resistive at low temperatures). There are also several vertical holes in the insert for demountable current leads and the LHe transfer line.

The lower section of the LHe dewar contains the slower and bias solenoids, and is connected to the upper section by two 1/2"O.D.×.065"w stainless steel tubes. The wires from the solenoids are fed to the upper section through the 1/2" tube designated as the "vent." The other 1/2" tube is the "fill" tube; a separate thin-walled 3/16"O.D. tube runs from the bottom of the lower section through the "fill" tube to a flange in the upper section where it can mate with the LHe transfer line. The slower and bias magnets are mounted to the bottom flange, which in turn is sealed to the lower LHe section with pure indium solder (indium does not superconduct at 4.2K). Sufficient room was left in this region for another magnet, such as a quadrupole magnet for focusing the atomic beam.

A future trap design might entail placing superconducting magnets in the vacuum region between the upper and lower sections of the LHe dewar. This would allow us to create extremely large or otherwise extraordinary fields in the region of the trapped atoms. These magnets would be heated primarily by radiation from the windows, and cooled by thermal conduction to the 4.2K walls of the LHe dewar. In order to provide a good thermal sink for these magnets, a disc-shaped area was machined away from the stainless steel flanges facing the trap region, leaving only a ~1/8" thickness of the poorly conducting alloy (see detail, Figure IV.3). To retain the

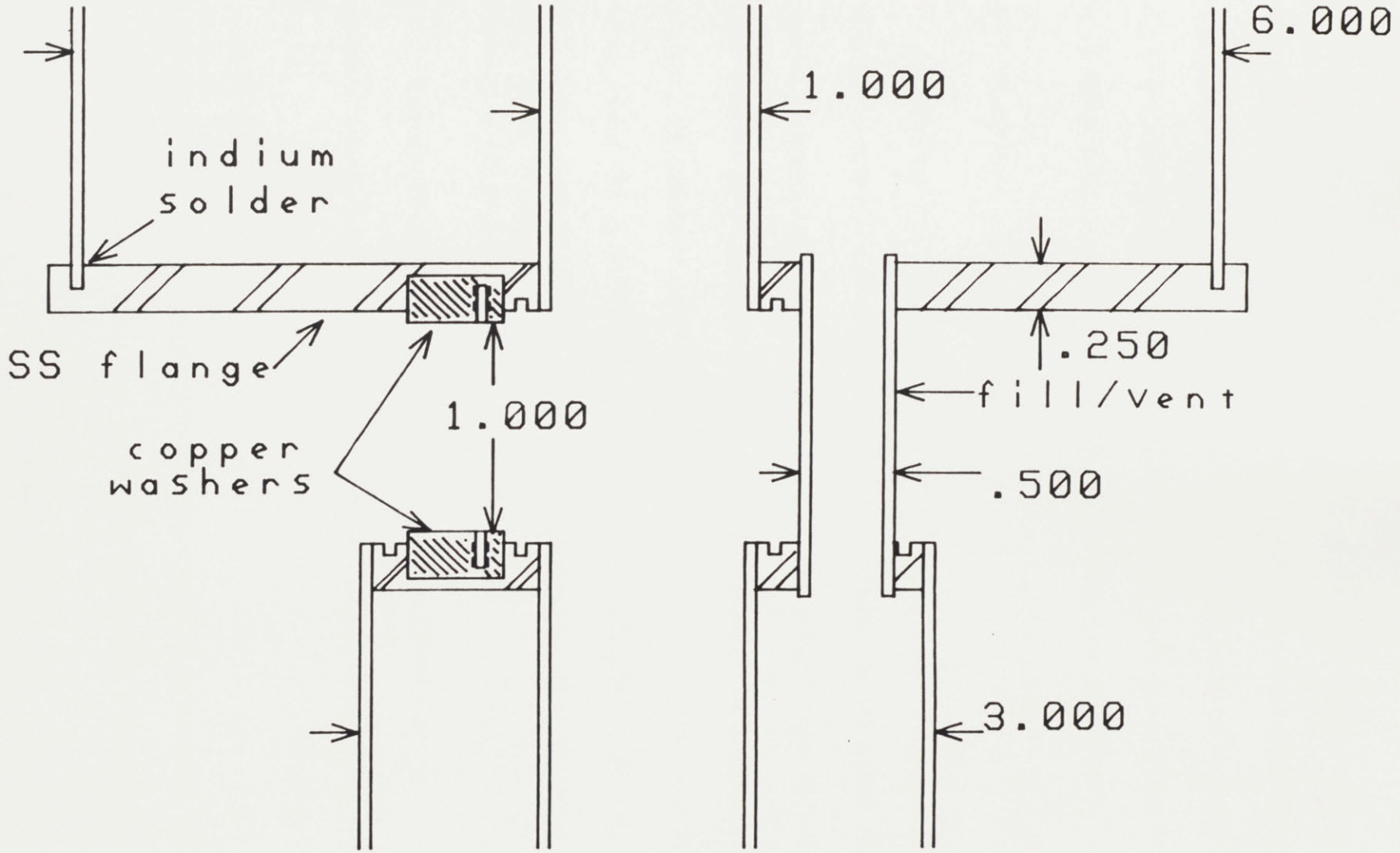

Figure IV.3 Detail of trap region

mechanical strength of the flanges, a "split washer" of OFHC (oxygen-free high conductivity) copper was indium soldered into each of the two thinned-out areas. A bolt circle was tapped into each washer to allow the magnets to be securely fastened to the LHe dewar; an indium gasket would be used to ensure good contact between the metal surfaces between these washers and any future magnet assembly.

IV.3.2 Loss Rate of the Liquified Gases

Estimating the loss rate of LN_2 and LHe from their respective containers is basically a matter of accounting for all the sources and sinks of heat in the pertinent system, and applying the conservation of energy. In general, there are two dominant heat sources on a particular storage reservoir: radiation from higher temperature surfaces, and thermal conduction down the neck supporting the reservoir from the top of the dewar. There are three ways to remove heat: boiling the liquid (using the latent heat of vaporization), warming the gas vapors as they rise out of the dewar (using the enthalpy of the gas), and radiating to a colder surface.

The rate of heat transfer $\dot{Q}$ due to thermal conduction along a solid of cross-sectional area A, length L, and thermal conductivity $\lambda(T)$ is given by

$$\dot{Q} = \frac{A}{L}\int_{T_1}^{T_2}\lambda(T)\,dT \qquad (1)$$

where T_1 and T_2 are the temperatures of the two ends of the material. We can write this in the useful form $\dot{Q} = (A/L)(I(T_1) - I(T_2))$, where the integrals

$I(T_0) \equiv \int_{T_0}^{T_{ref}} \lambda(T)dT$ have been determined for a number of common materials (Table IV.1 (HAN87)). We note that of the metals, OFHC copper is the best and stainless steel the worst thermal conductor in the temperature range of interest.

The radiative heat transfer between two surfaces with emissivities $\varepsilon_1, \varepsilon_2$, temperatures T_1, T_2, and common surface area A is given by (AND81)

$$\dot{Q} = \sigma A \frac{\varepsilon_1 \varepsilon_2}{\varepsilon_1 + \varepsilon_2} (T_2^4 - T_1^4) \qquad (2)$$

where $\dot{Q}$ is the rate of heat transfer and $\sigma = 5.67 \times 10^{-12} W \cdot cm^{-2} \cdot K^{-4}$ is the Stefan-Boltzman constant. Table IV.2 (HAN87) lists the emissivities of some common materials. The emissivity of a highly polished metallic surface will increase to 0.2-0.3 if it becomes coated with a light film of oil or frost. It is noteworthy that the intensity of 300K radiation peaks in the infra-red, where common glass is opaque: $\lambda_{peak} \sim hc/kT \sim 300 \mu m$.

A common strategy to reduce the radiative heat flow between two surfaces is to place ~10-30 layers of "super-insulation" between them (distributor: King Seeley Thermos Co., N.H.). This material consists of aluminized mylar, .00025" thick, and is crinkled to reduce the thermal contact between successive layers. If we assume that the thermal conduction is negligible, then N layers of super-insulation placed between two surfaces of fixed temperature and similar emissivity will reduce the heat flow between them by the factor N+1. An empirical formula which takes the conductivity

Table of thermal conductivity integrals

Temp K	OFHC Cu watts/cm	6063 Al watts/cm	Brass watts/cm	Stainless watts/cm	Manganese watts/cm	Nylon watts/cm	G-10 watts/cm	Glass watts/cm
6	6.1	.85	.05	.0063		.00032	.002	.0021
8	14.5	2.05	.13	.0159		.0008	.004	.0044
10	25.2	3.60	.23	.0293		.0015	.005	.0068
15	61.4	9.00	.59	.0816		.0041	.011	.0131
20	110	16.5	1.12	.163		.0082	.018	.0200
25	168	25.8	1.81	.277	.275	.0139	.026	.0279
30	228	36.5	2.65	.424	.635	.0208	.035	.0368
35	285	48.8	3.63	.607	1.06	.0290	.044	.0471
40	338	62.0	4.76	.824	1.54	.0385	.053	.0586
50	426	89.5	7.36	1.35	2.58	.0604	.070	.0846
60	496	117	10.4	1.98	3.74	.0859	.086	.115
70	554	143	13.9	2.70	4.98	.113	.102	.151
77	586	158	16.2	3.17	5.76	.131	.112	.175
80	606	167	17.7	3.49	6.28	.142	.120	.194
90	654	190	22.0	4.36	7.61	.173	.150	.240
100	700	211	26.5	5.28	8.98	.204	.185	.292
120	788	253	36.5	7.26	11.8	.269	.250	.408
140	874	293	47.8	9.39	14.7	.336	.320	.542
160	956	333	60.3	11.7	17.8	.405	.380	.694
180	1040	373	73.8	14.1	21.0	.475	.470	.858
200	1120	413	88.3	16.6	24.3	.545	.550	1.03
250	1320	513	128	23.4	33.9	.720	.780	1.50
300	1520	613	172	30.6	43.8	.895	.995	1.99

Table IV.1

APPARENT EMISSIVITIES 300K to 77K

Material	Condition	emissivity
Aluminum	polished, heavy anodized	0.32
Aluminum	polished, light anodized	0.21
Aluminum	wire brushed, steel wool	0.06
Aluminum	NRC-2	0.03
Aluminum	polished Kaiser foil	0.02
Brass	polished, clean	0.03
Brass	highly oxidized	0.6
Copper	polished, clean	0.02
Copper	highly oxidized	0.6
Chrome	plate	0.08
Gold	foil or plate	0.02
Nickel	polished	0.03
Silver	plate	0.02
Stainless	polished	0.06
G-10	cleaned	0.6
Glass	paint, carbon, lacquer, tape	0.9

Table IV.2

into account (HAN87) is

$$\dot{Q} = \left[\frac{A}{N}\right]\left[6.5\times10^{-12}\times(T_2^4 - T_1^4) + 6.7\times10^{-8} D^{1.5}(T_2 - T_1)\right] \qquad (3)$$

where $\dot{Q}$ is the heat flow in watts, A the area in cm^2, and D is the number of layers per centimeter (density) of super-insulation. We intend to add super-insulation to our dewar only if the liquid boil-off without it proves too costly.

We can estimate the boil-off of LN_2 using Eq. (2). We assume that the 300K radiation from the outer vacuum jacket is the dominant heat source on the LN_2 dewar, and that radiation from the LN_2 to the LHe dewar the primary heat sink. Using a surface area of ~11000 cm^2 and an emissivity per surface of ~.02, we obtain

$\dot{Q} \approx \sigma A\,(\varepsilon/2)(300^4 - 2{\cdot}77^4) \approx 5\,W$. Liquid nitrogen has a latent heat of 207 J/g and density of .81 g/cm^3 at 77K, so 1W corresponds to ~20 cm^3/hr; this implies us a boil-off rate of ~.1l/hr, for an LN_2 hold time of ~50 hr.

To estimate the loss rate of liquid helium, we must consider both radiative and conductive heat loads. The radiative load is small; using Eq. (2), we find $\dot{Q} \approx$ 17mW. The conduction load is from the 77K heat sink to the LHe reservoir via the walls of the top part of the upper section to the LHe dewar. A large part of this heat will be removed by the cold helium gas which is forced to rise along the outer wall of the LHe reservoir by the G-10 insert. We can estimate the LHe boil-off by assuming that the temperature of the walls decreases linearly from 77K to 4.2K. The heat load into the LHe is then given by

$$\dot{Q} = A\,\lambda(T{=}4.2K)\,\frac{dT}{dx}\ . \qquad (4)$$

The area $A \approx .9$ cm^2, and the conductivity of stainless steel at 4K is ~2.5 mW/cm·K; the temperature gradient $dT/dx \sim$ 7.3K/cm. The heat load is then $\dot{Q} \approx$ 16 mW. Using L=21.9 J/g and ρ=0.13g/cm^3 for He at the boiling point, we obtain an acceptable loss rate of ~5l/day.

It is be possible to reduce the helium loss by pumping on the liquid nitrogen dewar; this will lower the vapor pressure of the nitrogen gas and consequently the temperature of the boiling LN_2. A 15 CFM rotary vane pump should be sufficient to get the pressure down to 10 torr, where the LN_2 will be close to its freezing point of

55K. We want to avoid actually freezing the liquid, however, because we would lose thermal contact between the cold solid and the walls of the container. The conductive loss rate for helium in this case would be reduced to ~3.5*l*/day.

IV.4 The Superconducting Magnets

IV.4.1 Philosophical Comment

With the recent discovery of new superconducting materials with critical temperatures above the boiling point of nitrogen, those with a thorough technical understanding of the "old" superconductors may eventually be treated with the same mocking respect one gives to experts in vacuum tubes or manual typewriters. The "old" superconducting technology, however, has proven its reliablity for many years and is likely to prevail for many more years in research applications where high fields are required. For archival purposes at least we shall describe the design of the superconducting magnets in this apparatus. There are many good references on the subject of superconducting magnet design; Wilson's book (WIL83) is by far the most informative and practical.

The experiment can be divided into two regions with distinct requirements for the magnetic field (Figure IV.2). One is the "slower" region, where the thermal atoms effusing from the oven will be decelerated to a near stop; it is ~90cm long. The second region is the "trap" region, where the atoms are stopped and confined by the radiation pressure trap; it is ~5cm in length.

IV.4.2 The Slower Region

The field profile for the slower region is designed to keep an atom in resonance with the single frequency "slowing" laser over as great a distance as possible (PPM82). We will assume that the laser is circularly polarized and that the atom has a cycling transition (such as the $F, M_F = 2,2 \rightarrow 3,3$ transition in the sodium D2 manifold) so that we are effectively dealing with a two-level system. An atom will enter the slower region with an initial velocity v_0 and be subject to an approximately constant acceleration $a = \frac{\hbar k}{3m\tau} \approx 6.2\times10^7 cm\cdot s^{-1}$ for sodium when the laser is at saturation intensity ($a \approx 3\times10^8 cm\cdot s^{-1}$ for Li^7). The velocity as a function of distance z is then $v(z) = \sqrt{v_0^2 - 2az}$ (PPM84). To keep the atom resonant as it slows, we must offset the Doppler shift kv with a Zeeman shift μB. This resonance condition can be written as

apparent laser frequency = atomic transition frequency

i.e. $\omega_L + kv = \omega_0 + (\mu/\hbar)B$

where ω_L is the laser frequency, ω_0 the atomic transition frequency in zero field, and kv is taken to be positive. This gives us an equation for the field profile:

$$B(z) = \frac{\hbar(\omega_L - \omega_0)}{\mu} + \frac{\hbar k}{\mu} v(z) \qquad (2a)$$

$$= B_b + B_0\sqrt{1 - z/L}, \qquad (2b)$$

where $B_0 = \hbar k v_0/\mu$, $L = v_0^2/2a$, and B_b is a bias field whose purpose will be revealed shortly.

The maximum velocity of atoms which we are able to slow is restricted by the length of the slower magnet, which in our case is limited by the height of our ceiling to 90cm. We therefore expect to slow no atoms with initial velocities greater than ~1300m/s. This will have implications with regard to the operation of the oven (cf. Section IV.6.3), particularly when using lithium.

The slower magnet was wound on a 90cm long brass tube, 2-1/4" O.D.×.065"w. Brass was selected for a number of reasons: it is easy to machine; it can be soldered with indium; it has a relative thermal contraction from 300K to 4.2 K which is close to that of copper (and hence the wires); it has a fairly low enthalpy (so less LHe is required for cooling); and it has a relatively low electrical conductivity at 4.2K (so eddy currents will not be induced when the magnets are being charged). The tube was first painted with insulating epoxy (Miller-Stephenson Epon 815 resin and V-40 curing agent, 1:1 mixture by weight) and then divided into 1 cm segments with a black marking pen. The object was to wind a certain number of turns (accuracy: 1/10 turn) in each segment to create the proper field.

The "winding profile" was designed with the help of a series of computer programs. The first program designed the theoretical magnetic field by solving for v(z) given actual experimental parameters; it accounted for the fact that the slowing laser was focused, so that the acceleration was no longer constant but depended on z; it also subtracted the anticipated field of the trapping magnets and the expected fall-off of the bias field at the solenoid's ends. The field thus computed differed slightly from

the one obtained assuming constant a and B_b. The second program computed how many amp·turns to wind in each cm segment. This was done by inverting the matrix equation $\vec{B} = \overleftrightarrow{M} \cdot \vec{t}$. $\vec{B}$ is a 90-component vector whose components B_i specify the field at the position i; the 90 components of $\vec{t}$ specify the number of amp·turns at each position. $\overleftrightarrow{M}$ is a 90×90 matrix which adds the fields of all the current loops t_i to give B_i at each point in the magnet. $\overleftrightarrow{M}^{-1}$ therefore specifies the amp·turns given the field profile; the inversion takes ~1min on a DEC 11/34 microcomputer.

The solution for $\vec{t}$ thus obtained was not practical, however, because it called for negative windings to be made at the ends of the solenoid. To correct for this we averaged the number of amp·turns in each segment with those of the two segments on either side. The result is shown in Figure IV.4. The final turns profile which we used to wind the magnet is given in Table IV.3, for an assumed current of 70 amps.

The choice of superconducting wire for the slower and bias magnets was straightforward. One generally is concerned with the maximum current a wire can carry when immersed in a given field ("critical current"), the maximum temperature at which a wire will still superconduct ("critical temperature"), and the ability of a wire to protect itself in the event of a "quench" (when part of the wire suddenly goes normal). The fields we expect to generate, however, are so low (<<1 tesla), and the inductances so small (<<1 henry), that most type II superconductors would have been adequate for our purposes. We used a popular 54 filament Nb-Ti wire, embedded in a copper matrix (Supercon Inc., type 54S43). The ratio of copper to superconductor was

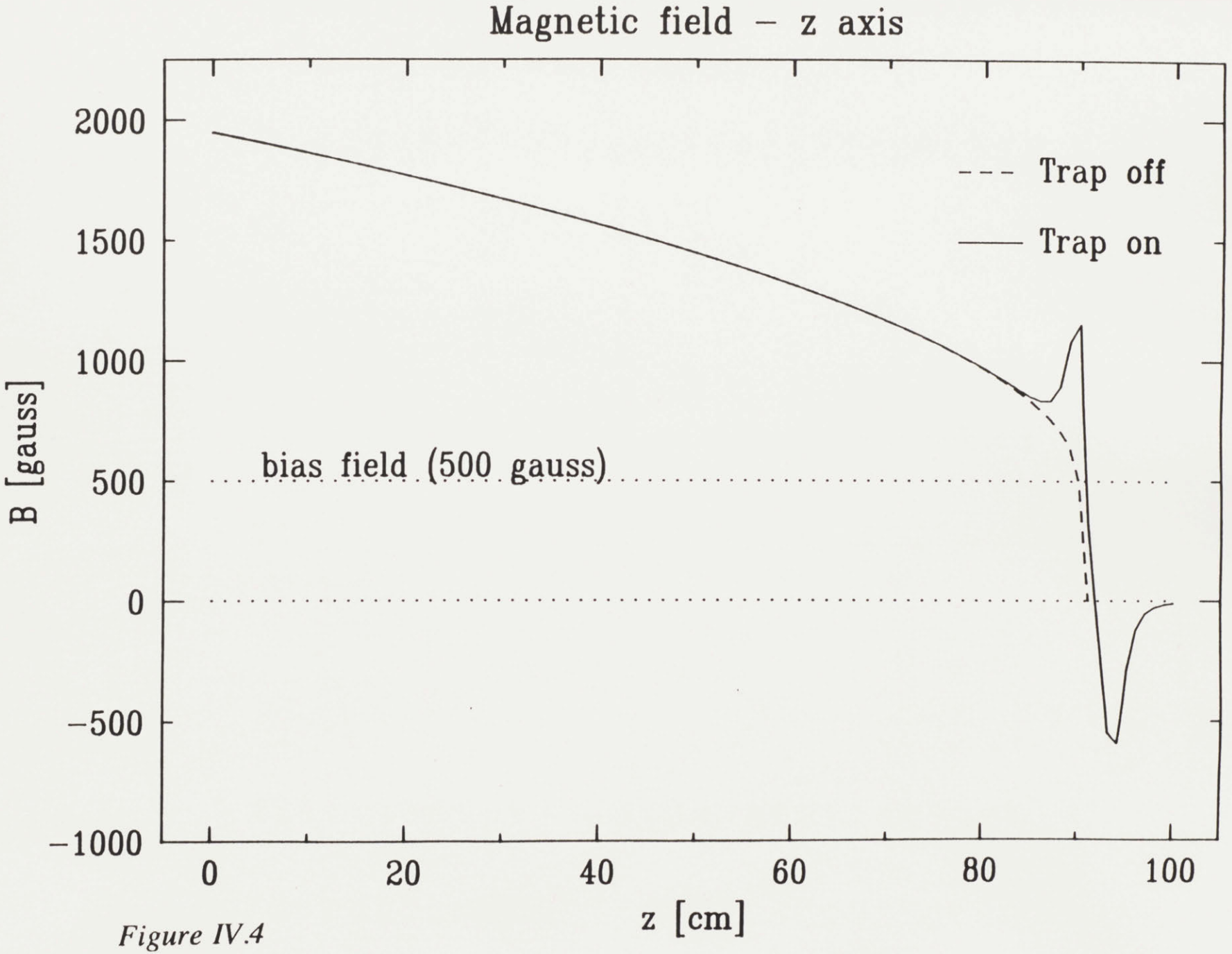
Magnetic field – z axis
Trap off
Trap on
bias field (500 gauss)
B [gauss]
z [cm]
2000
1500
1000
500
0
−500
−1000
0
20
40
60
80
100

Figure IV.4

z	turns	z	turns	z	turns
0	24.3	30	12.4	60	8.7
1	17.6	31	12.3	61	8.5
2	26.3	32	12.2	62	8.4
3	1.3	33	12.1	63	8.2
4	26.1	34	12.0	64	8.1
5	8.7	35	11.9	65	7.9
6	18.9	36	11.8	66	7.7
7	12.8	37	11.6	67	7.6
8	16.0	38	11.5	68	7.4
9	14.0	39	11.4	69	7.2
10	15.0	40	11.3	70	7.1
11	14.3	41	11.2	71	6.9
12	14.5	42	11.1	72	6.7
13	14.2	43	10.9	73	6.5
14	14.2	44	10.8	74	6.3
15	14.0	45	10.7	75	6.1
16	13.9	46	10.6	76	5.9
17	13.8	47	10.4	77	5.7
18	13.7	48	10.3	78	5.5
19	13.6	49	10.2	79	5.2
20	13.5	50	10.1	80	5.1
21	13.4	51	9.9	81	4.5
22	13.3	52	9.8	82	4.8
23	13.2	53	9.7	83	3.6
24	13.1	54	9.5	84	4.8
25	13.0	55	9.4	85	2.5
26	12.9	56	9.3	86	3.6
27	12.8	57	9.1	87	1.8
28	12.7	58	9.0	88	4.0
29	12.6	59	8.8	89	2.3

Table IV.3

1.35:1. The bare wire was .020" in diameter (24 AWG), and was coated with .0005" of formvar for electrical insulation. The critical current at low field is ~150amps, sufficient for our requirements.

The magnet was wound by mounting the tube on a lathe driven by a low speed DC motor. An odometer was connected to the mandril to count the total number of turns wound. We attempted to put the the required turns for each segment as close to the center of the segment as possible, since that most nearly approximated the winding configuration solved for by the program. After winding, a small current was passed through the wire and the resulting magnetic field measured with a Hall probe ("Gaussmeter"). The measurement is shown in Figure IV.5.

Using these field measurements, we also calculated the critical product

$$(B - B_b)\frac{dB}{dz} = \left[\frac{k}{\mu}\right]^2 \mathrm{v}\frac{d\mathrm{v}}{dz} = \left[\frac{k}{\mu}\right]^2 a \ ,$$

using Eq. (2a) and the chain rule. The requirement $a < a_{\max}$ therefore puts an upper limit on the quantity BB'; if BB' were to exceed this limit, the atom could not follow the field slope and consequently would drift out of resonance with the laser and cease to be slowed. A small glitch in the magnet winding profile might cause a spike in BB' which would bring it above the limit. These spikes were tolerated if the difference in μB between the two sides of the glitch was less than the power-broadened linewidth of the atomic transition; the atom in this case will not drift completely out of resonance, and will be recovered. A few windings had to be shifted slightly along the

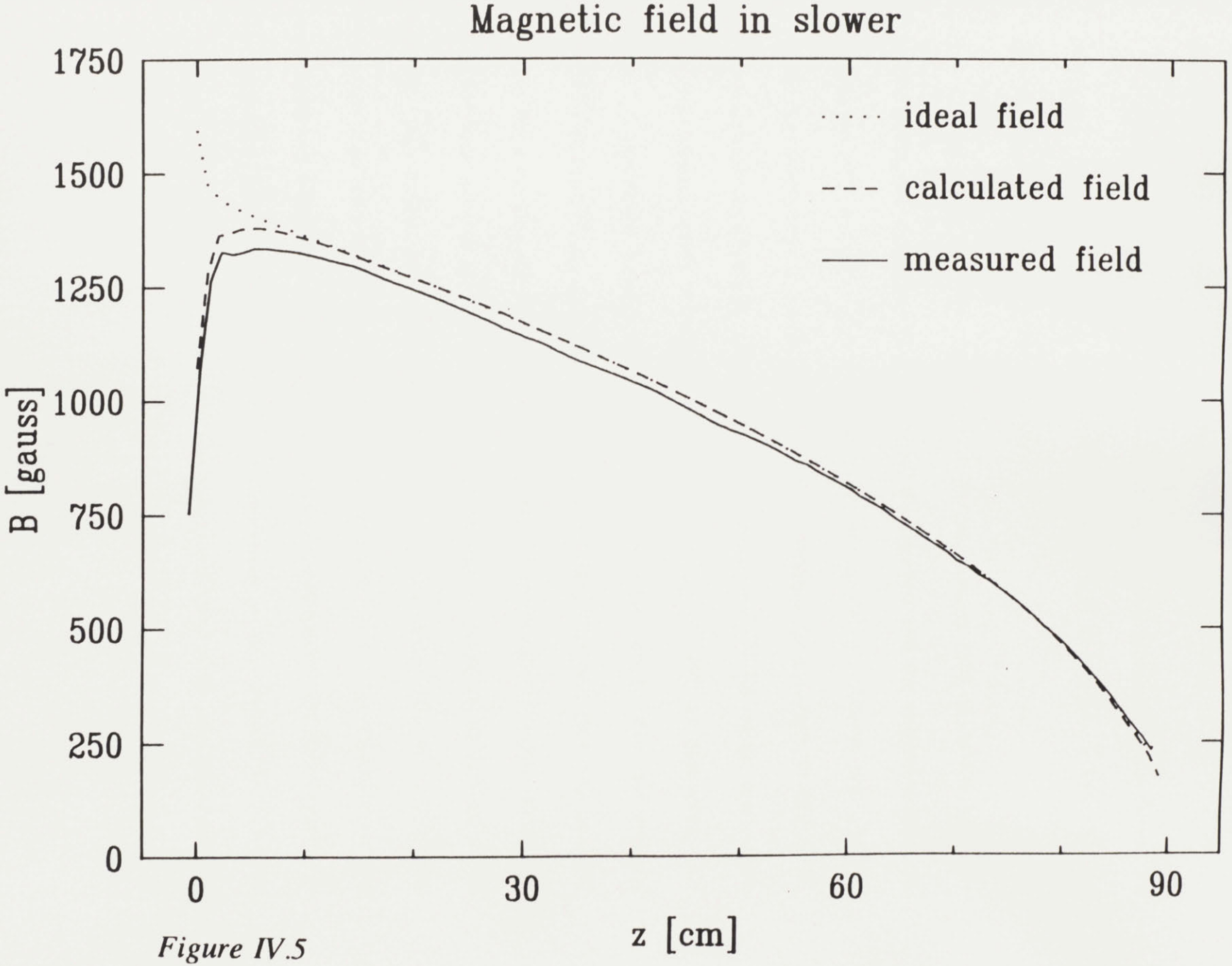
Magnetic field in slower
ideal field
calculated field
measured field
B [gauss]
z [cm]
1750
1500
1250
1000
750
500
250
0
0
30
60
90

Figure IV.5

tube to ensure that this condition was met.

After the measurements and corrections were made, the magnet was potted in the epoxy described above. It was allowed to cure for ~24 hr at a temperature slightly elevated by a bank of infra-red heat lamps.

A bias field B_b was superposed with the slowing field to ensure that the relatively high-intensity slowing laser would not interfere with the trapped atoms as it passed through the trap. The configuration of the optical system (see next section) made it convenient to choose a bias which would induce a Zeeman shift of ~856 MHz, or about half the hyperfine separation of the ground state. We therefore used a bias $B_b \approx 611 gauss$, which corresponds to a current density of ~490 amp·turns/cm. The rate of transitions induced by the slower in the trap would then be a factor $\sim\Omega^2/4\delta^2 \approx 3\times10^{-5}$ less than that of the trapping lasers. The bias field was designed using the same procedure as for the slowing magnet; the design minimized the roll-off of the field towards the extrema of the bias magnet by piling on extra turns at the ends. The magnet was then wound on a 1.375" O.D. brass tube and potted with epoxy. The body of the magnet had a turns density of ~17/cm, so we expect to need ~30amps to achieve the desired field. In running the experiment, the laser frequency is determined (within the range of an A-O modulator — see Section IV.5) by the requirements of the trap; the atoms in the slower will be brought into resonance with the laser by gradually increasing the bias field until the signal from the slowed atoms is maximized.

Once the correct currents are found for the bias and slower magnets at the start of an experimental run, they are not expected to change throughout the run. We therefore close the magnets' circuits with "superconducting switches," a small segment of superconducting wire which can be heated, causing it to "go normal." The wire then has a resistance of ~1Ω; a pair of demountable leads can be connected across the switch, and the magnet (which has no resistance) can be charged (Figure IV.6). After the magnets are charged fully, the switch is cooled, allowing it to superconduct; the leads can now be removed while current continues to flow through magnet. The bias and slower magnets are then operating in "persistent mode;" the 1/e time for current decay depends on the quality of the superconducting junctions made (see below) and can typically be months.

The construction of the superconducting switches is quite simple (Figure IV.7). Manganin heater wire (.020" dia., California Fine Wire Co.) and superconducting switch wire (Supercon) are wound onto a common brass spool and potted with the usual epoxy. This whole assembly is then inserted into a piece of copper tube (~1" O.D., 3" length) and filled with a thermally conductive epoxy (Stycast 2850FT plus catalyst 24LV, Emerson and Cuming Co.). Fewer filaments are used in the switch wire than in the magnet wire so that it is easier to make it go normal; one must therefore take care not to place the switches in a region of high field, lest they quench. We used 18 filament Nb-Ti embedded in a Cu-Ni matrix, with a diameter .015" plus formvar insulation. A pair of diodes (MR754) is placed in parallel to each switch to

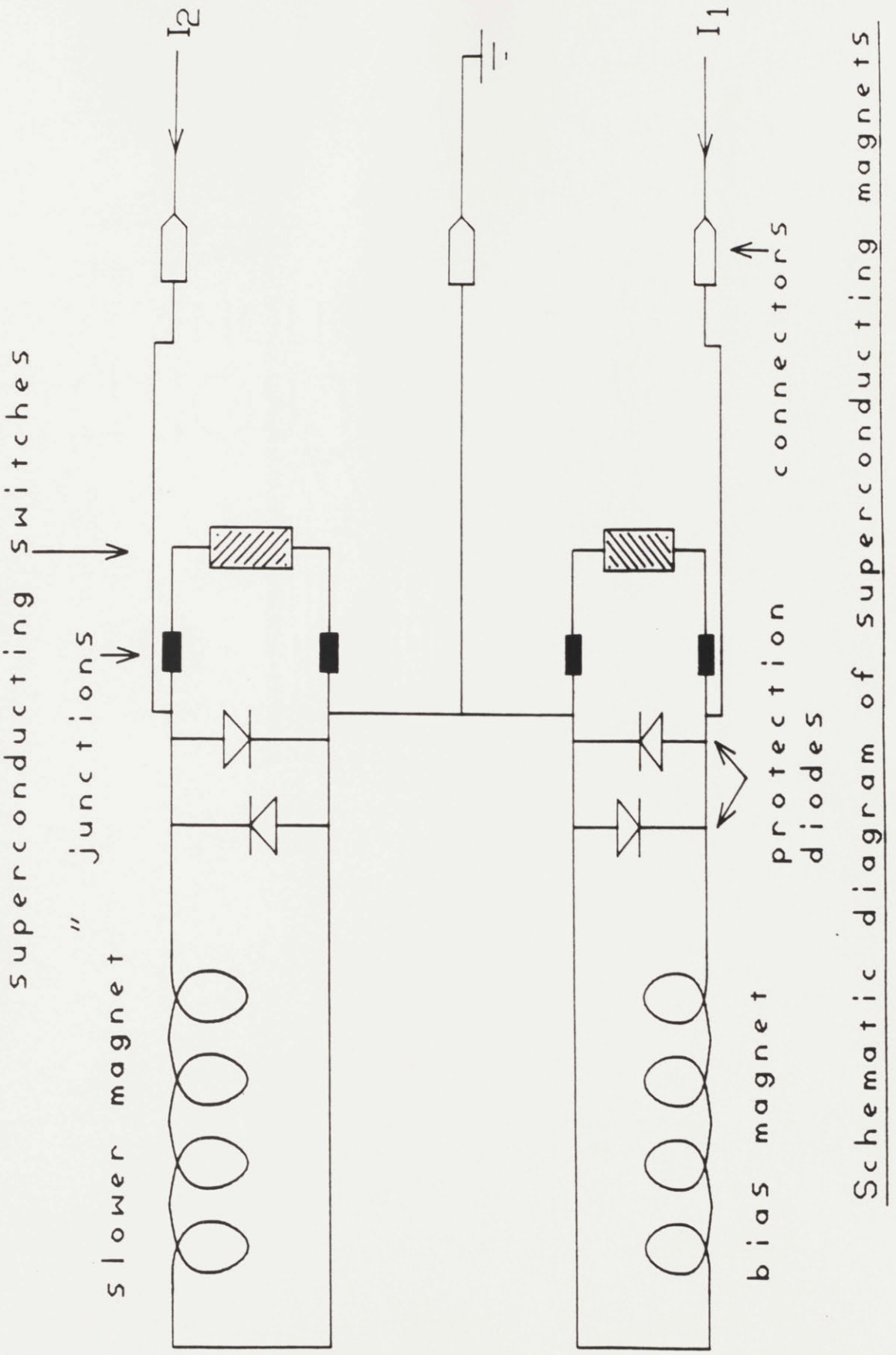
I2
I1
superconducting switches
" junctions
slower magnet
bias magnet
protection diodes
connectors
Schematic diagram of superconducting magnets

Figure IV.6

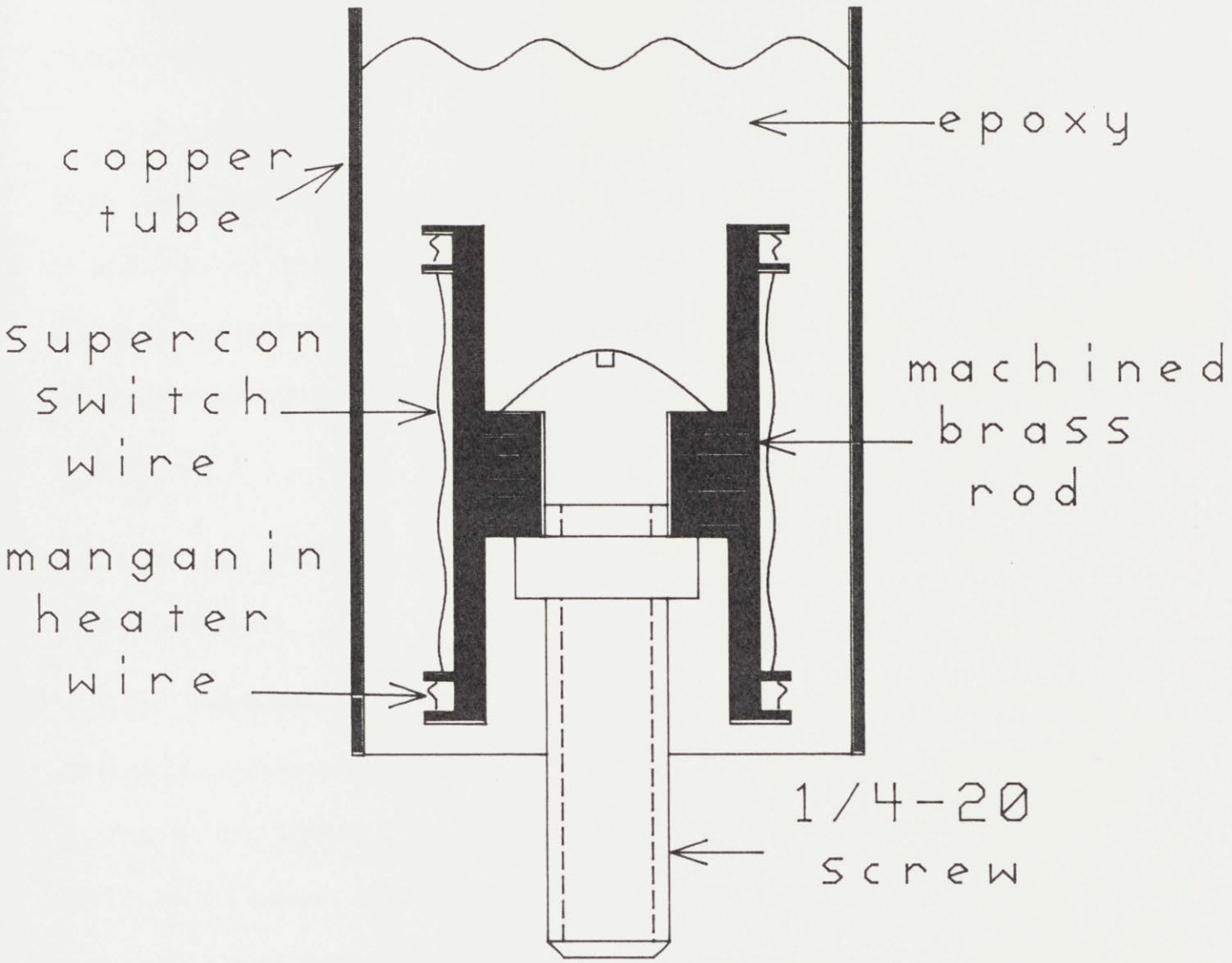
epoxy
copper tube
Supercon Switch wire
machined brass rod
manganin heater wire
1/4-20 screw
Superconducting Switch

Figure IV.7

protect it in the event of a quench; the diodes are capable of dissipating ~100 amps when they are immersed in LHe.

The maximum rate at which the magnets can be charged is determined by the ability of the switches to dissipate heat during charging. We intend to limit this ohmic heating in the switches to ~1W while charging. Since the resistance of the wire when normal is ~1.5Ω, we can have a maximum charging rate of ~1 amp per second per henry. The inductance of the bias magnet (assuming the field inside is uniform) is $\frac{4\pi^2 r^2 N^2 10^{-9}}{L} \approx 3\text{mH}$, where r is the radius and L the length in cm, and N the number of turns. We therefore can fully charge the bias magnet in ~.09 seconds, i.e. as fast as we please.

The demountable leads used to charge the magnets are designed to carry relatively high currents (as much as 150 amps) while generating as little heat as possible in the process. We opted to avoid the standard vapor-cooled lead (BFS75,BEI83) because of its tendency to trap air in its many pores — the air can then liquify, releasing its heat of vaporization and boiling away a lot of LHe. We chose instead to construct our leads using many (~50) strands of fine (30 AWG) copper wire inside a thin-walled stainless tube (for mechanical support). The tube was vented at the top and bottom to permit the cold vapors to flow next to the wires. Before inserting the lead, it is first purged of condensibles with helium gas, which is retained in the tube by placing one's thumb over the upper vent hole. The connectors

used (Huygin Industries series 6-X) are rated at 90 amps for continuous operation at room temperature, but can be pulsed to many (>10) times that value.

Since the slower and bias magnets are coaxial, the mutual inductance between them is significant. If one of the magnets is charged independently, an EMF will be induced across the other and change its current. It is therefore important to charge both of them at the same time and allow the currents to reach a steady state before closing the superconducting switches.

IV.4.3 The Trap Region

The field profile for the trap region will initially be the same as in the Bell experiment, albeit with the capacity to achieve much higher gradients. We have the additional capability of adding more superconducting coils, cooled perhaps by conduction, to create different fields and possibly different types of traps.

The trap magnet consists of "upper" and "lower" coils with opposing currents. The lower trap coil was wound at the end of the tube for the bias magnet, in a 3/8" space between a pair of brass flanges. The upper coil was wound on its own spool, 1-3/8" O.D.×3/8" long, and fastened to the lower flange of the upper section of the LHe dewar. Both coils were "wet wound" with 250 turns of wire; we used 54 strand NbTi in a copper matrix, with a Cu:NbTi ratio of 1.35:1. The wires had an O.D. of .011" and were insulated with a .0005" layer of formvar. The critical current at low field is 84 amps.

The two coils are wired in series, with the leads spiraling out around the perimeter of the G-10 insert as described above. The inductance of the system is $2(L-M)$, where L is the self inductance of 1 coil and M the mutual inductance between the two. Since the coils are separated by more than a radius, $M \ll L$; in any case, by neglecting M we obtain a conservative (high) value for the total inductance. For a single coil of radius a and N turns, we find (JAC75)

$$L = \frac{4\pi^2 a^2 N^2}{c^2} \int_0^\infty ds\, J_1^2(sa)$$

where J_1 is the first order Bessel function. By integrating this numerically, we find that $L = 7.2\pi^2 N^2 a \times 10^{-9}$H (with a in cm), which is about 8 mH for each of our trap magnets.

The minimum field gradient with which we observed trapping in the Bell experiment was ~5 gauss/cm. For the present geometry, we expect to have a gradient of 45 gauss/cm·amp, implying that a current of ~.1 amps will be sufficient to generate this minimum gradient. The maximum gradient at the critical current for the superconductor is ~4000 gauss/cm, about 200 times the maximum at Bell.

Since there are many layers of wire in each coil, a quench which occurs near the center of a coil's cross-section will induce a hot-spot which can propagate through the rest of the coil. If this propagation velocity is faster than the characteristic time for the magnet to conduct the heat away to the LHe, the entire coil will quench more or less simultaneously. Care must be taken in the system's design to ensure that this

does not lead to a catastrophic temperature rise in the superconductor causing it to melt. The worst case scenario is of an infinite propagation velocity and no cooling; for the dimensions of our trap coils, using the volumetric specific heat of the wire $C=2.5\times10^3$ J/m^3·K, we find that the temperature rise during such a quench is 80K/J. A current of 35 amps in the trap magnets would thus give a temperature of 400K after the quench. By performing a more detailed analysis (WIL83) one can show for higher currents as well that the coil dissipates the quench energy in the LHe before the temperature rise proves catastrophic.

IV.5 The Optical System

IV.5.1 Overall System

A schematic diagram of the optical system used in the experiment is shown in Figure IV.8. The setup downstream of the optical fiber is identical to that of the Bell experiment (cf. Chapter III). The upstream setup differs slightly from the Bell arrangement, though it utilizes many of the same components.

The upstream optics are located in a room separate from the dewar. About .5W of 589 nm laser light (~1 MHz linewidth) is generated by a Coherent CR-699 ring dye laser pumped by ~6W from a Spectra-Physics 171 Ar^+ laser. The light passes through the first acousto-optic modulator (AOM) (Isomet 1205C-2) which splits off part of the beam, giving it a positive frequency shift ν_1. The modulator is driven by a Leader LSG-17 signal generator and an ENI 603L power amplifier (3W max output), and can

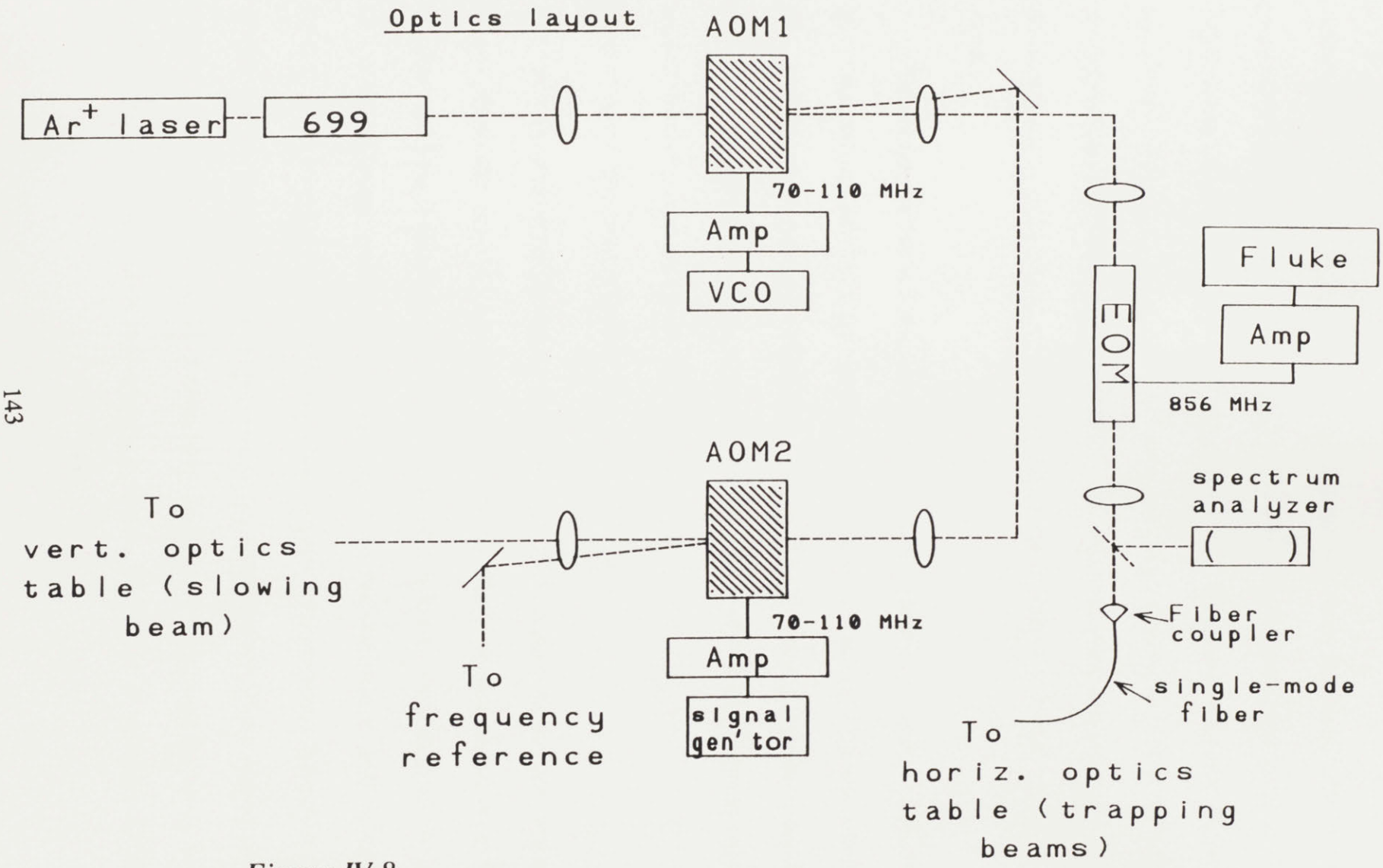
Optics layout
AOM1
Ar+ laser
699
70-110 MHz
Amp
VCO
Fluke
Amp
EOM
856 MHz
AOM2
spectrum analyzer
( )
To vert. optics table (slowing beam)
70-110 MHz
Amp
signal gen'tor
Fiber coupler
single-mode fiber
To frequency reference
To horiz. optics table (trapping beams)

Figure IV.8

deflect up to ~80% of the incident power into the first order sideband. The AOM is positioned at the common focus of a pair of anti-reflection coated plano-convex lenses (Melles-Griot 01-LPX-277/078—f=20cm) separated by 2f; this arrangement allows the modulation frequency ν to be varied over a ~30 MHz bandwidth without noticeably shifting the position of the modulated beam. The unshifted beam continues upstream to the electro-optic modulator (EOM), while the beam at $+\nu_1$ is directed to the second AOM.

The second AOM is configured with two lenses identical to the first. It is driven by a custom-built oscillator (see Section IV.5.2) and an ENI 603L power amplifier. The unshifted beam from the second AOM is used for the slower; note that it has a net positive frequency shift ν_1 with respect to the ring laser. The deflected beam acquires an additional negative frequency shift $-\nu_2$, giving it a total shift of $\nu_1 - \nu_2$. It is then directed to the frequency reference (see Section IV.5.2).

It is possible with this configuration to tune the frequency of the laser while the slower frequency remains constant. The reference beam is maintained at a fixed absolute frequency with respect to an atomic resonance line or a stablized He-Ne laser. The laser frequency, and hence the frequency of the trapping beams, will be detuned by $\Delta\nu_L = -(\nu_1 - \nu_2)$ from this reference; the slower, since it passes through the first AOM, will be detuned by $\Delta\nu_S = \Delta\nu_L + \nu_1 = \nu_2$. Consequently, if we change the RF frequency ν_1 of the first AOM, the trapping frequency will change by an equal and opposite amount, while the slower remains constant. The range of tuning is ~30 MHz,

the bandwidth of the AOM.

The trapping beam passes through an EOM constructed by T. Shirley, modeled after the one at Bell. A 1mm×1mm×25mm $LiTaO_3$ crystal rests in a resonant LC cavity formed by the crystal and flexible sheets of copper and beryllium-copper bent into a loop (Figure IV.9). Treating this circuit as a parallel LC resonator, we find a resonant frequency $\omega_0 = (LC)^{-1/2}$; L is the inductance of the two loops ($\sim\mu_0\pi r^2/l$ for each, where r is the radius and l the length) and C is the capacitance of the crystal $A\varepsilon/d$, where A is the area and $\varepsilon = 43$ is the dielectric constant at RF frequencies (KAM74). The resonant frequency of the cavity is coarse adjusted by sliding the copper clamp back and forth to change the size of the loop, and fine tuned by bending the foil slightly with a toothpick or similar implement. The Q of the cavity is ~50.

The crystal itself is attached to the copper base with a silver impregnated epoxy (Ohmex-AG, Transene Corp.). This creates good thermal contact between the crystal and the copper, preventing the crystal from warping during operation. To improve the optical transmission through the crystal, a glass window was secured near either face, and a drop of index-matching fluid (H-C oil series 27, HaloCarbon Products) placed in the interstice. The outside face of each window is anti-reflection coated.

The light emerging from the EOM is frequency modulated at the RF frequency ω_m. The relative power in the first order sidebands is given by $(J_1(\eta))^2$, where the *modulation index* $\eta \equiv (\omega_m/2c)\kappa E_m L$; κ is a constant describing the crystal, L is the

length of the crystal, and E_m is the amplitude of the applied electric field. The EOM is driven (by a Fluke 6060a synthesizer and ENI 603L amplifier) at ω_m = 856.2 MHz, which is about half the separation of the ground state hyperfine levels. If the laser is tuned halfway between the resonance frequencies of transitions from these two levels, the first order sidebands of the modulated light will be exactly resonant with these transitions. In practice, we tune ~10 MHz to the red of resonance in order to form the light trap. The modulated light is then coupled into the single-mode fiber and output onto the horizontal optics table on the dewar in the next room (Figure IV.10).

Since we are concerned more with the power in the slower beam than its spatial quality, it is sent directly to the dewar through a hole in the laser room wall. A mirror on the horizontal optics table reflects the beam up to the vertical optics table, together with the vertical trapping beam (Figure IV.11). Since the two beams are to have the same helicity, they share the same polarization optics. They are focused to slightly different points, however, by two separate mirrors. The mirror for the vertical trapping beam is placed at the waist of the intermediate focus of the slowing laser.

The vertical trapping beam is brought to a focus on a mirror just to the side of the source channel. The mirror is mounted on a rod connected to a gimbal assembly (Huntington VF-171-M) which can be adjusted exterior to the vacuum with micrometer drives in order to perfectly retroreflect the beam. A zero-order quarter wave plate suitable for the high intensity of the focused beam (Special Optics 8-8015-1/4-589) is positioned just above the mirror to reverse the polarization of the retroreflected beam.

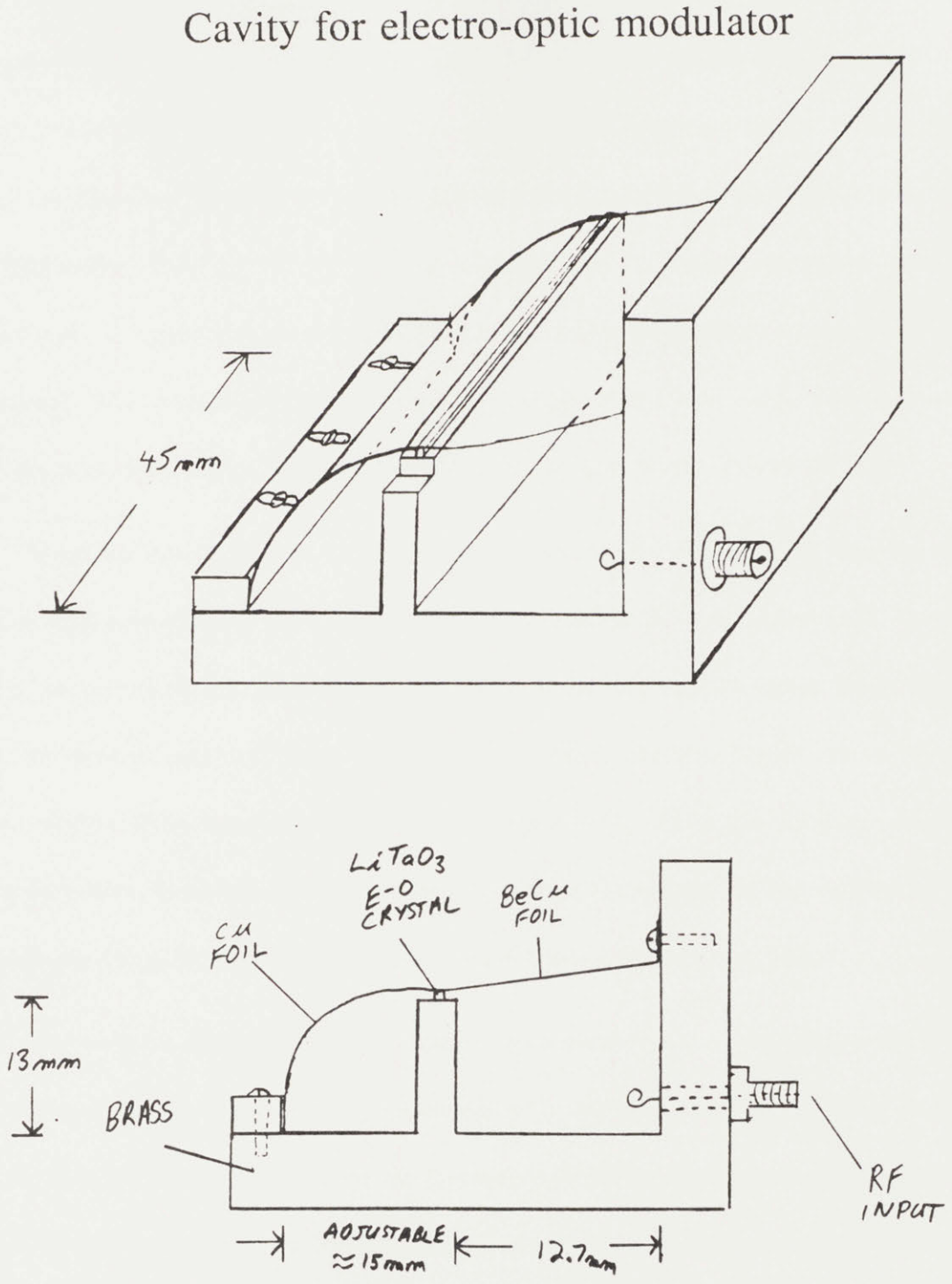
Cavity for electro-optic modulator
45mm
LiTaO3
E-O
CRYSTAL
BeCu
FOIL
Cu
FOIL
13mm
BRASS
RF
INPUT
ADJUSTABLE
≈15mm
12.7mm

Figure IV.9

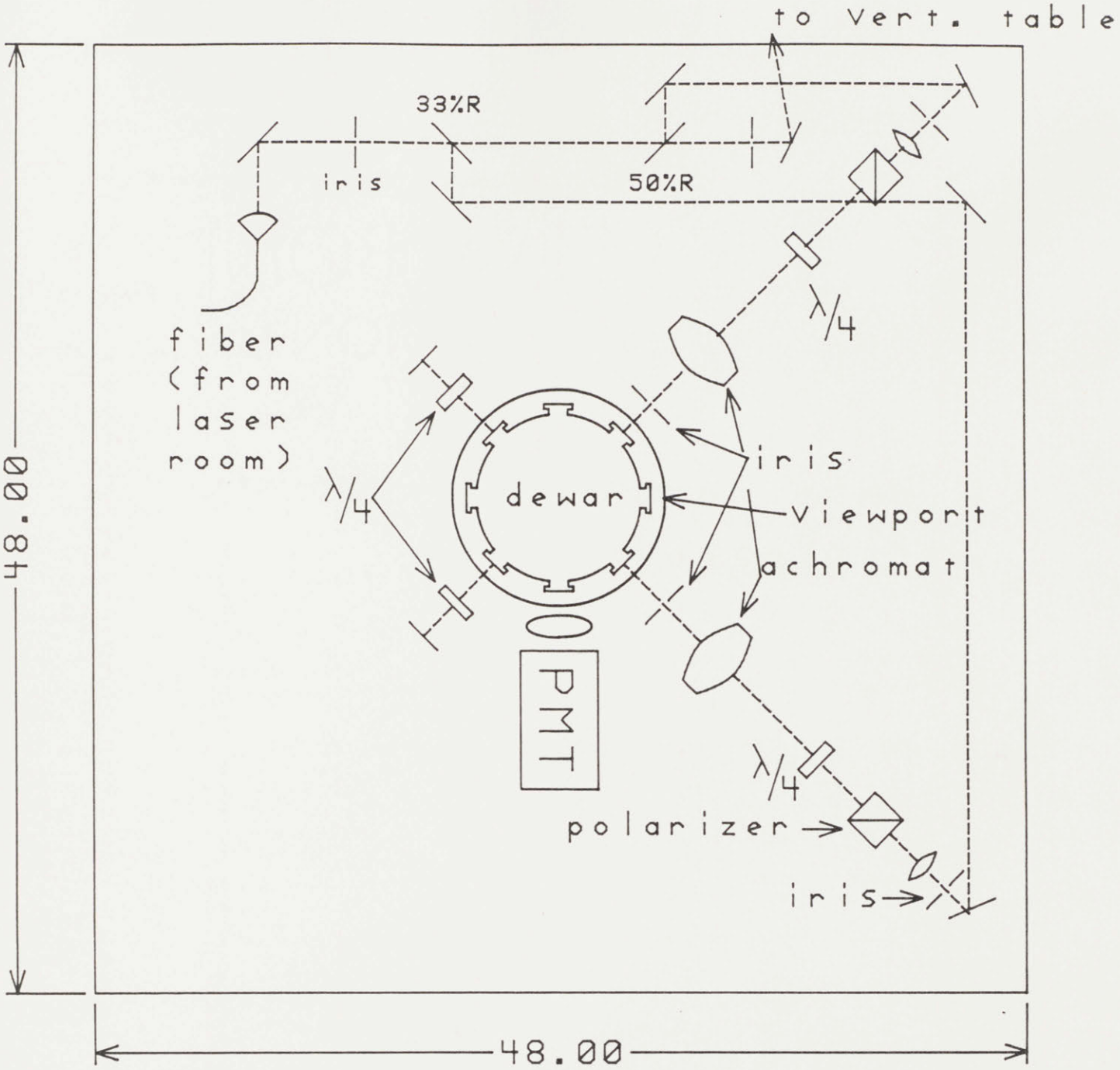
to Vert. table
33%R
iris
50%R
fiber (from laser room)
λ/4
iris
dewar
viewport
achromat
PMT
λ/4
polarizer
iris
48.00
48.00
Horizontal optics table layout

Figure IV.10

Vertical optics table

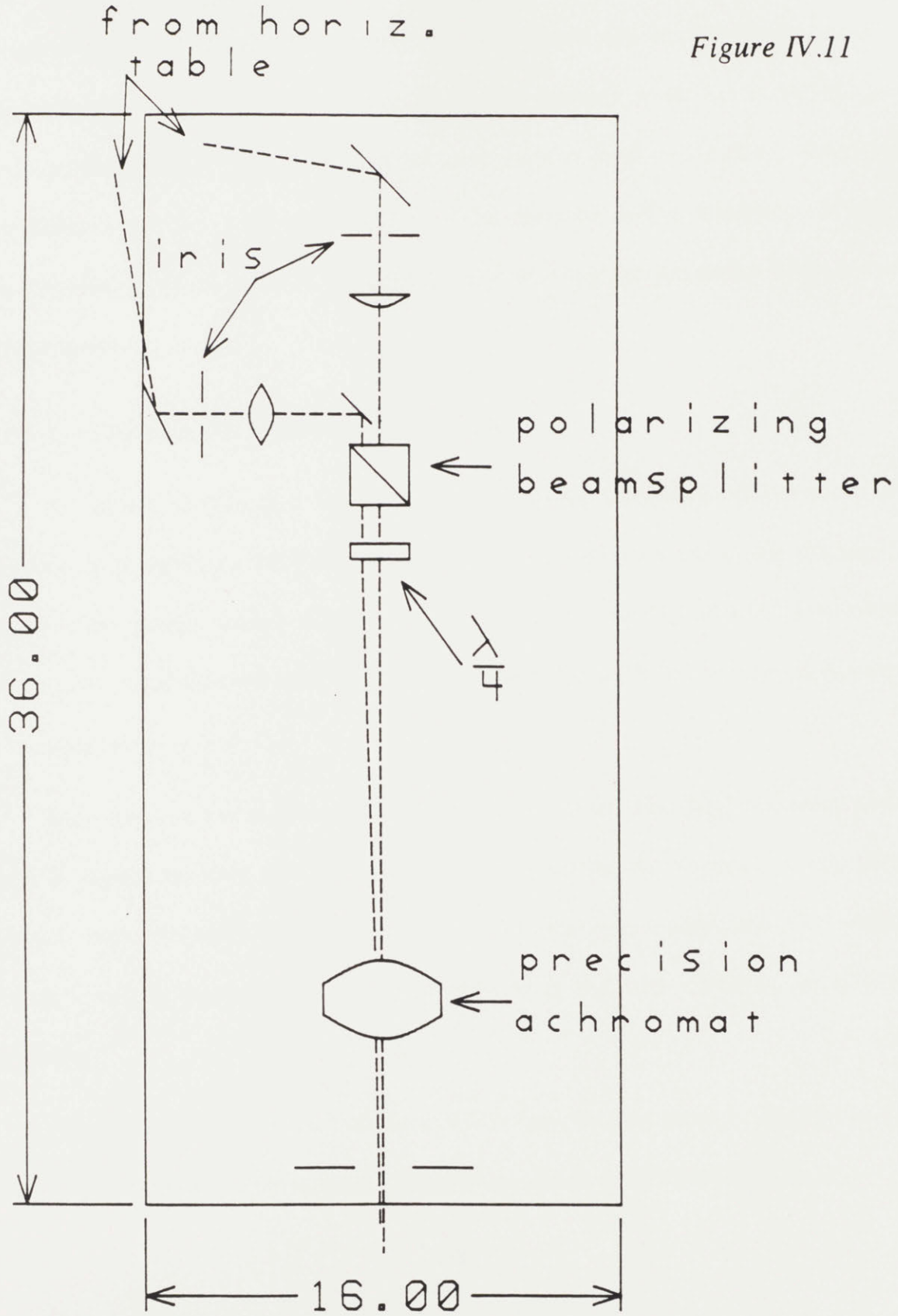

Figure IV.11

Once the vertical trapping beams are aligned, a small piece of a microscope slide is inserted into the trap region by means of a linear feed-thru on one of the dewar's horizontal view-ports. All six trapping beams are stopped down by means of iris diaphragms and made to fall on exactly the same point as seen on the slide. The slide is withdrawn and the beams expanded to ~1cm diameter before operating the trap. The diaphragms remain in place to facilitate re-positioning the the beams in the event of misalignment.

IV.5.2 Locking the Laser to a Frequency Reference

We intend to lock the ring laser to one of two frequency references. One reference is a stabilized He-Ne laser; the other is a crossover resonance (explained below) in the atomic species of interest. The goal of the locking scheme using either reference is to stabilize the laser against long-term (>10s) drift of the output frequency of the ring laser.

Both schemes are based on the same principle. When that laser frequency drifts from its desired location, an "error signal" is generated by the reference circuit. This signal is then integrated, buffered, and fed back to the laser control box. The control box then acts to reduce the error signal by moving the laser closer to the desired frequency.

The scheme utilizing the stabilized He-Ne laser is diagramed in Figure IV.12a. The red He-Ne light is sent through a Fabry-Perot etalon (FSR 300 MHz, finesse

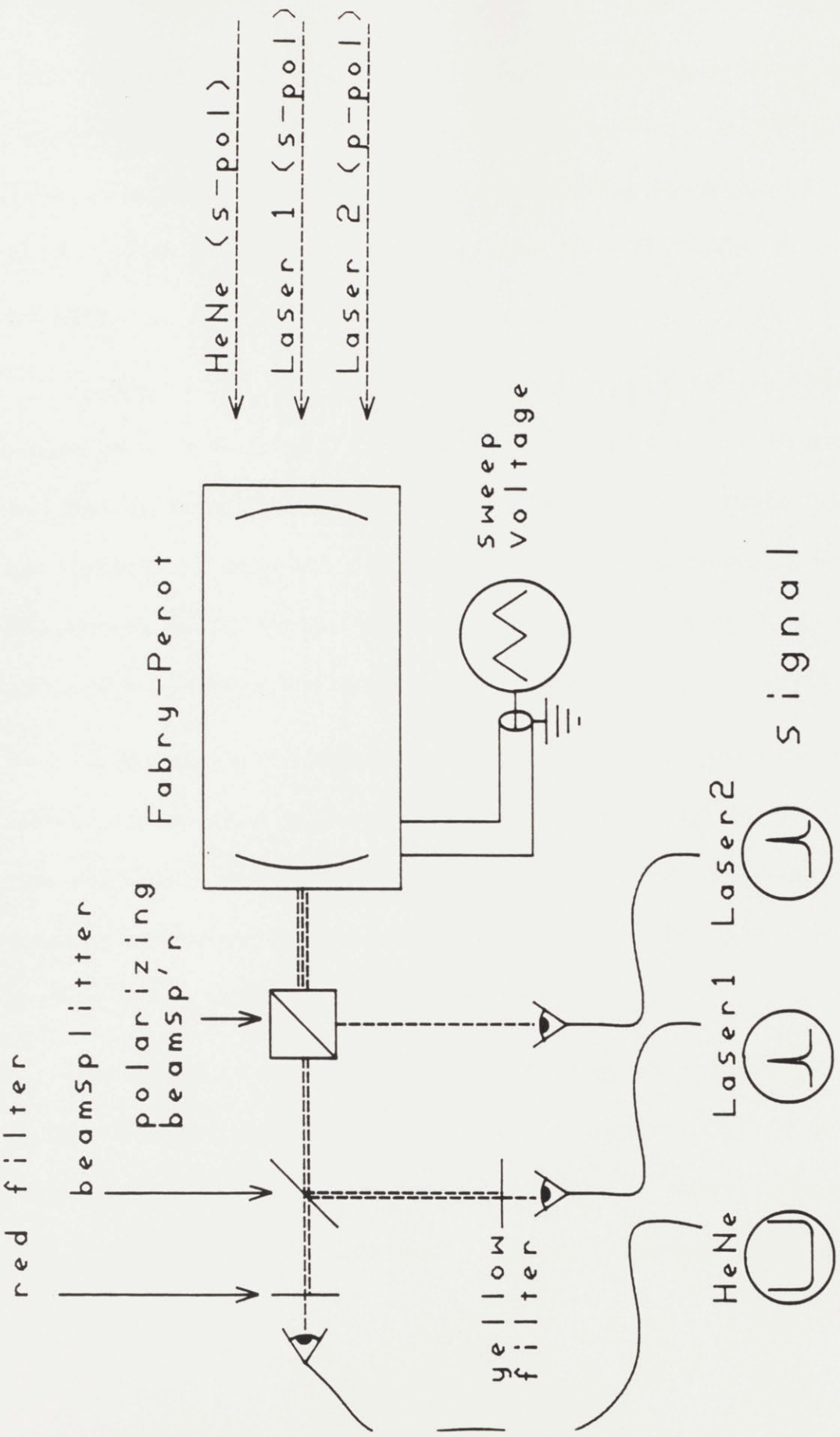

Figure IV.12a

~300), and its transmission detected by a "photop" (photodiode plus op amp — United Detector Technology UDT-455) behind a red band-pass filter. The PZT on the F-P mirror is used to sweep the cavity back and forth between two transmission peaks of the He-Ne; the PZT voltages at the endpoints are thus "locked" to the He-Ne frequency.

A beam from the ring laser is now passed through the F-P and detected by a separate photop after being discriminated by the appropriate filter. The transmission peak from this beam (the first peak if there are two) will fall somewhere between the two He-Ne peaks; this point will correspond to a certain fraction of the voltage difference on the PZT between the high and low parts of the sweep. By choosing this fraction with a 10-turn potentiometer, the ring laser can be locked to any point desired.

An advantage to this scheme is that at least two lasers can be locked to the same reference; the two must be distinguished after they pass through the F-P, perhaps by their polarization. A disadvantage is that it does not provide an absolute frequency reference; F-P transmission peaks occur every 300 MHz. An absolute reference *is* provided, though, by a saturated absorption gas cell.

The scheme for using the gas cell as a frequency reference is shown in Figure IV.12b. The cell (Quaracell Products type 137) is heated to ~200°C by two resistive "heater tapes"; the temperature is adjusted by changing the voltage across the heaters with Variacs. The absorption path length is ~20 mm; the beams enter the cell at an

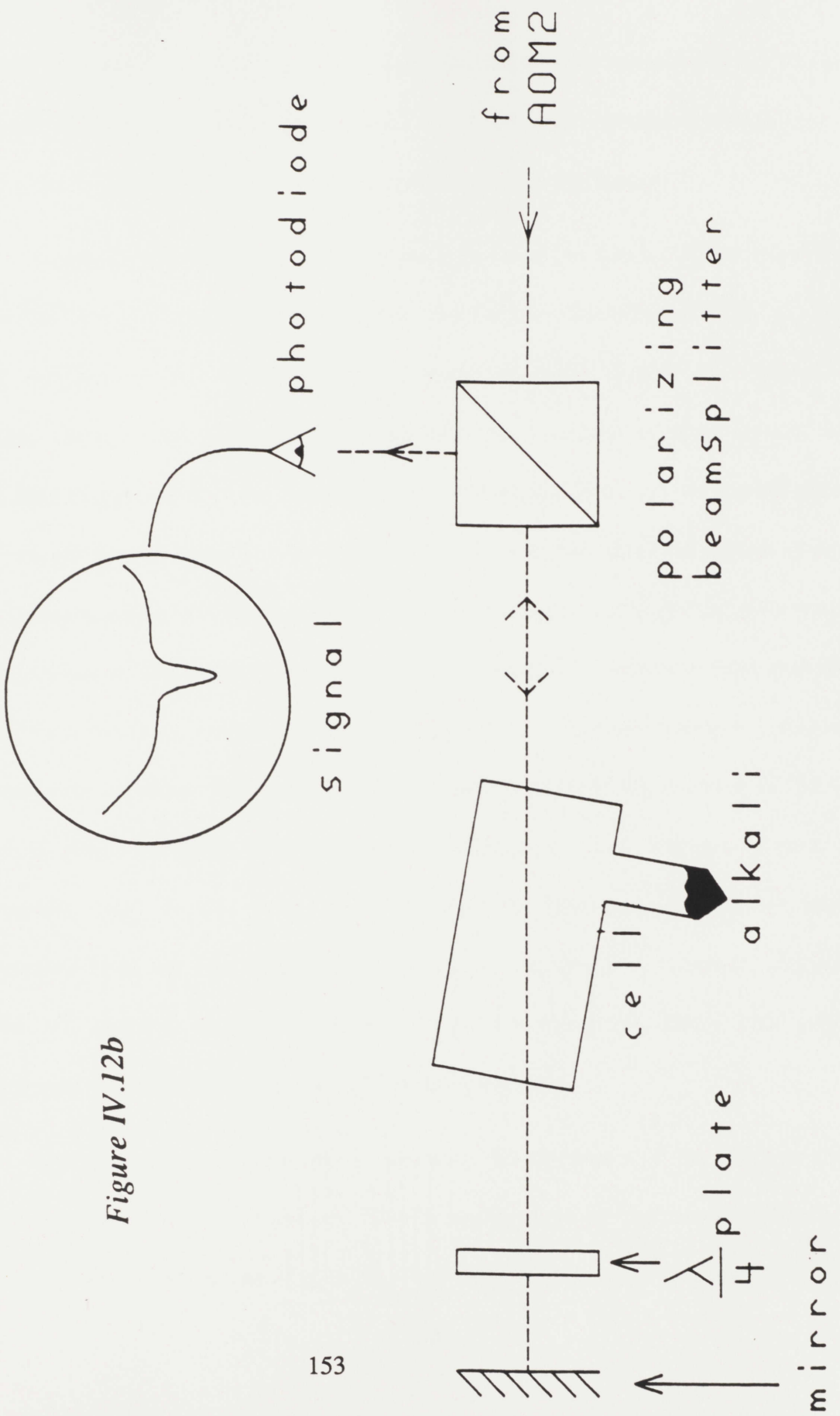

Figure IV.12b

oblique angle to the windows to keep spurious reflections away from the region of interest. A polarizing beamsplitter (NRC 05-FC16PB.3) and quarter-wave plate are used as an "optical diode" to prevent reflections back to the laser.

The cross-over resonance to which we lock occurs in species whose ground state hyperfine levels are separated by less than the Doppler linewidth (LEV84, e.g.). For most frequencies, one of the counter-propagating lasers (called the "pump" and "probe," though they can be equivalent) will be absorbed by those atoms whose velocities Doppler shift them into resonance. These velocities are in general *different* for the two ground states, so the two lasers will probe two different groups of atoms. The resonant atoms will consequently be optically pumped to the ground state which is not resonant at that velocity, resulting in a decrease of absorption than one would obtain in a two-level system. When the laser frequency is tuned *halfway* between the ground state transition frequencies, however, both transitions are resonant in the *same* velocity group, resulting in an increase in absorption. This increase is seen as a symmetric "dip" in the probe intensity when its frequency is halfway between resonances from the two levels. This serves as a convenient reference, because an EOM will generate sidebands evenly split around this point; hence both sideband frequencies can be placed near the appropriate transitions.

The error signal is generated by dithering the frequency of the reference beams about the "trough" of the crossover. This is readily done by frequency modulating the RF to the second AOM (see Fig. IV.8). We use a voltage-controlled-oscillator (a pair

of Avantek VTO-9120 oscillators (1-2 GHz) and a Mini-Circuits ZFM-150 mixer) and low-frequency signal generator to modulate ~80 MHz at 200 Hz with a deviation of ±1 MHz. The error signal is obtained by phase detecting the absorption signal at 200 Hz with an Evans 4110/4114. If the laser is exactly at the center of the line, the absorption signal will be at 400 Hz due to the symmetry of the line, and the error will be zero. Any drift of the laser will result in a 200 Hz component of the signal; this will generate an error signal whose sign depends on the relative phase of the driver and detector signals, i.e. the direction of the drift. The circuit is sensitive to drifts of several hundred kHz and should be able to lock the laser to ~1 MHz.

IV.5.3 Detection

An essential part of any experiment is to collect and record the data it produces. The data in this experiment will be the fluorescence from the cloud of trapped atoms. Our goal is to efficiently collect as much of this fluorescence as possible, measure its intensity, and analyze its spectrum.

The geometry for detection is illustrated in Figure IV.13. The light from the trap is collected by a precision achromat (corrected for spherical aberration—Melles Griot 01-LAO-059/078) and an aplanatic meniscus lens (to decrease focal length without adding to the aberration of the achromat—01-LAM-059/078). This pair is placed ~.75" from the center of the trap; it has $f/1.67$ and therefore will nominally collect ~3% of the light emanating from the atoms (a light-gathering mirror opposite

Figure IV.13

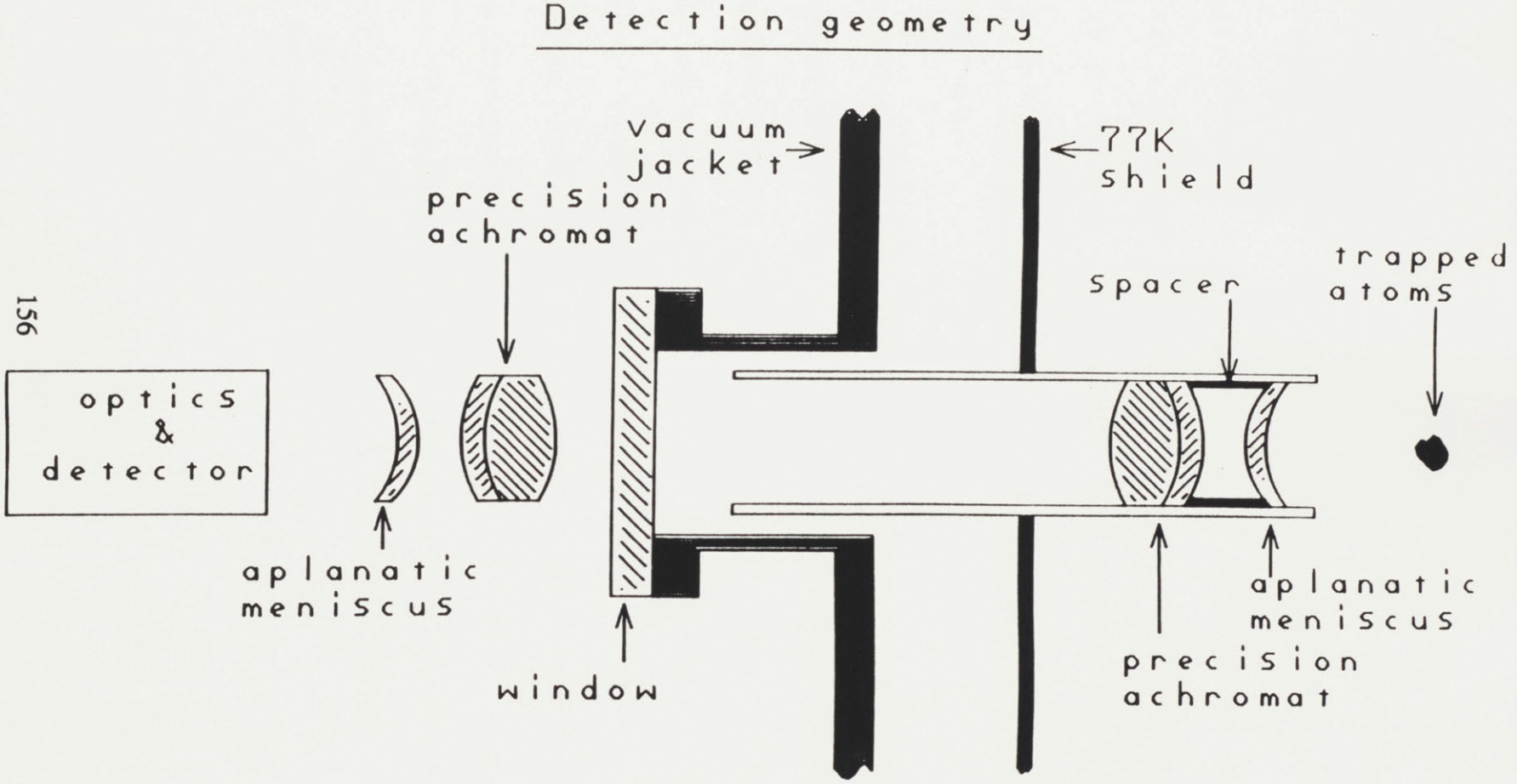
Detection geometry
vacuum jacket
77K shield
precision achromat
spacer
trapped atoms
optics & detector
aplanatic meniscus
window
aplanatic meniscus
precision achromat

the lenses can theoretically double this efficiency). A complementary pair of lenses identical to these is positioned just outside the vacuum chamber to complete the collection system symmetrically and thus form the optimum image of the trap.

In the initial stages of running the experiment, we will primarily be interested in the total fluorescence from the trap. This is most easily recorded by placing a PMT at the image of the trap, taking care to shroud it from extraneous light. The PMT efficiency is about 10%, more than sufficient considering the $\sim 10^{14}$ photons/sec collected by the optics.

In the later stages of experimentation, we will want to analyze the fluorescence using a monochromator (SPEX). To optimize its performance, the geometry of the input beam should match the grating geometry ($\sim f/7$) as closely as possible. This is accomplished with a secondary focusing lens placed beyond the image formed by the primary optics. The transmission of the monochromator is conservatively about 10^{-2}; if we include the collection and PMT efficiencies, reflective losses, and losses in the monochrometer entrance slit, we expect to record ~1 count per 10^5 photons emitted from the trap. The double monochrometer will also provide a rejection ratio of $\sim 10^8$ between the uninteresting photons emitted by the trapped atomic species and interesting ones produced by collisions, molecules, etc.

IV.6 Atomic Source

IV.6.1 Source Chamber and Related Hardware

The source of alkali atoms is a central part of the apparatus. Its design must be flexible enough to accommodate modification, maintenance, and the possibility of different atomic species. It must fit in the limited vertical space available to it, yet be sufficiently roomy to accommodate various accessories, pumps and gauges. The actual atomic source is a radiatively heated oven; the oven sits in a larger region called the "source chamber," which provides the required vacuum environment and the necessary accessories.

A schematic of the source chamber is shown in Figures IV.14a,b. The main enclosure for the oven is a 12" cube formed with 5/8-1" thick welded aluminum plates. The enclosure is evacuated by a $150 l/s$ turbo-molecular pump (Balzers TPH-170C, corrosive series) protected from the high flux of corrosive alkali by a water-cooled baffle (BFW-100M). The turbo is backed by an Alcatel ZM2008A rotary-vane roughing pump.

The main chamber is separated from the rest of the apparatus by a stainless steel channel directly above the oven nozzle (Figure IV.15). The channel has two purposes: to collimate the atomic beam en route to the dewar, and to isolate the high vacuum of the dewar region from the relatively high pressure of the source (it has a conductance of $\sim .06 l$/s). To keep it from becoming clogged with condensed alkali, it is heated

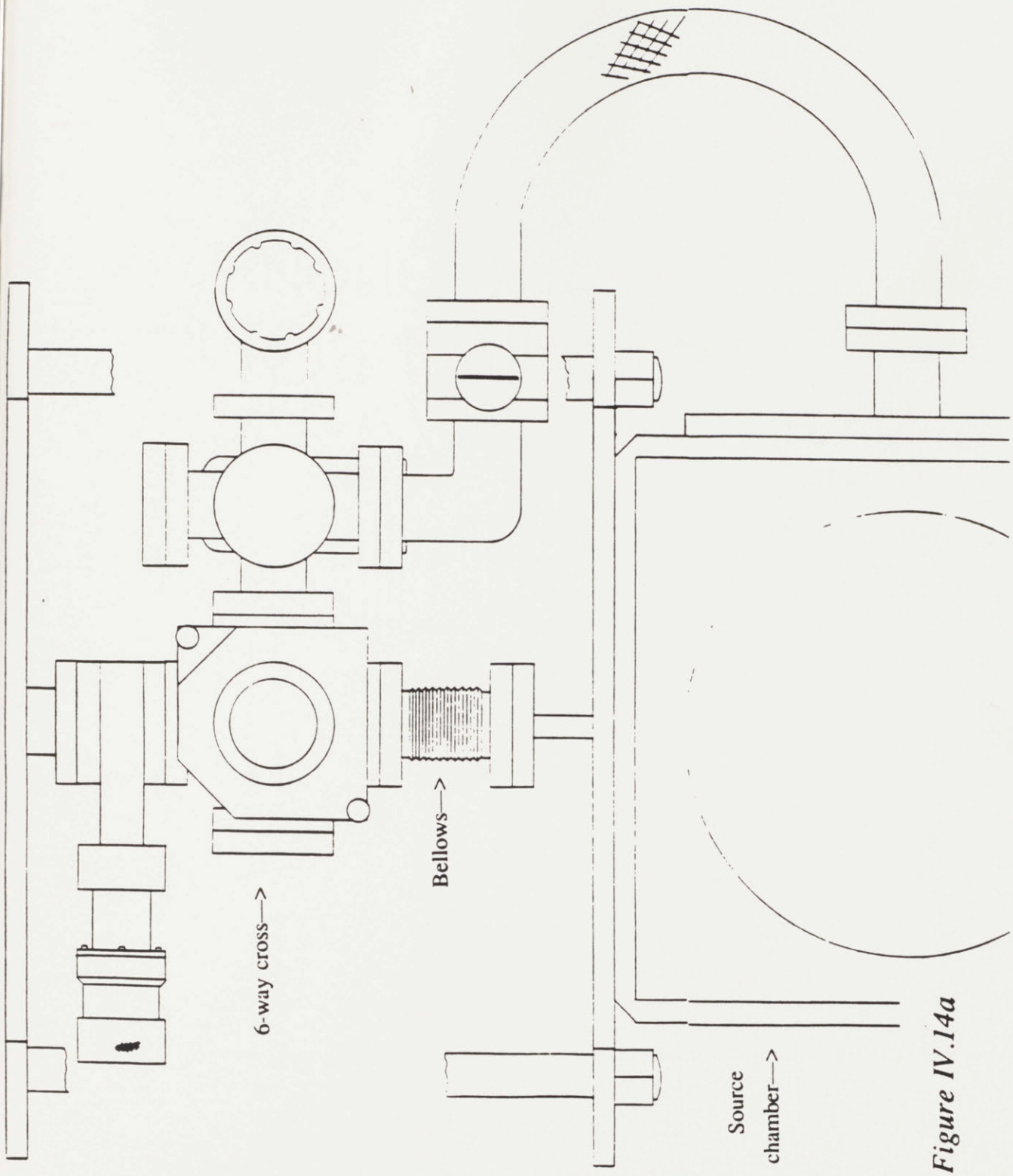

Figure IV.14a

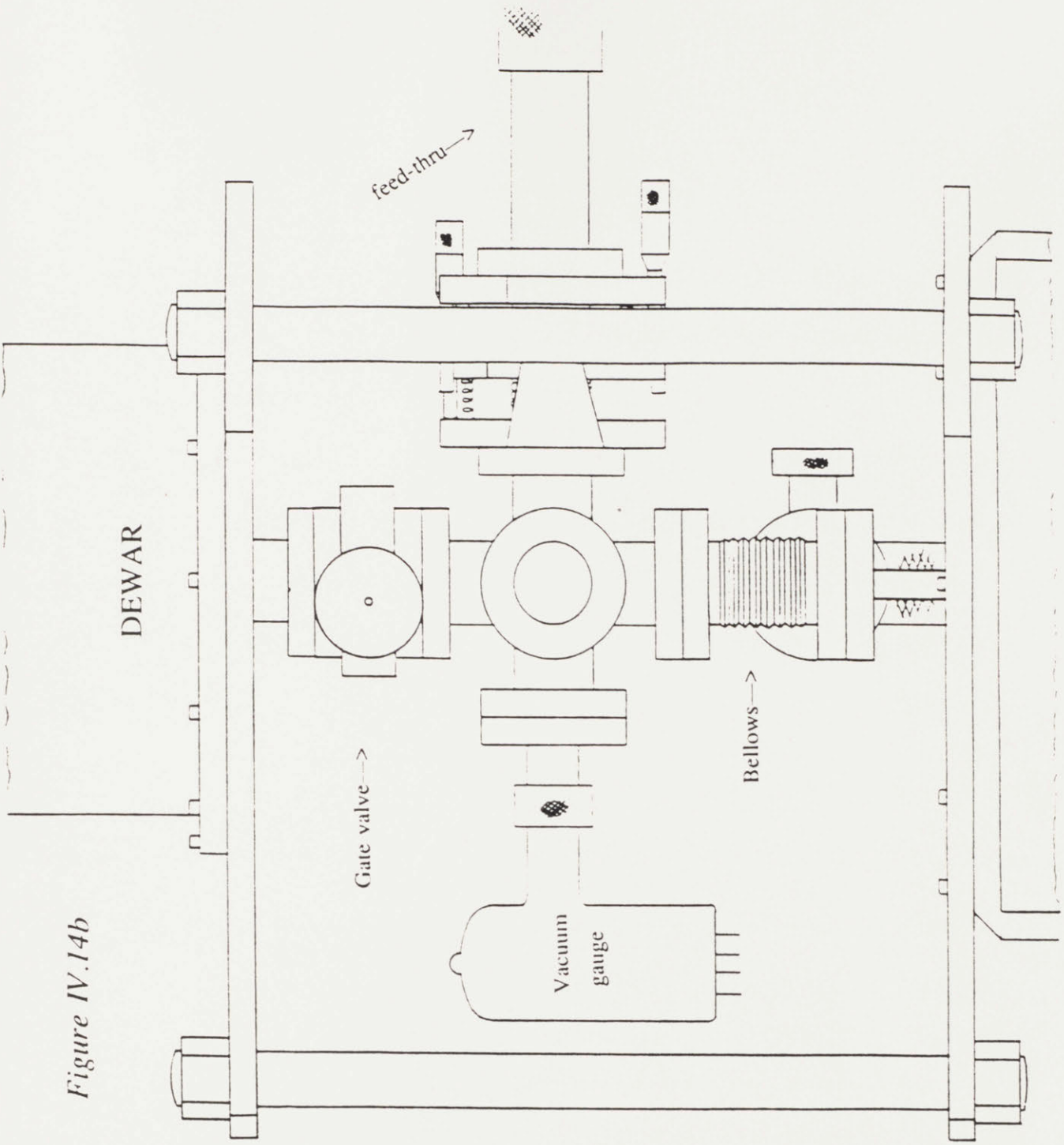

Figure IV.14b

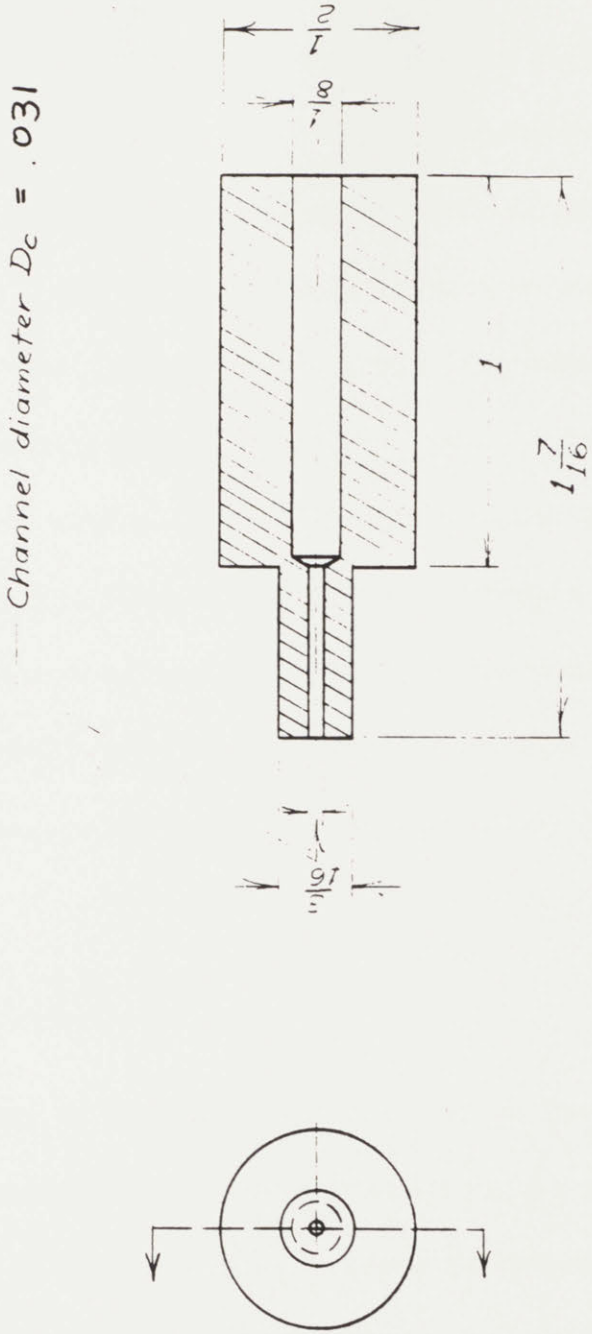

Figure IV.15

with a resistive wire (A.R.I. Industries) to several hundred degrees C.

A stainless steel bellows (MDC 150-X) connects the main chamber to a six-way cross (MDC 150-6) which in turn attaches to the dewar via a gate valve (MDC GV-1500V). The gate valve can be closed to completely isolate the dewar from the source region, necessary during the initial fire-up of the oven heaters (see next section) and for source maintenance while the dewar is cold. The cross has ports for an ionization gauge (Varian 0563-K2466-302), the gimbal mount for the retroreflecting mirror (cf. Section IV.5.1), a window (MDC VPH-150) for viewing the atomic beam, and a second six-way. The flexible hose shown (Huntington VF-155) circumvents the channel and allows the turbo to pump directly on the crosses and the dewar when the butterfly valve (MDC AV-150M) is open. An electrical relay sits in the cross just above the bellows; it controls a shutter which blocks the atomic beam when the relay is energized.

IV.6.2 The Alkali Oven

The purpose of the alkali oven is to provide atoms for experiment. It has sufficient temperature range to accommodate the various alkalis: lithium, sodium, etc. The oven itself is little more than a reservoir for molten alkali; a nozzle at the top allows some of the associated vapor to escape.

A cross-sectional view of the oven assembly is shown in Figure IV.16. The oven reservoir itself is fashioned from type 310 stainless. The alkali is loaded into the

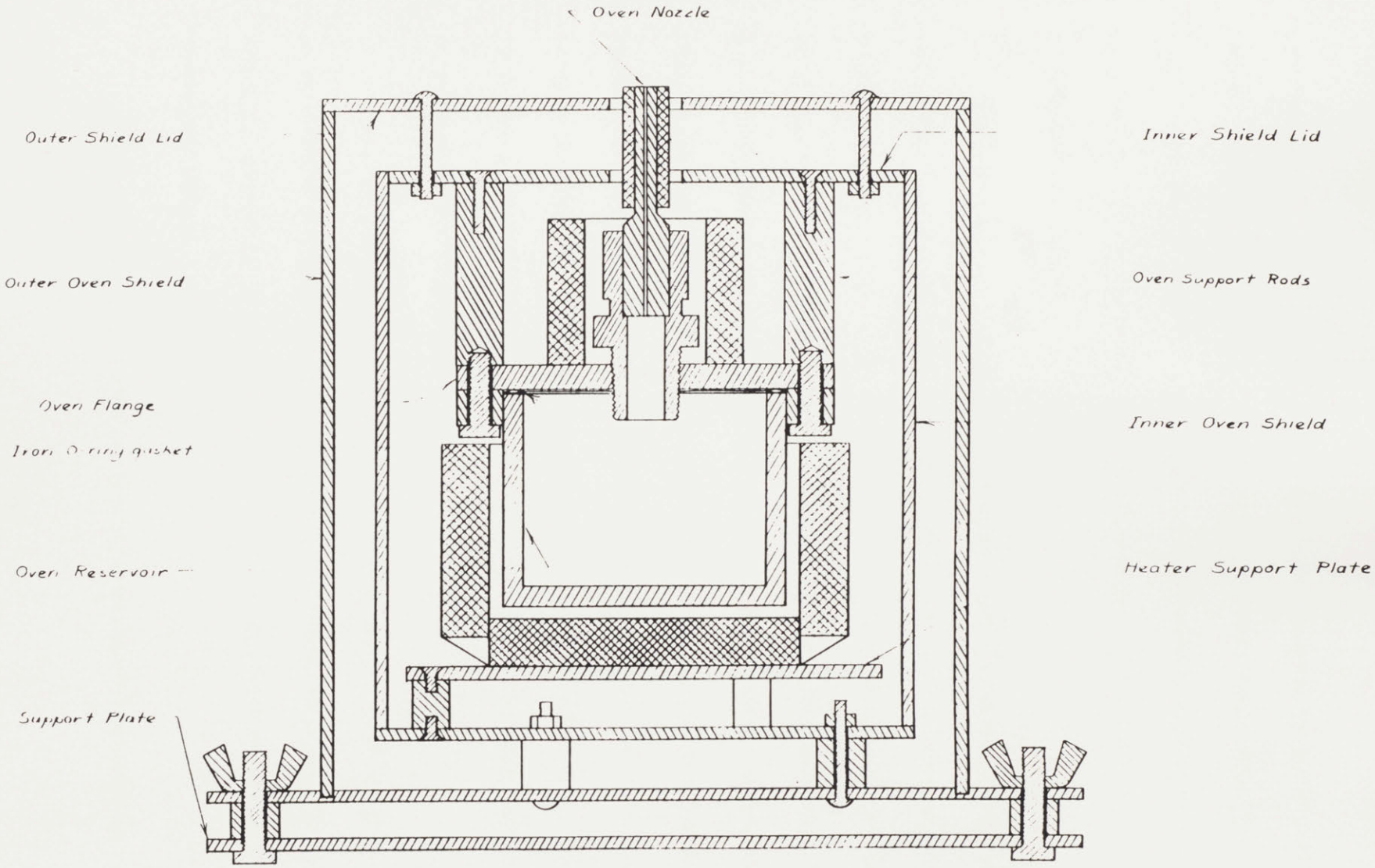
Oven Nozzle
Outer Shield Lid
Inner Shield Lid
Outer Oven Shield
Oven Support Rods
Oven Flange
Inner Oven Shield
Iron O-ring gasket
Oven Reservoir
Heater Support Plate
Support Plate

Figure IV.16

reservoir in an inert environment (dry nitrogen); the reservoir is then bolted together, with an iron gasket to provide a secure seal. The oven hangs from three stainless support rods, which ensure that the nozzle heater remains centered in the hole at the top of the shield. The nozzle (Figure IV.17) is secured to the top flange of the oven by a Swagelock connector.

The oven (MIG84) is radiatively heated by five Thermcraft resistance heaters: one for the baseplate (PH2004-S-3D 38V/170W), two half cylinders wired in series (with each other and the baseplate heater) for the body (RH251-S-1.62 38V/110W each), and two half cylinders wired in series for the Swagelock connector (RL111-S-1.62 57.5V/100W each). The nozzle is heated by a .035" tungsten wire secured to an alumina tube and encased in Sauereisen cement. All the leads from the heaters are insulated in ceramic "fish-spine" (Omega) and extracted from the shields through a notch at the top. The leads are then connected to electrical feed-thrus, which consist of Torr-Seal filled metal tubes with wires running through the inside, where they can be attached to power supplies.

The power supplies for the heaters are isolated from ground to permit operation in the event of a single short-circuit to ground. To reduce the chance of arcing in the hot alkali gas, the AC is rectified and somewhat filtered, giving maximum power for a given peak voltage.

The temperature of each oven component is monitored independently by several

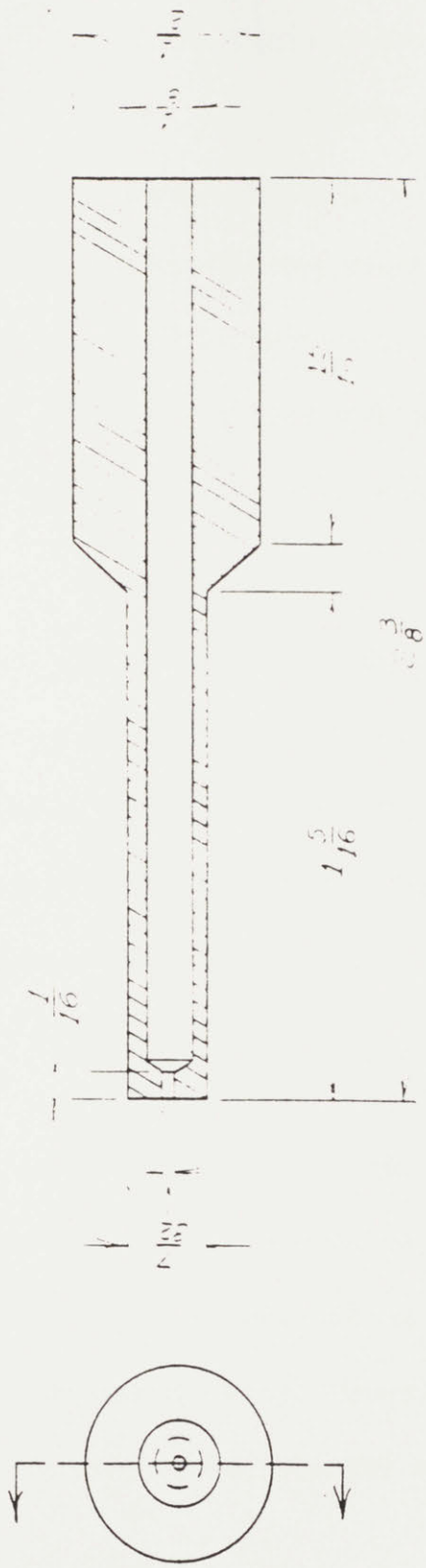

Figure IV.17

thermocouples. To prevent the nozzle from clogging, it is kept slightly hotter (~25°C) than the Swagelock connector, which in turn is slightly hotter than the body of the oven. To keep the demands on the heaters reasonable, the entire oven is enclosed in a multi-layer radiation shield which fills the indicated region. About 20 layers of .003" stainless shim stock is stacked above and below the oven, and a 20 layer spiral of the shim is wound around the perimeter. The outer and lower covers are cooled by circulating water through a copper refrigerator tube which is silver-soldered to these covers.

The oven shield support plate is fastened to an x-y translator (two NRC 420-05 translation stages) which in turn is secured to the base of the source chamber. The translator drives are connected to flexible cables which go to rotary feed-thrus on a source chamber flange. The horizontal position of the oven can thus be adjusted from the outside to maximize the flux of alkali into the dewar.

IV.6.3 Expected Performance

Having now provided a physical description of the apparatus, we can estimate the flux of atoms that we expect to be able to load into the trap. This is an important consideration, for it determines the ultimate density we can hope to achieve in the light trap. We shall make our analysis general, and provide numerical estimates for sodium and lithium. Table IV.4 lists some of the properties of sodium and lithium for comparison and reference.

Property	Na^{23}	Li^{7}	units
a	103,300	137024	
b	7.553	7.229	
λ (D2)	589.6	670.8	nm
ΔE_{fs}	17.19	.34	cm^{-1}
ΔE_{hfs} (grnd)	1772	803	MHz
$\hbar k/M$	2.9	8.4	cm/s
τ_N	16	27	ns
Melting pt.	98	186	°C
v_{max} (L=90cm)	1300	1600	m/s
a_{max}	9.7×10^{7}	1.6×10^{8}	cm/s^2
N_γ ($v_{max} \rightarrow 0$)	43000	19000	
v_{perp}	6	12	m/s
I ($v<v_{max}$)	10^{15} (@ 500°C)	2×10^{14} (@ 750°C)	s^{-1}

Table IV.4

We shall assume that the oven is an effusive source of atoms of mass M and absolute temperature T. This is a poor approximation in some respect, because we will almost certainly operate in a regime where the mean free path of the atom λ is much less than the nozzle diameter w (for sodium at 300°C, $\lambda \approx .01$ cm). The flow from the nozzle will therefore be partially hydrodynamic; for an order of magnitude estimate of the flux, however, this approximation will suffice.

The kinetic theory gives the flux dQ from a nozzle of area A into the element of solid angle $d\Omega$ as (RAM56)

$$\frac{dQ}{d\Omega} = \frac{n\bar{v}}{4\pi} A \cos\theta \tag{1}$$

where $\bar{v} \equiv 1.13\sqrt{2kT/M}$ is the mean atomic velocity inside the source, n the density, and θ the azimuthal angle. The total flux of the source into a cone defined by the angle θ_0 is obtained by integrating this expression:

$$Q = \frac{n\bar{v}}{4} A \sin^2\theta_0 \, . \tag{2}$$

If we consider the gas to be ideal, then we may write

$$Q = 1.13P\sqrt{\frac{2}{MkT}} A \sin^2\theta_0. \tag{3}$$

Since the gas in the oven is just the vapor above a molten metal, the pressure P is the vapor pressure of the metal at the temperature T. This may be obtained empirically from the relation (WEA75)

$$P(T) = 10^{-\frac{.05223a}{T}+b} \; torr \; . \tag{4}$$

Values for the constants a and b are given in Table IV.4 for sodium and lithium.

The distribution of velocities in the oven is Maxwellian. The distribution in the beam, however, is skewed by an additional factor of v since the faster atoms in the oven have more chances to escape. If $I(\mathrm{v})d\mathrm{v}$ is the beam intensity for atoms with velocities between v and $\mathrm{v}+d\mathrm{v}$, then the normalized expression is (RAM56)

$$I(\mathrm{v}) = 2Q\,\frac{\mathrm{v}^3}{\alpha^4}\,e^{(-\mathrm{v}^2/\alpha^2)} \; , \tag{5}$$

where $\alpha \equiv \sqrt{2kT/M}$. By integrating this we get the total number of atoms in the beam with velocities less than v_0:

$$I(\mathrm{v}<\mathrm{v}_0) = Q\left[1 - \left[1 + \frac{\mathrm{v}_0^2}{\alpha^2}\right] e^{(-\mathrm{v}_0^2/\alpha^2)}\right] . \tag{6}$$

Note that as we increase T, the total flux will increase due to the rise in vapor pressure; the most probable velocity $\mathrm{v}_p = 1.22\alpha$ will increase as $T^{1/2}$, indicating that the entire atomic distribution will shift upward in velocity as we raise the source temperature.

Recall (Section IV.4.2) that our slower of length L can stop atoms with a maximum velocity $\mathrm{v}_{\max} = \sqrt{2La_{\max}}$. There is therefore an optimum temperature to which the oven should be heated to produce the greatest number of "stoppable" atoms. In the regime in which we are able to operate, this number increases monotonically with temperature, suggesting that we should run our oven as hot as possible. Aside

from the increased consumption of alkali, other *dis* advantages to hot operation are discussed below.

It is instructive to calculate how many atoms we expect to be able to load into the trap. The azimuthal angle subtended by the trap is $\theta_0 \approx .5/120 = 4\text{mrad}$. Taking the slower length $L = 90$ cm, we get $v_{max} \approx 1300$ m/s for sodium and 1600 m/s for lithium 7. We find that $\sim 10^{15}$ sodium atoms per second will be available for the trap.

It is unlikely that we will be able to slow this many atoms, however. We see from Table IV.4 that an atom with velocity v_{max} requires ~43000 photons to be stopped; since most of the stopped atoms will have initial velocities less than this, however, we will assume an "average" ~35000 photons per atom. With a laser power of ~100mW, we have $\sim 3\times 10^{17}$ photons per second available for slowing, enough for $\sim 10^{13}$ atoms/sec. We therefore have enough light for only ~1% of all "stoppable" atoms from the source. In practice we will probably be no more than 10% efficient, however, so we expect to load atoms into the trap at a rate of $\sim 10^{12}$ per second.

IV.6.4 Ultimate Limits

There are several factors which will serve to limit the ultimate performance of our trap. One limiting process will be the collisions between unstopped atoms in the atomic beam and stopped atoms in the trap, knocking the trapped atoms out. The rate that an atom will be expelled by this process is

$$R = I_{beam} \times \frac{\sigma_{Na-Na}}{A}\ , \tag{3}$$

where I_{beam} is the flux of atoms through the trap region, σ_{Na-Na}~2000Å^2 is the collision cross-section and A is the area of the trap. We find that the collision rate per atom is ~125/sec, implying a lifetime of ~8 msec. This indicates that it may be desirable to reduce the oven temperature and to chop the atomic beam for studying long-time trap effects.

The ultimate densities which can be obtained in a radiation pressure trap may be limited by the ideal gas law $n = P/kT$ (PWR86). Once the trapped gas becomes optically dense, the laser beams will form a "wall" for the trapped atoms, which will feel a pressure P at most equal to the total radiation pressure. For lasers having an intensity of 10 mW/cm^2, we have $P = 3\times10^{-6}$ dyne/cm^2, yielding a maximum density at $T = 240\mu K$ of $n = 10^{14}$ cm $^{-3}$. A warning: one may have to reflect the trapping lasers' retro beams at a slight angle to avoid casting a shadow on the trapped atoms from their absorption of the incident beam.

One would like the loading rate of the slower to be as high as possible to maximize the trap densities and the signal from collision processes. A high field-gradient in the trap, which is conducive to high densities, tends to reduce the size of the capture disc by Zeeman shifting atoms far from resonance when they are even a small distance from the trap center, thereby reducing the loading rate. There are a number of possible ways to increase the capture disc of the trap, however, yet still

retain the high field gradient near the center. For example, one could create additional frequency components in the trapping lasers which would be resonant with the atoms at the higher field. The field could be "rolled-off," perhaps, by installing smaller coils closer to the trap center, which would add to the field near the center but subtract from it as you move away. Yet another possibility is to place a focusing magnet — quadrupole or hexapole — to bend the off-axis atoms back to the center using their magnetic moments. The conception of other ideas is left to the ingenuity of future experimenters.

CHAPTER V — CONCLUSION

The primary accomplishment reported in this thesis is the conception and demonstration of the first spontaneous force light trap for neutral atoms. The key breakthrough was the fundamental realization that the internal structure of an atom could be utilized to circumvent the "optical Earnshaw theorem" (GOA82) and form a stable trap (PWR86). Using Jean Dalibard's idea for a gradient field as a starting point, we developed a scheme that would trap most paramagnetic atoms in three dimensions. The trap for sodium was constructed by adding several components to S. Chu's "optical molasses" setup at Bell Labs. We trapped a gas of sodium atoms for longer times and at higher densities than in any trap previously reported (though our records have since been broken (HKD87)). We measured some of the basic properties of the trap such as its lifetime, size, and strength, and compared these measurements with the predictions of a theoretical model. We also observed some evidence of binary collisions amongst the trapped atoms.

The collaboration with Bell provided the most expeditious route to test our ideas for the light trap. The experimenters were able to team up for only about a month, however, before other factors interceded to force the author to return to M.I.T. and the apparatus to depart with its owner S. Chu for Stanford University. Consequently, we had to limit the time spent on any one measurement, and refrain altogether from examining some potentially interesting phenomena. For example, it would have been nice to do a more detailed study of the trap strength versus laser frequency to compare

with the model's predictions. The velocity distribution of the trapped atoms should have been accurately pinned down by devising a setup to quickly and simultaneously shut off the laser beams and the magnet currents. A reliable way to positively chop the lasers should have been implemented to remove the disagreement on the lifetime in the magnetic trap alone. The effect of changing the separation between the laser sidebands should have been tested, especially when the upper sideband was tuned to the red of the $F=2 \rightarrow F'=2$ transition. Et cetera.

The experiment conducted at Bell was only an appetizer, serving to whet our appetite for the research we hope to perform in the new M.I.T. apparatus. Possible entrees include:

- A detailed examination of loss rates under a number of laser and field conditions at very high densities.

- Spectroscopy of the atoms undergoing non-linear decay to try to identify the precise loss mechanism. We would be especially vigilant for detecting laser-induced molecular formation (TWJ87), associative ionization (WEI80), and collisional heating effects (GAP88). A grating monochromator could be supplemented by a channeltron to detect any ions that are produced (GOU87).

- Resonant-collision spectroscopy. If two colliding atoms are in excited states whose energies sum to that of a third excited state, the collision will be resonant. One example of such a collision is Na(ns) + Na(ns) $\rightarrow$ Na(np) + Na((n-1)p), where an

electric field is used to tune the levels so that the energy of the ns state is halfway between the energies of the np and the (n-1)s states. A trap is a good environment to study such collisions because the spectroscopic linewidths will not be broadened by the atomic motion.

• Investigations of other types of spontaneous force traps and hybrid traps. Of primary interest are light traps which spin-polarize the trapped atoms, simplifying the collisional calculations and possibly reducing the recombination rate.

• Slowing and trapping lithium. Lithium is available as either a Boson (Li^7) or as a Fermion (Li^6); we could choose one or the other for our trap by a judicious selection of the frequency for the laser sidebands. Lithium as a Boson is a better candidate for Bose-Einstein condensation than sodium, since the critical temperature T_c at a given density goes as the mass^{-1} (BPK87); at densities which we realistically hope to achieve, however, T_c is still ~2-3 orders of magnitude below the Doppler cooling limit, so this difference is of marginal utility. Lithium as a Fermion, though, can be interesting, because S-wave collisions are symmetry forbidden between two atoms with parallel spin. Since the trapped atoms are cold enough to inhibit collisional orders above S-wave (the maximum partial wave is given by $(l_{\max} + \frac{1}{2})\lambda \approx 2\pi b$, where λ is the deBroglie wavelength and b the semi-classical impact parameter (PRI85, p.XI-B-4.1)), the total collision cross-section should vanish at low temperatures (though above the Doppler limit). This might allow the trap density to increase far beyond what we have thus far seen, perhaps to the point where

the atoms form a degenerate Fermi sea.

The apparatus was intentionally designed to be versatile in order to accommodate these and other experiments which we conceive. Anything unexpected which we discover in the course of experimentation will simply be icing on the dessert cake.

References

ADH86 A. Aspect, J. Dalibard, A. Heidemann, C. Salomon, and C. Cohen-Tannoudji, *Phys. Rev. Lett.* **57**, 1688 (1986).

ALE75 L. Allen and J. Eberly, *Optical Resonance of Two–Level Atoms*, J. Wiley and Sons (New York), 1975.

ASG83 A. Ashkin and J. Gordon, *Opt. Lett.* **8**, 209 (1983).

ASH70a A. Ashkin, *Phys. Rev. Lett.* **24**, 156 (1970).

ASH70b A. Ashkin, *Phys. Rev. Lett.* **25**, 1321 (1970).

ASH78 A. Ashkin, *Phys. Rev. Lett.* **40**, 729 (1978).

ASH84 A. Ashkin, *Opt. Lett.* **9**, 454 (1984).

ASK72 G. Askar'yan, *Sov. Phys. JETP* **15**, 1088 (1962).

BAG87 V. Bagnato, Ph.D. thesis, M.I.T. (unpublished).

BEI83 R.F. Berg and G.G. Ihas, *Cryogenics*, August 1983, p. 437.

BFA78 J. Bjorkholm, R. Freeman, A. Ashkin, and F. Pearson, *Phys. Rev. Lett.* **41**, 1361 (1978).

BFS75 Yu.L. Buyanov, A.B. Fradkov, and I.Y. Shebalin, *Cryogenics*, April 1975, p. 193.

BLM79 V. Balykin, V. Letokhov, and V. Mushin, *JETP Lett.* **29**, 560 (1979).

BLM87 V. Bagnato, G. Lafyatis, A. Martin, E. Raab, R. Ahmad-Bitar, and D. Pritchard, *Phys. Rev. Lett.* **58**, 2194 (1987).

BLS84 V. Balykin, V. Letkhov, and A. Sidorov, *JETP Lett.* **40**, 1027 (1984).

BLS84 V. Balykin, V. Letokhov, and A. Sidorov, *Opt. Comm.* **49**, (1984).

BPI85 J. Bolinger, J. Prestage, W. Itano, and D. Wineland, *Phys. Rev. Lett.* **54**, 1000 (1985).

BPK87 V. Bagnato, D. Pritchard, and D. Kleppner, *Phys. Rev. A* **35**, 4354 (1987).

CAB86 M. Carrera-Patino and R. Bory, *Phys. Rev. A* **34**, 4728 (1986).

CAB87 A. Cable, private communication.

CBA86 S. Chu, J. Bjorkholm, A. Ashkin, and A. Cable, *Phys. Rev. Lett.* **57**, 314 (1986).

CHA43 S. Chandrasekhar, Rev. Mod. Phys. **15** (1943).

CHB85 S. Chu, L. Hollberg, J. Bjorkholm, A. Cable, and A. Ashkin, *Phys. Rev. Lett.* **55**, 48 (1985).

CDL77 C. Cohen-Tannoudji, B. Diu, and F. Laloe, *Quantum Mechanics*, J. Wiley and Sons (New York), 1977.

COH86 C. Cohen-Tannoudji, Lectures at Helsinki Summer School (unpublished) (1986).

COM23 A.H. Compton, *Phys. Rev.* **22**, no. 5 (1923).

COO79 R. Cook, *Phys. Rev. A* **20**, 224 (1979).

COO80 R. Cook, *Phys. Rev. A* **21**, 268 (1980).

COR77 A. Corney, *Atomic and Laser Spectroscopy,* Clarendon Press (Oxford), 1977.

COS35 E.U. Condon and G.H. Shortly, *The Theory of Atomic Spectra*, Cambridge Univ. Press (Cambridge), 1935 (reprinted 1985), p. 108.

DAC85 J. Dalibard and C. Cohen-Tannoudji, *J. Opt. Soc. Amer. B* **2**, 1707 (1985).

DHS87 J. Dalibard *et al.*, to be published.

DRC83 J. Dalibard, S. Reynaud, and C. Cohen-Tannoudji, *Opt. Comm.* **47** (1983).

EBH85 W. Ertmer, R. Blatt, J. Hall, and M. Zhu, *Phys. Rev. Lett.* **54**, 996 (1985).

EIN17 A. Einstein, *Physik. Zs.* **18**, 121 (1917), translated in D. ter Haar, *The Old Quantum Theory*, Pergamon Press (Oxford, 1967) pp. 167-183.

FRI33 O. Frisch, *Z. Phys.* **86**, 42 (1933).

GAP88 A. Gallagher and D. Pritchard, to be published.

GOA80 J. Gordon and A. Ashkin, *Phys. Rev. A* **21**, 1606 (1980).

GOR84 J. Gordon, *Prog. Quant. Elec.* **8**, 177 (1984).

GOU86 P.L. Gould, Ph.D. thesis, p. 74 (unpublished).

GOU87 P.L. Gould, private communication.

HAN87 R.G. Hanson and Associates, Tech. Pub. no. RG386, Santa Barbara, CA.

HAS75 T. Hansch and A. Schawlow, *Opt. Comm.* **13**, 68 (1975).

HEE63 C.V. Heer, *Rev. Sci. Instr.* **34**, p. 532 (1963).

HKD87 H.F. Hess *et al.*, *Phys. Rev. Lett.* **59**, 672 (1987).

JAC75 J.D. Jackson, *Classical Electrodynamics*, 2nd edition, J. Wiley and Sons (New York), 1975.

JAV86 J. Javanainen, *Phys. Rev. Lett.* **57**, 3164 (1986).

KAM74 I.P. Kaminov, *Introduction Electrooptic Devices*, Academic Press (New York), 1974.

KPT78 K.-J. Kugler, W. Paul, and U. Trinks, *Phys. Lett.* **72B**, 422 (1978).

KYS77 E. Kyrola and S. Stenholm, *Opt. Comm.* **22**, 123 (1977).

LAL60 L. Landau and E. Lifshitz, *Electrodynamics of Continuous Media*, Pergamon Press (New York), 1960, p. 54.

LEB01 P. Lebedev, *Ann. Phys.* (*Leipzig*) **6**, 433 (1901).

LEM77 V. Letokhov and V. Minogin, *Phys. Lett.* **61A**, 370 (1977).

LEP76 V. Letokhov and B. Pavlik, *Appl. Phys.* **9**, 229 (1976).

LET68 V. Letokhov, *Sov. Phys. JETP* **7**, no. 9 (1968).

LEV84 M.D. Levenson, *Introduction to Non-linear Laser Spectroscopy,* Academic Press (New York), 1984.

LMP76 V. Letokhov, V. Minogin, and B. Pavlik, *Opt. Comm.* **19**, 72 (1976).

LMP78 V. Letokhov, V. Minogin, and B. Pavlik, *Sov. Phys. JETP* **45**, 698 (1978).

LOU64 W. Louisell, *Radiation and Noise in Quantum Electronics,* McGraw Hill (New York), 1964, p. 165.

LOU73 R. Loudon, *The Quantum Theory of Light*, Clarendon Press (Oxford), 1973.

MAS71 Massey, *Electronic and Ionic Impact Phenomena,* vol. 3, p. 1324, Oxford (1971).

MAX91 J.C. Maxwell, *Electricity and Magnetism,* 3rd edition, Dover (New York), 1891—reprinted in 1954.

MIG84 A. Migdall, Ph.D. thesis (unpublished).

MIJ82 V. Minogin and J. Javanainen, *Opt. Comm.* **43**, 119 (1982).

MIN80 V. Minogin, *Opt. Comm.* **34** (1980).

MIS79 V. Minogin and O. Serimaa, *Opt. Comm.* **30**, 373 (1979).

MPP85 A. Migdall *et al.*, *Phys. Rev. Lett.* **54**, 2596 (1985).

NHT78 W. Neuhauser, M. Hohenstatt, P. Toscek, and H. Dehmelt, *Phys. Rev. Lett.* **41**, 233 (1978)

PHI86 W.D. Phillips, Lectures at Helsinki Summer School (unpublished) (1986).

PHM82 W. Phillips and H. Metcalf, *Phys. Rev. Lett.* **48**, 596 (1982).

PMP85 J. Prodan *et.al.*, *Phys. Rev. Lett.* **54**, 992 (1985).

PPM82 J. Prodan, W. Phillips, and H. Metcalf, *Phys. Rev. Lett.* **49**, 1149 (1982).

PPM84 W. Phillips, J. Prodan, and H. Metcalf, *Prog. Quant. Elec.* **8**, 119 (1984).

PRC87 M. Prentiss and A. Cable, private communication.

PRI85 D. Pritchard, lecture notes to 8.421, to be published.

PRI83 D. Pritchard, *Phys. Rev. Lett.* **51**, 1336 (1983).

PRI84 D. Pritchard, *Prog. Quant. Elec.* **8**, 209 (1984).

PWR86 D. Pritchard, C. Wieman, E. Raab, R. Watts, and V. Bagnato, *Phys. Rev. Lett.* **57**, 310 (1986).

RAM56 N.F. Ramsey, *Molecular Beams*, ch. II , Clarendon Press (Oxford), 1956.

RPC87 E.L. Raab, M. Prentiss, Alex Cable, Steven Chu, and D.E. Pritchard, *Phys. Rev. Lett.* **59**, 2631 (1987).

SAG87 R. Stoneman, M. Adams, and T. Gallagher, *Phys. Rev. Lett.* **58**, 1324 (1987).

SDA87 C. Salomon *et al.*, *Phys. Rev. Lett.* **59**, 1659 (1987).

SDG81 K. Safinya *et al.*, *Phys. Rev. Lett.* **47**, 405 (1981).

SML78 S. Stenholm, V. Minogin, and V. Letokhov, *Opt. Comm.* **25**, 107 (1978).

SOB63 I.I. Sobel'man, *Intro. the Theory of Atomic Spectra*, Pergamon Press (New York), 1963.

STW84 W.C. Stwalley, *Prog. Quant. Elec.* **8**, 203 (1984).

TWJ87 H. Thorsheim, J. Weiner, and P. Juliene, *Phys. Rev. Lett.* **58**, 2420 (1987).

VAD81 H. Anderson, ed. *Physics Vade Mecum*, American Institute of Physics (New York) 1981.

WDW78 D. Wineland, R. Drulinger, and F. Walls, *Phys. Rev. Lett.* **40**, 1939 (1978).

WEA75 R.C. Weast, ed., *Handbook of Chemistry and Physics,* CRC Press, (Cleveland), 1975.

WEI80 J. Weiner, *J. Chem. Phys.* **72**, 2856 (1980).

WIB87 D. Wineland et al., *Phys. Rev. A* **36**, 2220 (1987).

WIE87 C.E. Wieman, private communication (1987).

WII79 D. Wineland and W. Itano, *Phys. Rev. A* **20**, 1521 (1979).

WIL83 M. Wilson, *Superconducting Magnets*, Clarendon Press (Oxford), 1983.

WIN84 W. Wing, *Prog. Quant. Elec.* **8**, 119 (1984).

WSL59 Wuerker, Shelton, and Langmuir, *J. Appl. Phys.* **30**, 342 (1959).

YSH86 Yang *et al.*, *Phys. Rev. A* **34**, 2962 (1986).

Acknowledgements

I could not have written the preceding pages without the assistance, advice, and encouragement of numerous people.

My advisor, Dave Pritchard, is a superb physicist and a terrific motivator. I am priviledged to have been taught by him.

Steven Chu gave me the opportunity to perform our experiment in his laboratory at Bell, assisted in the initial set-up, and advised us during experimental runs via telephone from Japan. Alex Cable did most of the actual work at Bell — his highly skilled efforts enabled us to accomplish twice as much in half the time (yes, a factor of four gain) than would have been possible without him. Mara Prentiss also played a major and indespensible role in my visit to Holmdel and subsequent data analysis.

Jean Dalibard's idea for trapping an atom in one-dimension had the characteristics of many truly great ideas: it superficially was extraordinarily simple, yet it had a deep and profound influence on his scientific peers.

Many of my associates at M.I.T. had direct and/or indirect contributions to this thesis. Rick "Spike" Stoner, Xe-Sun Sun, and Debbie Lew all worked diligently and ably on the design and construction of the M.I.T. light trap — and continue to do so. Rick also contributed many of the professional-quality drawings in this thesis. Mark Anderson assisted in the design of the optical system and the magnets — presumably he is happy in his present surroundings at Berkeley. Though Sam Osofsky elected to

diversify his undergraduate experience just after the success of the Bell experiment, his contributions to the early development of spontaneous force traps were skilled and numerous. Tim Shirley built the cavity and electronics for the electro-optic modulator.

Phil Gould introduced me to lunchtime hoops, an activity whose importance I cannot overstate; he also helped me straighten out the problem of the ultimate temperature in a laser-cooled gas. Greg Lafyatis and Alejandro Martin, past and present "post-docs" in my group, were always willing to summon their vast experience to assist me when requested. Vanderlei Bagnato was a valued co-worker on an earlier experiment; he and Kris Helmerson also gave me much useful advice for the construction of the current experiment.

May others ameliorated the quality of my stay here with friendship and technical assistance. Pete Magill, Brian Stewart, Robert Weisskoff, and Eric Cornell were always available when needed. Mike Kash, Barbara Hughey-Beckwitt, Scott Paine, and George Welch, truly fine people all, were never too busy to answer a question or to lend stuff; Mike's vast resources of knowledge and literature proved especially helpful.

Dan Kleppner greatly improved the quality of this work with his diligent proofreading, as well as his subsidy of the coffee fund. Andrea Gelinas provided highly capable administrative assistance.

I probably will never be able to fully appreciate the love of my parents, to

whom I have dedicated this thesis.

To all: Thank you.